



UNIVERSITÀ
DEGLI STUDI
DI PADOVA

UNIVERSITA' DEGLI STUDI DI PADOVA

Dipartimento di Ingegneria Industriale DII

Corso di Laurea Magistrale in Ingegneria Meccanica

Analysis of transmission error by means of a novel flex-to-flex gear contact
method with model order reduction

Relatore: Prof. Alberto Doria

Correlatori: Prof. Wim Desmet
Dr. Tommaso Tamarozzi

Andrea Russo

Matr. 1057593

Anno Accademico 2014/2015

Ai miei genitori

This thesis work was developed at the Catholic University of Leuven in collaboration with Siemens Industry Software NV. Research activities at Siemens Industry Software were supported by DEMETRA project, under the MARIE CURIE European Programme.

I wish to thank for the support on this work Prof. Alberto Doria, Prof. Wim Desmet, Tommaso Tamarozzi, Bart Blockmans, Alessandro Toso, Antonio Palermo, Shadi Shweiki.

Abstract

In recent years simulation tools revealed to be a valid alternative for the design of mechanical systems in many industrial applications.

Simulations of gear transmission is still a computationally demanding task due to the high accuracy required in the determination of specific local quantities. Model order reduction techniques can reduce the computational effort and allow the solution of mechanical systems in a reasonable amount of time. Recently a novel flex-to-flex model order reduction method for gear transmission was developed at the PMA research group of KU Leuven. A simulation code for gear transmission was implemented based on this new approach and it was numerically validated with an other commercial software.

At Siemens Industry Software NV a gear test-rig, concurrently developed by Siemens Industry Software NV, KU Leuven and Unical, is available for experimental tests on various spur gear pairs.

This thesis work illustrates the main aspects of the method and the code. Then a spur test-rig gear pair is both modelled and simulated on the code and tested with quasi-static measurements on the test-rig. Furthermore code parameters influence is discussed. Experimental and numerical transmission errors are analysed and compared.

Results are finally discussed and future research works are suggested.

Contents

Abstract	4
1 Introduction and Objectives	8
1.1 Gear transmission and simulation	8
1.2 A novel simulation approach	9
1.3 Structure of the work	9
2 Gears, Concepts and Geometry	11
2.1 Cylindrical gears	11
2.1.1 Spur gear geometry	12
2.1.2 Cylindrical gear pair	15
2.1.3 Transmission error	19
2.2 Technical data of implemented gears	20
2.2.1 Test gears	21
2.2.2 Test gear pair parameters	21
2.3 Chapter's remarks	24
3 Non-linear Parametric Model Order Reduction Technique for Gear Simulations	25
3.1 Review of model reduction techniques in dynamic contact analysis	25
3.1.1 Time-domain CMS methods employing real modes . .	26
3.1.2 Static modes switching method	28
3.1.3 Parametric and non linear model order reduction . . .	29
3.2 Definition of the parametric basis matrix	30
3.2.1 Computation of the global contact shapes	30
3.2.2 Interpolation of the global contact shapes	33
3.3 Derivation of the equations of motion	36
3.3.1 Floating frame of reference formulation	36
3.3.2 Kinetic and potential energy of the flexible gear	37
3.3.3 Equations of motion of the gear	39
3.4 Computer implementation	40
3.4.1 The pre-processing phase: computing the basis vectors	41

3.4.2	The processing phase: solving the equations of motion	42
3.4.3	Contact forces computation	43
3.5	Chapter's remarks	46
4	Correlation and model updating	47
4.1	Modal analysis	47
4.2	Numerical model and design of experiments	48
4.3	Model correlation	49
4.4	Chapter's remarks	53
5	Simulation Parameters Analysis	54
5.1	System model and types of analysis	54
5.2	Mesh analysis	55
5.2.1	Adopted model and meshing strategy	56
5.2.2	Mesh refinement along tooth flank	56
5.3	Penalty factor analysis	61
5.4	MOR analysis	64
5.5	Numerical effects	68
5.5.1	No convergence of a single shape	68
5.5.2	Oscillation on flat zones	68
5.5.3	Oscillations on transitory zones	69
5.6	Chapter's remarks	72
6	Experimental Measurements	73
6.1	Gear test-rig: basic concepts and instruments	73
6.2	Experimental results	76
6.2.1	Test operating conditions	76
6.2.2	Signal components	78
6.2.3	Experimental results	79
6.3	Chapter's remarks	82
7	Numerical results and comparison	83
7.1	Operating conditions	83
7.1.1	Numerical model	83
7.1.2	Pre-processing and applied torques	84
7.2	Numerical results	85
7.2.1	Static results	85
7.2.2	Dynamic results	89
7.2.3	Contact evolution	90
7.3	Comparison with experimental results	92
7.3.1	Signal decomposition	92
7.3.2	Amplitude	95
7.3.3	Shape	96
7.3.4	Contact ratio	99

7.4	Chapter's remarks	102
8	Conclusions	103
8.1	Simulation parameters analysis	103
8.2	Correlation and transmission error results	103

Chapter 1

Introduction and Objectives

1.1 Gear transmission and simulation

Gear transmissions are mechanical components that can be found in many industrial machinery and their role is crucial in every application. These elements are ones of first born mechanical systems in history and their evolution have always increased together with the mechanical industry development. Today companies R&D department and University research activities are still focused on gears transmission to improve the design know-how. The most important research fields in gears are related to the improving of the following performances:

- Efficiency
- Noise level
- Durability

These complex components transfer forces through mechanical contact interactions associated with elastic deformations and high dynamic stresses. The accurate prediction of these quantities is essential for sustainable and cost-efficient design of gearboxes above all for companies in the field of automotive and wind energy industry.



Figure 1.1: Automotive and wind turbine gearboxes

Nowadays most companies have numerical instruments integrated in their production process, from design to the manufacturing phase. Gear transmission design is also based on computer aided design, and recent developments have brought many commercial software to produce new simulation packages dedicated to gears transmission. These kind of systems present various difficult numerical problems to be implemented and this impedes the diffusion of simulation software due to a too high computation time.

1.2 A novel simulation approach

Traditional finite-element methods allow to perform static analysis, but are usually too demanding for the execution of dynamic simulations, in particular if contact interactions between the flexible members are considered. The KU Leuven research group PMA (Production Manufacturing Automation) developed an efficient method for performing such analyses. A novel code, named MUTANT (MULTibody Transient ANalysis of Transmissions) has recently been created based on this method. Its accuracy was demonstrated by comparison with commercial finite element software and evaluated to be 1 to 2 orders of magnitude faster than other approaches of similar accuracy [7]. This novel method is based on a MOR (Model Order Reduction) technique. Many mathematical models in various branches of numerical simulations implement the MOR approach to reduce their large size dimensions. By a reduction of model's degrees of freedom, an approximation to the original model is obtained, named reduced order model, which can be evaluated with lower accuracy but in significantly less time.

Gear transmission is an example of a large-scale dynamical system, which needs an high number of degrees of freedom to reach values of accuracy required by companies. Therefore applying a MOR technique on the model of this system is a logic and useful strategy.

1.3 Structure of the work

Concurrently KU Leuven, Siemens Industry Software NV and University of Calabria, developed a gear test-rig that is fully equipped to perform meshing analysis of gear pairs. This test-rig has been designed within the DEMETRA (DEsign of MEchanical TRAnsmiSSion) project and it's available at Test and Simulation Division of Siemens Industry Software NV for this thesis work. Data can be collected for different pre-load torques and speeds, regarding shaft torques, velocity, transmission errors, etc. In this thesis a set of two identical spur gears is available and a numerical model of the gear pair is updated to obtain a correlated numerical model and various numerical analyses are conducted on it. Consequently the gear pair is tested on the test-rig obtaining transmission error measurements and comparing them with

numerical solutions.

This thesis is organized as follows:

Chapter 1 introduces the work and its organization.

Chapter 2 discusses gears concepts and adopted gear pair technical data.

Chapter 3 presents theoretical basis of the MOR method.

Chapter 4 studies the parameters influence on the numerical code.

Chapter 5 presents the model updating of the gear pair.

Chapter 6 presents the experimental measurements of transmission error on the test-rig.

Chapter 7 provides comparison of numerical and experimental transmission errors.

Chapter 8 shows concluding remarks.

Chapter 2

Gears, Concepts and Geometry

2.1 Cylindrical gears

Gears are used in various types of machinery as a transmission component in every branch of mechanical industry. In this chapter basic concepts about the geometry and the parameters of a single gear are introduced, afterwards the main notions on gear pairs are presented and the transmission error is deeper discussed.

The most common way to classify gears is by category type and by the orientation of axes: parallel axes gears, intersected axes gears (conical) and non-parallel and non-intersecting axes gears. Spur and helical gears are parallel axes gears, bevel gears are intersecting axes gears, screw or crossed helical belong to last category.

Since meshing of paired parallel axis gears or intersecting axis gears involves simple rolling movements, they produce relatively minimal slippage and the efficiency is high.

In this chapter basic concepts are introduced only about cylindrical gears.

Category	Efficiency (%)
Parallel	98.0 – 99.5
Intersecting	98.0 – 99.0
Non parallel and non intersecting	30.0 – 95.0

Table 2.1: Efficiency of gears types

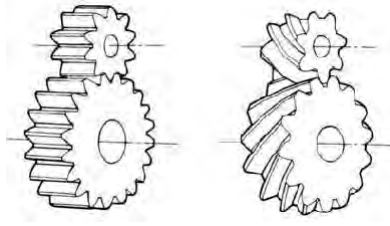


Figure 2.1: Spur and helical gears. Source: [9]

2.1.1 Spur gear geometry

In this part, the geometry of gear teeth is described.

The nominal dimensions of involute gear teeth are uniquely determined by the diameter of the reference cylinder, the associated basic rack and its position in relation to the reference circle. The nominal dimensions are defined by the following parameters, which are independent of each other:

Number of teeth, z

Standard basic tooth profile

Normal module, m_n

Profile shift coefficient, x

Tip diameter, d_a

Face width, b

Basic rack tooth profile

The generation process is based on zero backlash engagement with a basic rack. A rack is the profile of the conjugate gear of infinite pitch radius and the standard basic rack (according to ISO 53) is the one used in the present work.

It presents (see figure 2.3):

- Straight flanks
- The datum line is the straight line on which the nominal dimensions of tooth thickness and space width are defined as equal to half the pitch
- Same pressure angles for the left and right flanks
- Addendum plus bottom clearance equal to the dedendum

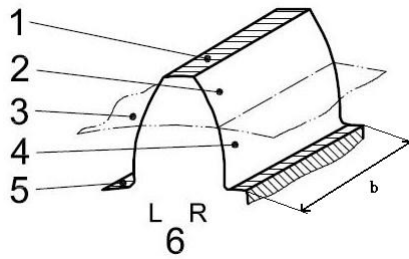


Figure 2.2: Components of a spur gear tooth: 1. top land 2. addendum flank 3. reference cylinder 4. dedendum flank 5. bottom land 6. datum face. Source: [9]

The basic rack tooth profile is defined in a normal section. The flanks of the basic rack tooth profile of involute teeth are straight lines. Tooth thickness, s and space width, e , on the datum line of the basic rack ($P - P$) in the reference plane are equal and they give the pitch of the gear, p . The standard basic rack tooth profile for involute teeth is standardized in ISO 53. In this chapter various parameters are represented through the rack tooth profile and not on the gear.

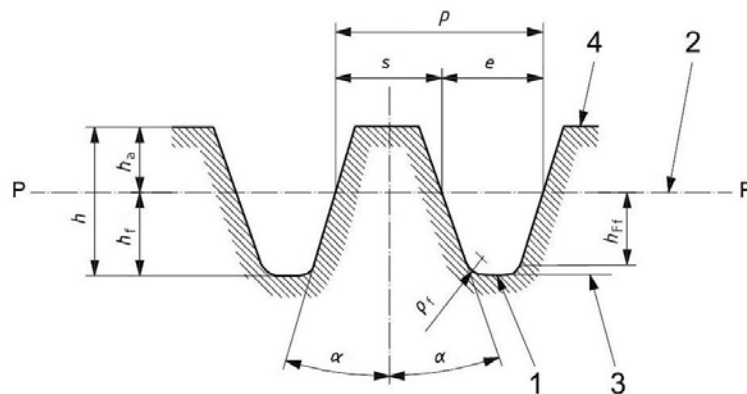


Figure 2.3: basic rack profile: 1. basic rack profile 2. datum line 3. root line 4. tip line. Source: [9]

Reference cylinder, reference circle, reference diameter

The reference cylinder is the reference surface for the cylindrical gear teeth. Its axis coincides with the axis of the gear and it's represented in figure 2.2. The reference circle is the intersection of the reference cylinder with a transverse plane section. The reference diameter, d is determined by:

$$d = |z|m \quad (2.1)$$

Module, face width

The module of the basic rack is found as the pitch of the rack divided by π . The normal module m_n , of the cylindrical gear is found as the module of the standard basic rack tooth profile (module series ISO 54). For a spur gear, the module is $m = m_n$.

The face width, b , is the length of the toothed part of the cylindrical gear measured in the axial direction on the V-cylinder, shown in figure 2.2.

Profile shift

The profile shift, xm_n , for involute gear teeth is the displacement of the basic rack datum line (ϕd) from the reference cylinder (ϕp). The tooth thickness, $\curvearrowright s$, is the circular tooth thickness on the theoretical pitch diameter. The magnitude of the profile shift can be made non dimensional by dividing by the normal module, and it is expressed by the profile shift coefficient, x . Positive profile shift increases the tooth thickness on the reference cylinder, as can be seen in figure 2.4 on the right, whereas negative values give a less thick tooth on the reference cylinder.

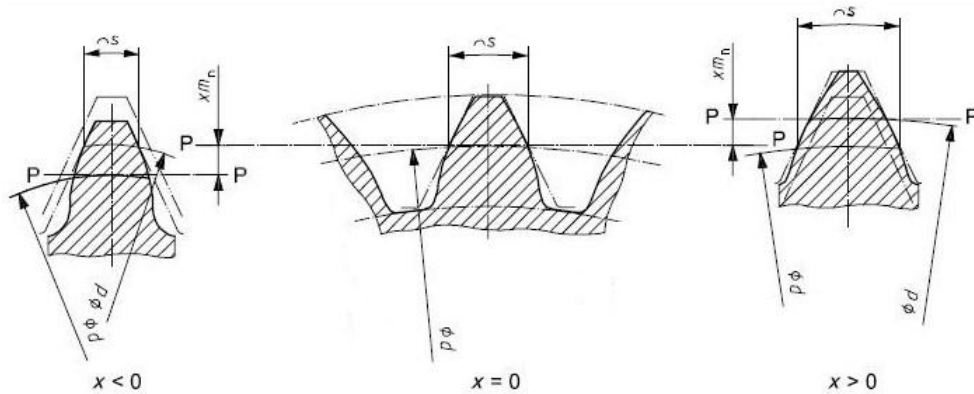


Figure 2.4: Profile shift xm_n . Source: [9]

Angular pitch, addendum and dedendum

The angular pitch, τ , is the angle laying in transverse sections that results from dividing a circle into z equal parts.

$$\tau = 360/|z| \quad (2.2)$$

A change to the addendum in relation to the addendum determined in the standard basic rack tooth profile is expressed by the tip alteration.

The tip alteration is made non-dimensional by dividing by the normal module, and it is expressed as the tip alteration coefficient, k . The addendum,

h_a , and the dedendum, h_f , of a cylindrical gear are stated on the basis of the reference circle (Figure 2.3). Their values are calculated from:

$$h_a = \frac{|d_a - d|}{2} = h_{aP} + xm_n + km_n \quad (2.3)$$

$$h_f = \frac{|d - d_f|}{2} = h_{fP} - xm_n \quad (2.4)$$

h_{aP} and h_{fP} are the addendum and dedendum of the rack profile, they are represented in 2.3 and are here identified by the subscript P . h_{Ff} is the depth of dedendum form, given by the introduction of the root radius ρ_f .

2.1.2 Cylindrical gear pair

A pair of gears can only mesh correctly if the pitches and the pressure angles are the same. The requirement that the pressure angles must be identical becomes obvious from the following equation for base pitch p_b :

$$p_b = \pi m \cos \alpha \quad (2.5)$$

If the pressure angles are different, the base pitches cannot be identical.

Gear ratio and transmission ratio

The gear ratio, u , of a gear pair is the ratio of the number of teeth of the wheel, z_2 , to the number of teeth of the pinion, z_1 :

$$u = \frac{z_2}{z_1} \quad (2.6)$$

The driving gear introduces rotation to the gear pair and effects the rotation of the driven gear. The transmission ratio, i , of a gear pair is the ratio of the angular speed (rotational speed) of the driving gear (a) to that of the driven gear (b):

$$i = \frac{\omega_a}{\omega_b} = \frac{n_a}{n_b} = -\frac{z_b}{z_a} \quad (2.7)$$

Center distance

In a transverse section of two mating gears, the line which connects the two axes is called the line of centres. The center distance, a_w , is the working distance between the gear axes of the two gears on the line of centres.

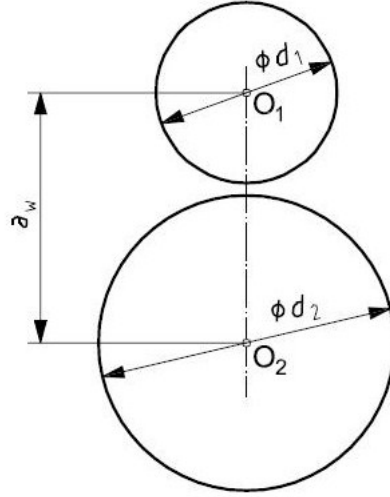


Figure 2.5: Center distance a_w . Source: [9]

Pressure angle

The working transverse pressure angle, α_{wt} , is that pressure angle whose vertex lies on the pitch circle (working pitch circle), and it can be seen in figure 2.6. If the backlash is zero results:

$$\alpha_{wt}^{-1} = \alpha_t^{-1} + \frac{2 \tan \alpha_n}{z_1 + z_2} (z_1 + z_2) \quad (2.8)$$

Tooth engagement refers to the meshing of a gear with its mating gear. The tooth engagement is influenced by the geometry of the gear pair, the mutual contact of the tooth flanks and the sliding conditions.

Plane of action, zone of action, contact line

The plane of action of a spur gear is tangent to the base cylinders. The intersection of two planes of action (one for each tooth flank) is parallel to the gear axes and is the pitch axis. The zones of action are the parts of the planes of action which are limited by the usable tip cylinders of the gear and mating gear and by the face-width and by the start of the involute. A zone of action is linked to the flank that is normal to it. Hence, one of the planes of action is linked to the right flanks and the other to the left flanks.

At any instant in time, the intersection of the zone of action with the corresponding tooth flanks of a gear pair is known as the contact line. With the

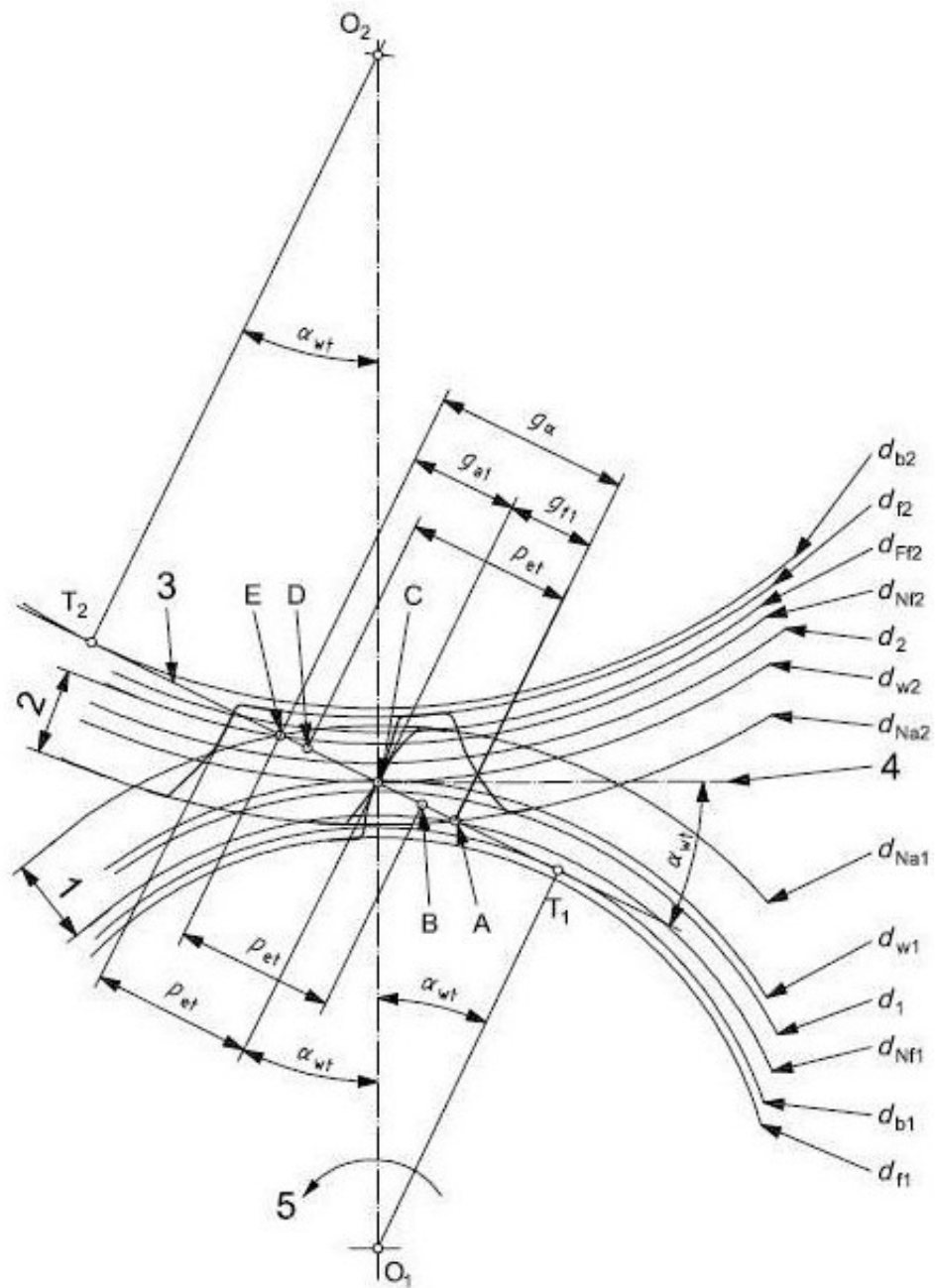


Figure 2.6: Gear pair meshing. 1. radial part of active flank gear 1 2. radial part of active flank gear 2 3. line of action 4. tangent to pitch circles 5. direction of rotation of driving pinion. Source: [9]

rotation of the gears around their axes, the contact lines move through the zone of action.

In figure 2.6 the significant diameters and segment of contact lines are shown for gear 1 and 2. d_b is the base diameter, d_f is the root diameter, d_{Ff} is the root form diameter, d_{Nf} is the start of active profile diameter, d is the reference diameter, d_w is the working pitch diameter, d_{Na} is the active tip diameter.

Line of action, path of contact, point of contact

Lines of action are where the planes of action intersect transverse sections. A line of action is inclined to the common tangent to the pitch circles at the pitch point (pitch circle tangent) by the working transverse pressure angle, α_{wt} and it contacts the two base circles at the points T_1 and T_2 .

A path of contact is that part of the line of action which is within the zone of action. The starting point, A, of the path of contact is at or near the tip circle of the driven gear. The finishing point, E, of the path of contact is at or near the tip circle of the driving gear.

The lines of action intersect the center line at pitch point C. Pitch point C is also the point at which the two lines of action intersect.

Length of the path of contact

In figure 2.6 the path of contact is shown, divided in different components, g_a and g_f , length of addendum and dedendum path of contact. The length g_α of the path of contact (length between points A and E) of two mating spur gears is given by:

$$g_\alpha = \frac{1}{2} [\sqrt{d_{Na}^2 - d_b^2} + \frac{z_2}{|z_2|} (\sqrt{d_{Na}^2 - d_b^2} - 2a_w \sin \alpha_{wt})] \quad (2.9)$$

Contact ratio

The contact ratio, ϵ (Figure 2.6) is the ratio of the path of contact to the normal base pitch:

$$\epsilon = \frac{g_\alpha}{p_e} \quad (2.10)$$

The total contact ratio defines how much a gear is engaged (path of contact) on an angular pitch. For the efficiency of the transmission is necessary a path of contact higher than the angular pitch. Usually in gear pairs design, values higher than $\epsilon = 1.2$ are used, maximum values do not go over $\epsilon = 2$ to keep always at least one tooth in contact. If a value of $\epsilon = 1.3$ is assumed, it means that one tooth stays in contact 1.3 times one angular pitch, and therefore two teeth are in contact at the same time for 0.3 times one angular pitch.

2.1.3 Transmission error

Theoretically, for two gears with perfect involute and an infinite stiffness, a constant rotation of the input shaft would result in a constant rotation of the output shaft.

Due to various factors these two rotations are never equal. This error in motion is called transmission error (TE), citing [36]: "transmission error is the difference between the angular position that the output shaft of a drive would occupy if the drive were perfect and the actual position of the output".

$$TE(t) = R_{b,p}\theta_p(t) + R_{b,g}\theta_g(t) \quad [mm] \quad (2.11)$$

where $R_{b,p}$ and $R_{b,g}$ are the base radius of the pinion and the gear, and θ_p and θ_g the rotations. The transmission error quantifies the gearbox's imperfections when transferring energy from input to output in a metric of the gearbox's efficiency. The higher the transmission error, the higher the risk of an amplified dynamic variation of the shaft's rotational speed or torque. This would imply an increasing in noise and vibration of the system.

The transmission error can be divided in two categories:

- **MTE**, Manufactured Transmission Error. In this category all the manufacturing error given by the construction of the gear are included. Furthermore all the errors coming from inaccuracy of the working condition are taken in account, for example the eccentricity of the shafts or the angular misalignment of the gears.
- **LTE**, Loaded Transmission Error. In this category there are all errors given by the torque applied on the gears. It's a component of error due to the stiffness of the whole gear but mostly of the tooth, therefore directly dependent on the geometry and micro geometry of the tooth.

In Figure 2.7 a generic TE measurement is shown and its two most clear sources are indicated. The eccentricity, which is a first order signal and the teeth passing component, whose orders are given by the number of teeth of the gears and its integer multiples. The graphics to represent the TE can have on the x-axis the rotation angle of one of the two shafts; if the gear pair has $u = 1$ the shaft angles are equals. From the literature, the teeth passing component of the TE should presents a square distribution. In figure 2.8 a theoretic TE is shown. For this thesis work graphics on teeth passing component of TE is very important and further discussion on it will be presented in next chapters.

Assuming for the actual gear pair $1 < \epsilon < 2$ (for higher values of ϵ refer to [36]), it has to be noticed that the contact ratio can be obtained by simple observations on the TE distribution. A square shape is the theoretical

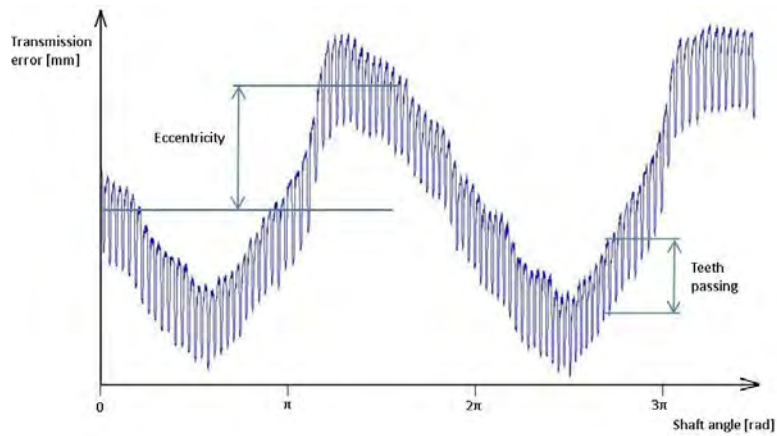


Figure 2.7: Different TE components

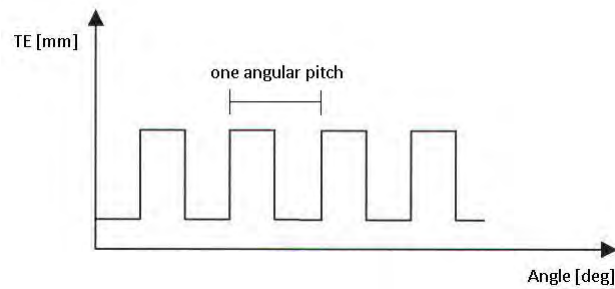


Figure 2.8: TE squared distribution

distribution expected for $\Delta\theta$ on a gear pair. The upper part of TE represents the section of an angular pitch in which the flexibility of the system is higher (higher angles difference) which means that only one tooth is in contact. The lower part, more rigid, is the one with two teeth in contact. Considering the length of these two segments along one angular pitch, the contact ratio ϵ can be obtained.

2.2 Technical data of implemented gears

This work presents a comparison of the numerical method with experimental measurements. This was achieved through an available gear test-rig and gear pair at Siemens Industry Software NV in Leuven (Belgium). Further details of the test-rig are presented in the following chapters.

In this section the gears used for the comparison are shown and the mainly geometrical parameters are calculated.

2.2.1 Test gears

The gear pair consists of two identical spur gears with the technical draw presented in figure 2.9. Gear quality is 3, according to ISO 1328. The main features are:

- Material 16MnCr5
- Heat treatment, case hardening
- Surface hardness after grind, 60 HRc

Gear tooth modifications

Special focus has to be taken on the modification of tooth profile. There are various way to modify gears and every type of modification leads to different working results, with a different TE shape obtained.

Here some of most common methods are briefly introduced, using [10] as main reference.

Tooth Profile Modification: it generally means removing material in a transverse plane and uniformly across the face width. It enables the tooth to avoid interfering with the mating gear.

Crowning and End Relief: crowing means making the tooth surface slightly convex in the direction the face width, while end relief is the chamfering of both ends of tooth surface.

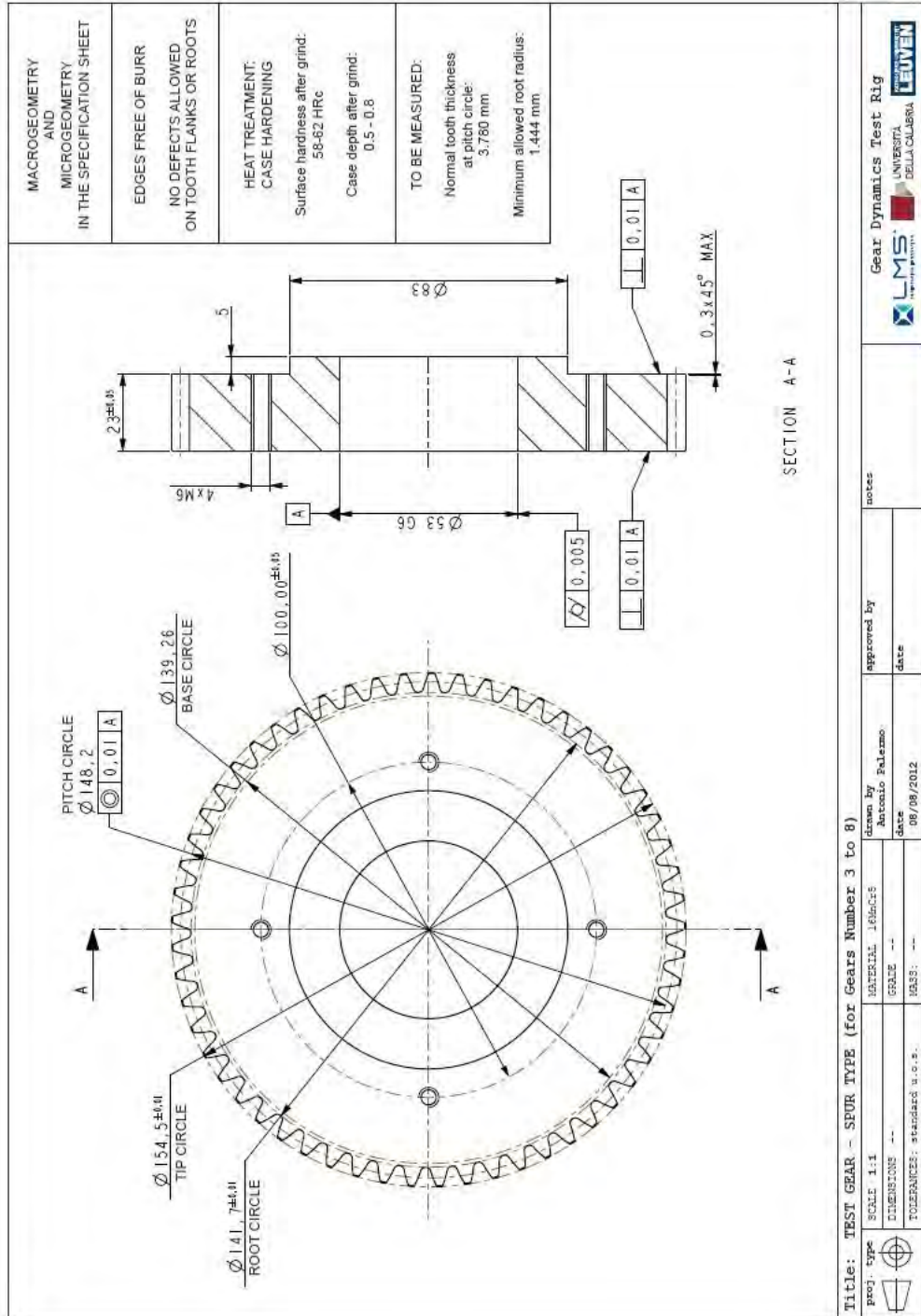
Topping and Semitopping: the top or tip diameter is cut simultaneously with the generation of the teeth, while the semitopping is the chamfering of the tooth's top corner.

The adopted gears do not present modifications of the micro-geometry, so the shape of the TE of the gear pair is expected to show sudden variations, as stated in the previous section.

2.2.2 Test gear pair parameters

The geometrical parameters of the gear pair are reported in table 2.2. The values of module and the reference pressure angle are given by the basic rack profile adopted whereas the center distance is chosen.

Values are expressed in millimetres and degrees.



Title: TEST GEAR - SPUR TYPE (for Gears Number 3 to 8)		drawn by	Antonio Palermo	approved by		notes
proj. type	SCALE 1:1	MATERIAL	16AlCr5	date		
DIMENSIONS	--	SCALE	--	date		
TOLERANCES	standard u.o.s.	MASS	--	date		



Figure 2.9: Test gear, Technical draw

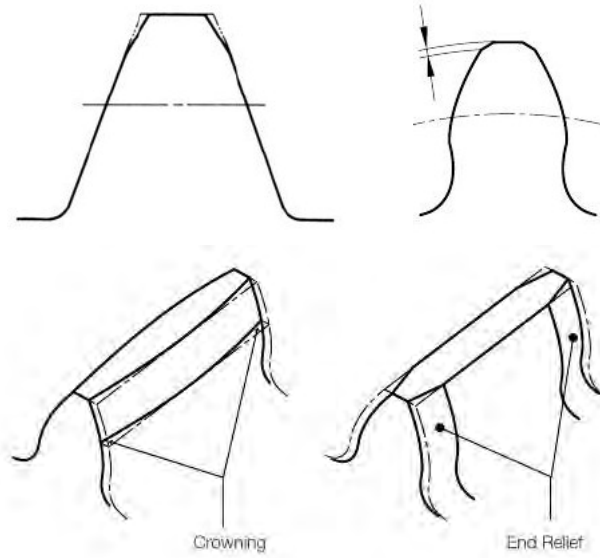


Figure 2.10: Profile modification, topping, crowning and end relief. Source: [10]

Item	Symbol	Value
Module	m	2.6
Reference pressure angle	α	20
Number of teeth	z	57
Center distance	a	150
Profile shift coefficient	x	-0.160
Reference diameter	d	148.2
Base diameter	d_b	139.262
Working pitch diameter	d_w	150
Tip diameter	d_a	154.50
Root diameter	d_f	141.70
Tooth thickness	\widehat{s}	3.780
Nominal contact ratio	ϵ	1.45

Table 2.2: Technical data of the gear pair

2.3 Chapter's remarks

In this chapter the main concepts on a single gear and gear pair have been discussed. Only some parameters concerning gears are needed in this work and main formulas have been presented to allow the calculation of them. The transmission error will be the most important element along this thesis work. It will be used as the main parameter of comparison for testing code features and the main result for experimental tests and numerical solutions. In the last part of the chapter the available gear pair at Siemens Testing and Simulation Division were discussed in terms of main features and technical data.

Chapter 3

Non-linear Parametric Model Order Reduction Technique for Gear Simulations

3.1 Review of model reduction techniques in dynamic contact analysis

Contact problems in multibody dynamics are characterized by variations in location and size of the contact area. If a flexible body is modelled using finite elements, there is a multitude of possibly loaded degrees of freedom which in a gear pair are the degrees of freedom at the teeth flanks.

Furthermore contact problems generally need highly refined meshes to correctly identify stress gradients in relatively small volumes of stressed material.

These considerations lead to a:

- Very non-linear problem due to multibody formulation, flexibility problem and contact problem
- High number of degrees of freedom

Therefore to perform a gear pair simulation a Model Order Reduction (MOR) scheme is required to reduce the computational effort.

At the KU Leuven in the department of Mechanical Engineering the PMA research group (Production, Manufacturing, Automation) is working on the solution of mechanical systems using MOR techniques. Recently a novel flex-to-flex gear contact method using MOR was developed and the objective of this new method is to solve systems characterized by problems types proposed above [5][7]. Consequently a novel computational code named MUTANT (MULTibody Transient ANALysis of Transmissions) for the simulation

of gear transmission systems was built, based on the theoretical concepts expressed by this new approach. The developing of the method and the code was entirely done at PMA group of KU Leuven.

The code is currently at its early stage but it has already been validated against other commercial simulation software in [7], leading to very promising results in terms of accuracy of the solution and computational speed.

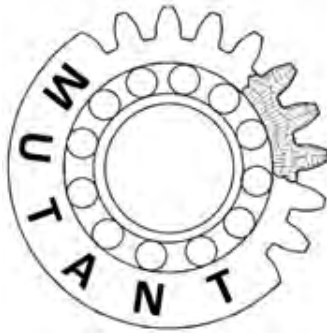


Figure 3.1: MUTANT code logo

In this section there is a review of model order reduction techniques, which heads afterwards to the definition of the novel method applied to gear transmission systems.

3.1.1 Time-domain CMS methods employing real modes

In this part MOR techniques, belonging to the class of projection-based methods, are considered.

These methods approximate the state vector in a basis of reduced dimension and project the governing equations of the system onto a dimensionally reduced subspace.

Component Mode Synthesis (CMS) is a MOR scheme frequently used in structural dynamics.

According to [1], CMS techniques should have the following characteristics:

- Accuracy and efficiency: the method should produce accurate system predictions while minimizing computer memory requirements and execution time.
- Component independence: the component data for one component should be independent of the data from other components.
- Synthesis generality: the synthesis procedure should be general, there shouldn't be limitations on the component modes choice.

- Static solution capability: pseudo-static solutions should be obtainable using the CMS coupled model.

From a not damped FE model of a generic mechanical system one obtains:

$$\mathbf{m}\ddot{\mathbf{x}} + \mathbf{k}\mathbf{x} = \mathbf{f} \quad (3.1)$$

\mathbf{x} is the vector of the n degrees of freedom (DOF) of the structure. A CMS method attempts to reduce the number of DOF introducing an approximation in the solution. In [1], Craig proposed a particular CMS method, below the basis of this CMS mode sets are introduced, considering only real component modes. Here this reduction strategy is presented.

Through the transformation matrix ϕ the physical coordinates \mathbf{x} are expressed in terms of the generalized coordinates \mathbf{q} :

$$\mathbf{x} = \phi\mathbf{q} \quad (x_1 x_2 \dots x_n)^T = \begin{bmatrix} \phi_{11} & \dots & \phi_{1nr} \\ \vdots & \ddots & \vdots \\ \phi_{n1} & \dots & \phi_{nnr} \end{bmatrix} (q_1 q_2 \dots q_{nr})^T \quad (3.2)$$

The transformation matrix consists of preselected component modes of the following types: dynamic eigenvectors and static shape vectors.

Dynamic eigenvectors are the normal modes of the system and are obtained by solving the following eigenproblem:

$$(\mathbf{k} - \omega_q^2 \mathbf{m})\Phi_q = \mathbf{0} \quad (3.3)$$

Whereas the static shape vectors (also called attachment modes) are calculated as the static displacement vector resulting from an imposed unit displacement on one coordinate of a set of physical coordinates. In the specific case of gear models, the static shapes vectors (or attachment modes) are computed for all the DOF on the external surfaces of teeth that have to undergo contact forces.

$$\mathbf{k}\mathbf{x} = \mathbf{f}_i = \{00 \dots 010 \dots 0\}^T \quad (3.4)$$

A static shape vector for each DOF involved in the contact is obtained.

Normal modes are needed to take into account the global deformations of the component, whereas the static shape vectors allow the solution to include local deformations. These two types of deformation are clearly evident in a mechanical system such as gears where static modes can reproduce teeth deformation.

To calculate attachment modes the system is solved for every possible contact element of one tooth, along flank and root fillet elements and along the width direction of the gear. Consequently, through the symmetry of the body, all attachment modes sets are obtained performing a rotation of every

vector around the gear axis.

First three static vectors are shown in figure 3.2. The component mode syn-

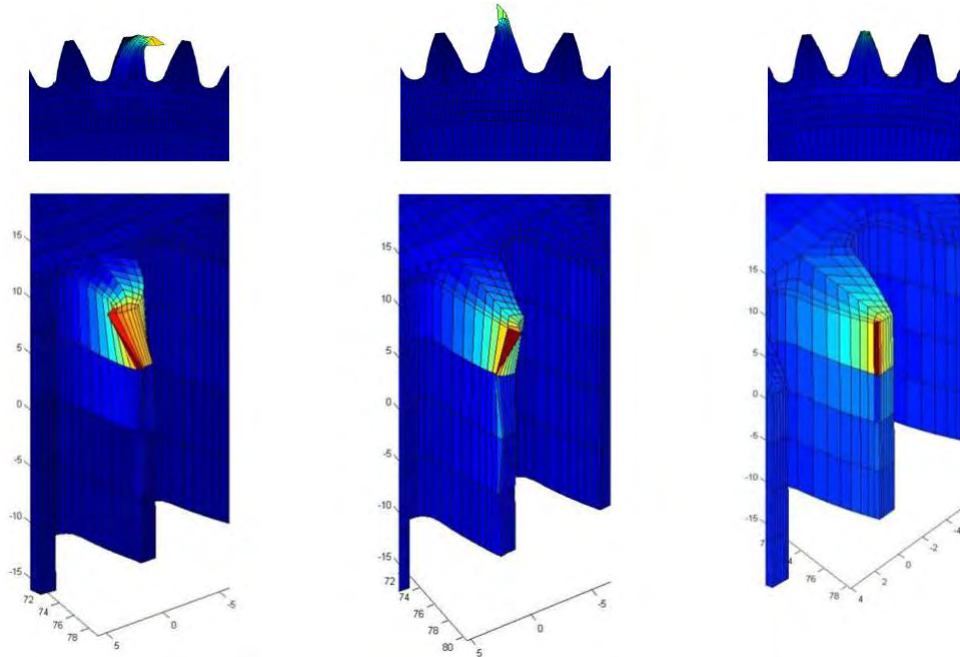


Figure 3.2: First, second and third attachment modes (first contact element)

thesis presented by Craig retains only the eigenvectors and augments these with constraint modes to obtain a well defined global and local solution.

3.1.2 Static modes switching method

A static shape vector for each degree of freedom that can possibly be loaded during the simulation must be added to the reduction basis. Consequently, as in gear pairs a very fine mesh is required to obtain results convergence, the precedent MOR technique brings to a reduced model having several hundreds or even thousands degrees of freedom which leads to a computational effort still too high.

This dependence between the number of DOF and the reduction basis was partly avoided, with a statically complete and computationally tractable procedure for dynamics contact problem by the Static Modes Switching (SMS) method [2] which was applied to the gear contact problem in [3]. Based on the observation that at each time step of the simulation only few out of many boundary DOF will be loaded simultaneously, SMS makes use of a discontinuously changing basis matrix of minimal dimensions, contain-

ing only those static shape vectors that contribute to the solution in that very instant of the simulation.

To yield valuable results, the approach should be combined with time integration schemes that present high-frequency numerical damping in order to soften the influence of discontinuities that result from removing and adding static shape vectors from the basis matrix.

The SMS approach yields a reduced-order models having significantly less degrees of freedom as compared to CMS-based ROM, but its efficiency remains sensitive to the FE refinement because the smaller the elements, the higher the number of degrees of freedom involved in the contact analysis and the higher the number of static shape vectors that has to be included in the basis matrix. Furthermore the efficiency decreases as the number of simultaneous contact zones (e.g. the number of teeth in contact) increases.

3.1.3 Parametric and non linear model order reduction

The dynamic simulation of a gear pair is characterized by contact forces moving along flanks of interacting teeth. When modelling these systems, the idea of parametrization of the location of contact zones in the full-order model rises. It is important to keep control of reduced-order model and to do this the introduced parameter dependency should be preserved along the reduction process. The latter is the goal of Parametric Model Order Reduction (PMOR).

Parametric model reduction is a technique which generates reduced models that approximate the original full-order model through a range of parameters. These parameters can be introduced in the model in several ways, representing, for example, material parameters, component geometry, system configuration, or boundary conditions.

In this system the applied parameter is the angular rotation of the gears which directly defines the contact load location and then the reduction strategy. It can be seen afterwards that the present case is a different parametric dependence, in the sense that the system matrices of the full-order models (i.e. the mass, damping and stiffness matrices in structural dynamics) are parameter independent, whereas the reduced-order matrices become parameter-dependent only after the process of model reduction.

The interpolation of locally reduced models has also been investigated in the field of non-linear model order reduction (NLMOR) [33]. Here, the local ROMs are typically obtained through linear interpolation of the full-order model at discrete points along a reference trajectory [4].

Parametric and non-linear model reduction techniques have the potential of reducing the dimensions of large-scale dynamic contact problems considerably further than classical MOR techniques. The accurate simulation of a

gear pair can be achieved through this reduction strategy with a reasonable computational effort. The main challenges with this procedure are the correct interpolation between local reduced models and the system dynamic behaviour along the parameter variation.

3.2 Definition of the parametric basis matrix

The PMA research group of the Department of Mechanical Engineering developed this novel gear contact method using MOR technique to perform numerical simulations on gear transmission systems. A gear transmission system fully presents the problem types listed in the first part of this chapter.

- High problem non-linearity
- High number of degrees of freedom

Therefore the application of this new method on this mechanical system is highly suitable.

In this section and in the following ones, the main mathematical and numerical concepts of this new solution strategy are introduced to better understand the global working approach of the method.

In typical gear contact problems, the number n of nodal degrees of freedom in gears finite element models is $n \approx 10^5 \div 10^6$.

In order to reduce the computational effort associated with these large-scale FEM, the vector of nodal displacements of the i -th gear is approximated in a basis of reduced dimension \mathbf{V}_i . The basis matrix \mathbf{V}_i consists of a constant set $\Phi^i \in R^{n \times n_k}$ of n_k eigenvectors augmented with a parameter-dependent set $\Psi^i \in R^{n \times n_t}$ of n_t static shape vectors, i.e. $\mathbf{V}_i = [\Phi^i \Psi^i]$. The vector of generalized elastic coordinates $\boldsymbol{\eta}_i$ is partitioned accordingly as $\boldsymbol{\eta}_i^{iT} = [\boldsymbol{\eta}_k^{iT} \boldsymbol{\eta}_t^{iT}]$ where $\boldsymbol{\eta}_k^i \in R^{n_k \times 1}$, $\boldsymbol{\eta}_t^i \in R^{n_t \times 1}$ and $n_k + n_t = n_\eta$. The static shape vectors in Ψ^i are obtained by interpolating among a set of global contact shapes.

3.2.1 Computation of the global contact shapes

A global contact shape is defined as the deformation pattern of a gear obtained from a static contact analysis of the gear pair, locked at a certain configuration and submitted to defined external forces. The driven gear is held fixed at a certain angular position θ_2 and the angle of the driving gear θ_1 is adjusted in order to have the two gears coming into contact. An external torque T_1 is applied to the driving gear and the following system of non-linear equations is solved for $\theta_1, \mathbf{u}_f^1, \mathbf{u}_f^2$:

$$\begin{bmatrix} 0 & \mathbf{0} & \mathbf{0} \\ \mathbf{0} & \mathbf{K}_{FE}^1 & \mathbf{0} \\ \mathbf{0} & \mathbf{0} & \mathbf{K}_{FE}^2 \end{bmatrix} \begin{Bmatrix} \theta_1 \\ \mathbf{u}_f^1 \\ \mathbf{u}_f^2 \end{Bmatrix} = \begin{Bmatrix} T_1 \\ \mathbf{0} \\ \mathbf{0} \end{Bmatrix} + \mathbf{Q}_c \quad (3.5)$$

Where \mathbf{K}_{FE}^1 and \mathbf{K}_{FE}^2 are the gears FE stiffness matrices and \mathbf{Q}_c is the vector of generalized contact forces. The solution vectors \mathbf{u}_f^1 and \mathbf{u}_f^2 represent the deformation patterns of the respective gears at static equilibrium. These vectors are referred to as the global contact shapes of the gear pair at the configuration (θ_1) while undergo the external torques $(T_1, T_2 = u \cdot T_1)$, where u is the transmission ratio of the gear pair (Figures 3.3 and 3.4). The global contact shapes are used to construct the set of static shape vectors Ψ^i .

In order to obtain static (matrix \mathbf{K}_{FE}) and dynamic (matrix \mathbf{M}_{FE}) decoupling between the coordinates corresponding to Ψ^i and Φ^i , the global contact shapes obtained from the precedent system are made residual with respect to the columns of Φ^i . The goal of this procedure is to yield mass and stiffness diagonal matrices. This objective is due to the fact that the solution of a system presenting diagonal matrices, is computationally faster [34].

The starting reduction space of the MOR scheme is $[\Phi, \Psi]$. The following approach is implemented to obtain the residual global contact shapes, referring to [5]. A set of kept eigenvectors Φ and a single global contact shape \mathbf{S} are the inputs, forming the matrix $\mathbf{V} = [\Phi, \mathbf{S}]$ and the matrices $\tilde{\mathbf{M}}$ and $\tilde{\mathbf{K}}$:

$$\tilde{\mathbf{M}} = \mathbf{V}^T \mathbf{M}_{FE} \mathbf{V} \quad \tilde{\mathbf{K}} = \mathbf{V}^T \mathbf{K}_{FE} \mathbf{V} \quad (3.6)$$

These matrices can always be written in a full symmetric structure through an arbitrary set of shape vectors. A generalized eigenvalue problem for the pencil $(\tilde{\mathbf{K}}, \tilde{\mathbf{M}})$ can be solved:

$$\tilde{\mathbf{K}} \phi - \omega^2 \tilde{\mathbf{M}} \phi = \mathbf{0} \quad (3.7)$$

Where ω^2 is the eigenvalues vector and ϕ is the eigenvector of the reduced system. A new set of reduced matrices is obtained:

$$\begin{aligned} \tilde{\mathbf{M}}^{ortho} &= [\phi_1^T, \phi_2^T \dots \phi_{n_k}^T] \tilde{\mathbf{M}} [\phi_1, \phi_2 \dots \phi_{n_k}] \\ \tilde{\mathbf{K}}^{ortho} &= [\phi_1^T, \phi_2^T \dots \phi_{n_k}^T] \tilde{\mathbf{K}} [\phi_1, \phi_2 \dots \phi_{n_k}] \end{aligned} \quad (3.8)$$

Through the solution of the eigenvalue problem two diagonal matrices are obtained. By mass-orthonormalization of $[\phi_1, \phi_2 \dots \phi_{n_k}]$, the reduced mass matrix $\tilde{\mathbf{M}}^{ortho}$ becomes the identity matrix and $\tilde{\mathbf{K}}^{ortho}$ is the orthogonalized diagonal reduced stiffness matrix.

The obtained reduction space $[\Phi, \tilde{\Psi}]$ has the same dimensions as the starting one. Only a change of basis is performed and the final mass and stiffness matrices present the following block diagonal form with the set of global shapes vectors independent with respect to the kept normal modes

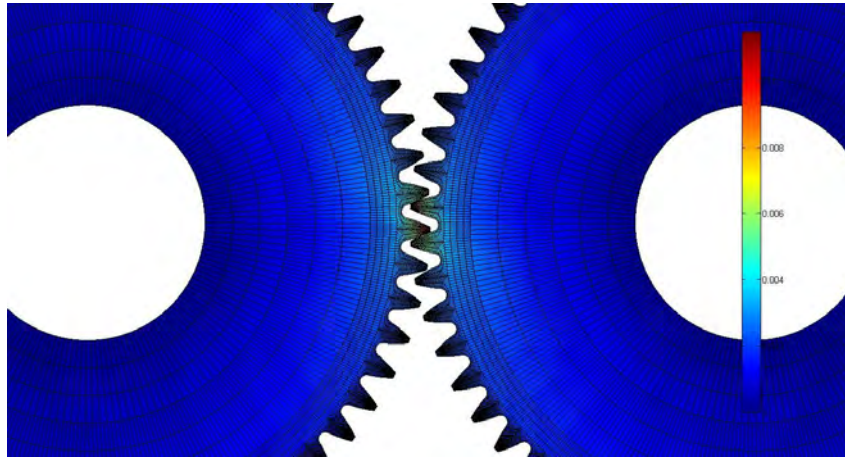


Figure 3.3: Two Static solutions of the precedent system, two and one teeth in contact (Displacement)

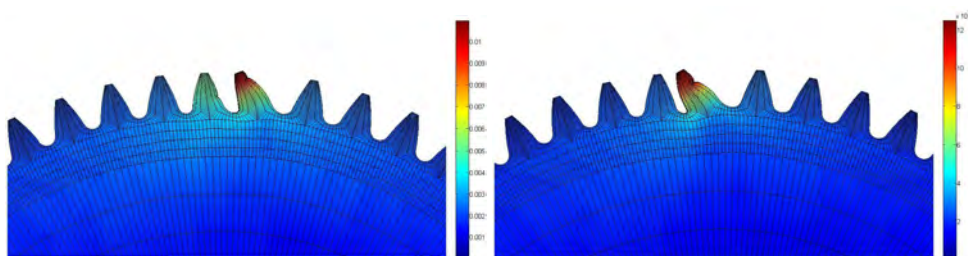


Figure 3.4: Two global contact shapes of driving gear, two and one teeth in contact (Scaled displacement)

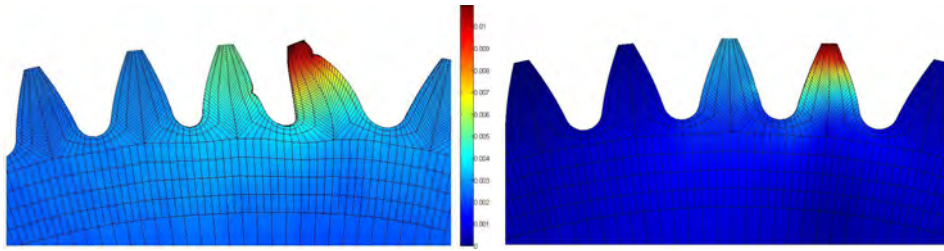


Figure 3.5: Unresidualized and residualized shape, driving gear, two teeth in contact

vectors:

$$\begin{bmatrix} * & & & & & & & \\ & * & & & & & & \\ & & * & & & & & \\ & & & * & * & * & * & \\ & & & * & * & * & * & \\ & & & * & * & * & * & \\ & & & * & * & * & * & \end{bmatrix}$$

3.2.2 Interpolation of the global contact shapes

The calculated set of global contact shapes is not directly adopted as reduction space. Equation 3.5 can be solved for different values of torque, accordingly to the required working conditions of the simulation. This brings to a number of global contact shapes sets equal to the number of adopted torque values in the solution of equation 3.5. Only a few of these global contact shapes, depending on the number of different torques implemented, are inserted in the final reduction space. These are obtained by interpolating among the $\tilde{\Psi}$ set of global contact shapes, based on the current configuration of the gear pair.

This set has been constructed in the last section by solving the static contact problem for n_θ different gear pair configurations between the initial and final positions of the simulation, therefore in one angular pitch. At each particular configuration n_t different torques are applied to the driving gear, forming a set of $n_s = n_\theta \times n_t$ global contact shapes.

The relation between the torque applied and the nodal displacement of the structure is not linear and to obtain an accurate solution with different applied torque values a set of torque values should be used in the preprocessing phase to evaluate the global contact shapes. Doing this, different applied torques in the static preprocessing phase allow to build a model which can be used correctly for different torque values in the next processing phase.

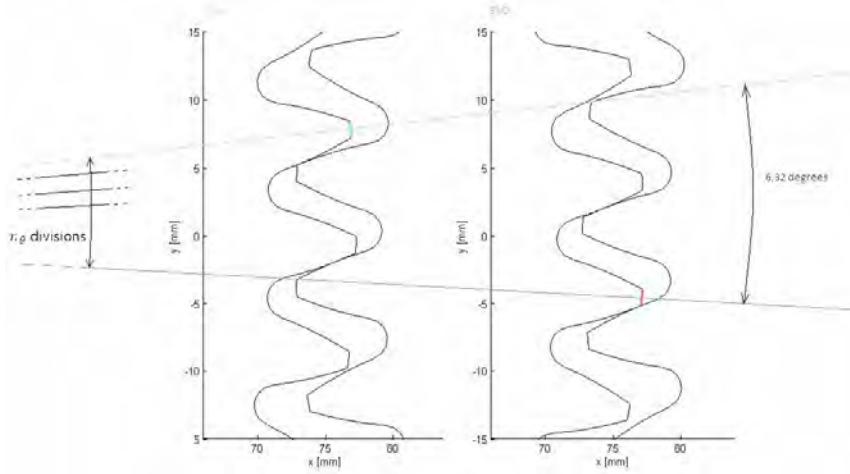


Figure 3.6: $n_\theta + 1$ global contact shapes calculated for an angular pitch

In this work a maximum value of $n_t = 2$ was chosen. An interpolation with respect to the applied torque is possible but is not performed in this method. Consequently the final basis matrix will be composed by the kept normal modes vectors plus the torque related shapes. A suitable set of participation factors is automatically obtained in the solution of the reduced system to take into account the different influence of every torque shape. If only one torque value needs to be used in the processing phase, the participation factors yield to a solution where only the first torque related shape participate in the solution.

Possible choices of interpolation are polynomial or spline interpolation of arbitrary order. Higher orders of interpolation functions bring to higher complexity of the system matrices. The choice of an interpolation scheme must be done taking into account accuracy of the solution, complexity of the system and number of discrete points to be used. Furthermore, care should be taken when there are discontinuities in the solution, since their representation is highly dependent on the adopted interpolation scheme. In the case of a gear pair, we have clear discontinuities in the evolution of the simulation, given by the entrance and leaving of contact of a teeth pair, as better discussed in the next chapter. In this work, a linear interpolation scheme is used to construct the static shape vectors in the MOR phase. This choice enables an efficient evaluation of the equations of motion and on the other side needs a larger number of global contact shapes to be calculated to obtain better solution representations on the discontinuities zones.

Global contact shapes at angle $\theta^i = \theta_s^i$ are defined by \mathbf{S}_s^i and the ones at angle $\theta^i = \theta_{s+1}^i$ by \mathbf{S}_{s+1}^i . Consequently the matrix of static shape vec-

tors can be called Ψ^i at an intermediate angle θ^i using the following linear interpolation formula:

$$\Psi^i = (1 - p)\mathbf{S}_s^i + p\mathbf{S}_{s+1}^i \in R^{n \times n_t} \quad (3.9)$$

Where p is a parameter depending only on the angular position θ^i of the gear through the following relation:

$$p = (\theta^i - \theta_s^i)/(\theta_{s+1}^i - \theta_s^i) = (\theta^i - \theta_s^i)/(\Delta\theta^i) \quad 0 < p < 1 \quad (3.10)$$

Where $\Delta\theta^i$ is the angular increment in the angular range considered. Due to the performed parametrization, Ψ^i , and therefore \mathbf{V}^i , continuously varies in time, and their variability must be analysed to observe influences on the dynamic simulation. To do this their first and second derivatives with respect to time were calculated:

$$\dot{\Psi}^i = \frac{\delta\Psi^i}{\delta\theta^i}\dot{\theta}^i = \Psi_{\theta}^i\dot{\theta}^i \quad (3.11)$$

$$\ddot{\Psi}^i = \frac{\delta^2\Psi^i}{\delta\theta^{i2}}\dot{\theta}^{i2} + \frac{\delta\Psi^i}{\delta\theta^i}\ddot{\theta}^i = \Psi_{\theta\theta}^i\dot{\theta}^{i2} + \Psi_{\theta}^i\ddot{\theta}^i \quad (3.12)$$

Assuming a linear interpolation scheme, the last equation becomes $\ddot{\Psi}^i = \Psi_{\theta}^i\ddot{\theta}^i$. Substituting $\Psi^i = f(p)$ one obtains:

$$\dot{\Psi}^i = \Psi_{\theta}^i\dot{\theta}^i = \dot{\theta}^i(\mathbf{S}_{s+1}^i - \mathbf{S}_s^i)(\Delta\theta^i)^{-1} \quad (3.13)$$

$$\ddot{\Psi}^i = \Psi_{\theta}^i\ddot{\theta}^i = \ddot{\theta}^i(\mathbf{S}_{s+1}^i - \mathbf{S}_s^i)(\Delta\theta^i)^{-1} \quad (3.14)$$

It has to be taken into consideration the fact that differences between two consecutive global shapes strictly depends on the chosen angular increment $\Delta\theta^i$. Higher values of $\Delta\theta^i$ yield to less global shapes along one angular pitch, but more different each other. Finally the reduction matrix \mathbf{V}^i is composed of a constant set of eigenvectors Φ^i and a configuration-dependent set of interpolated global contact shapes $\Psi^i(\theta^i)$:

$$\mathbf{V}^i(\theta^i) = [\Phi^i \quad \Psi^i(\theta^i)] = [\Phi^i \quad (1 - p(\theta^i))\mathbf{S}_s^i + p(\theta^i)\mathbf{S}_{s+1}^i] \quad (3.15)$$

It's important to notice that its first and second derivatives are non-zero:

$$\dot{\mathbf{V}}^i(\theta^i) = \mathbf{V}^i(\dot{\theta}^i) = \dot{\theta}[\Phi_{\theta}^i \quad \Psi_{\theta}^i] = \dot{\theta}[0 \quad (\mathbf{S}_{s+1}^i - \mathbf{S}_s^i)(\Delta\theta^i)^{-1}] \quad (3.16)$$

$$\ddot{\mathbf{V}}^i(\theta^i) = \mathbf{V}^i(\ddot{\theta}^i) = \ddot{\theta}[\Phi_{\theta}^i \quad \Psi_{\theta}^i] = \ddot{\theta}[0 \quad (\mathbf{S}_{s+1}^i - \mathbf{S}_s^i)(\Delta\theta^i)^{-1}] \quad (3.17)$$

Note that the number of basis vectors in \mathbf{V}^i only depends on the number of kept eigenvectors and on the number of torques, not on the dimensions of the FEM of the gear. This is one of the main advantages of the method, which allows highly-refined mesh system to be solved in a reasonable amount of time.

3.3 Derivation of the equations of motion

In this section, the equations of motion of a pair of flexible gears are obtained. The gears are kept fixed on their axes of rotation without angular misalignments. The energetic formulation (Lagrange's procedure) is used. Gears are represented by FEM whose vectors of nodal displacements are approximated in a basis of reduced dimension according to Eq. 1.2, with the basis matrix as defined in Eq. 1.15. FEM are composed of lumped-mass solid elements having three translational degrees of freedom per node.

3.3.1 Floating frame of reference formulation

The dynamic formulation of the equations of motion of the two deformable gears that undergo large translational and rotational displacements are developed using the floating frame of reference formulation (FFR). This approach is widely presented by [6], here the basic concepts are illustrated.

In the floating frame of reference formulation, the configuration of each deformable body (two gears) in the multibody system is identified by using two sets of coordinates:

- Reference coordinates: define the location and orientation of the selected body reference.
- Elastic coordinates: describe the body deformation with respect to the body reference.

The global position of an arbitrary point on the deformable body is thus defined by using a coupled set of reference and elastic coordinates.

A global fixed coordinate system is chosen to define the connectivity between the different bodies in the multibody system. For an arbitrary body in the system, body i , a body reference $\mathbf{X}_1^i \mathbf{X}_2^i \mathbf{X}_3^i$ is selected, whose location and orientation w.r.t. the global coordinate system are defined by a set of reference coordinates, $\mathbf{q}_r^i = [\mathbf{R}^{iT} \quad \boldsymbol{\theta}^{iT}]^T$. R^i is the set of Cartesian coordinates, whereas $\boldsymbol{\theta}^i$ is the rotational one.

The body coordinate system $\mathbf{X}_1^i \mathbf{X}_2^i \mathbf{X}_3^i$ is the floating frame of reference, it can be chosen wherever but it has not to be rigid motion between the system and its body. The FFR approach separates the complete motion of a flexible body into the non linear motion of the body's reference, which is a rigid motion (rotation of the gear along its axis), and the linear elastic deformation of the body with respect to this reference (deformation of the gear). The last can be described using linear FE theory, allowing to apply MOR techniques to reduce the dimensions of the model.

The global position \mathbf{r}^{ij} of the j -th node of the i -th gear can be expressed as:

$$\mathbf{r}^{ij} = \mathbf{R}^i + \mathbf{A} \mathbf{u}^{ij} = \mathbf{R}^i + \mathbf{A}^i (\mathbf{u}_o^{ij} + \mathbf{u}_f^{ij}) \quad (3.18)$$

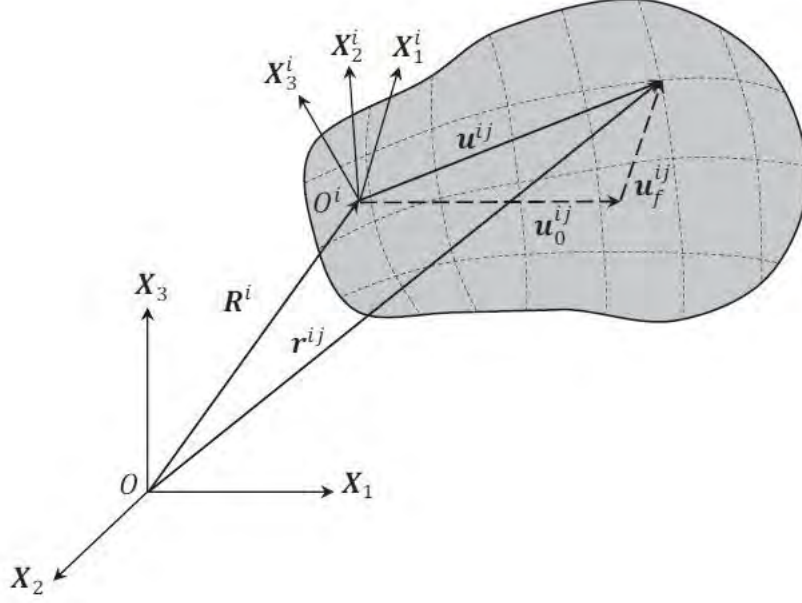


Figure 3.7: Flexible body reference systems and coordinates. Source: [7]

where \mathbf{u}_o^{ij} and \mathbf{u}_f^{ij} represent, respectively, the deformed and undeformed positions of node ij w.r.t. the local reference $\mathbf{X}_1^i \mathbf{X}_2^i \mathbf{X}_3^i$, and \mathbf{A}^i is the transformation matrix of the gear, which defines the orientation of the local reference w.r.t. the global reference $\mathbf{X}_1 \mathbf{X}_2 \mathbf{X}_3$. As the gears only rotate around the global axis \mathbf{X}_3 , the transformation matrix is:

$$\mathbf{A}^i = \begin{bmatrix} \cos \theta & -\sin \theta & 0 \\ \sin \theta & \cos \theta & 0 \\ 0 & 0 & 1 \end{bmatrix}^i \quad \dot{\mathbf{A}}^i = \dot{\theta}^i \begin{bmatrix} -\sin \theta & -\cos \theta & 0 \\ \cos \theta & -\sin \theta & 0 \\ 0 & 0 & 1 \end{bmatrix}^i = \dot{\theta}^i \mathbf{B}^i \quad (3.19)$$

Then the reduced-order model of the i -th gear can be obtained by approximating the vector of nodal displacements \mathbf{u}_f^i with the \mathbf{V}^i basis.

$$\mathbf{r}^{ij} = \mathbf{R}^i + \mathbf{A}^i(\mathbf{u}_o^{ij} + \mathbf{u}_f^{ij}) \approx \mathbf{R}^i + \mathbf{A}^i(\mathbf{u}_o^{ij} + \mathbf{V}^{ij} \boldsymbol{\eta}^i) \quad (3.20)$$

where $\boldsymbol{\eta}^i$ is the corresponding vector of generalized elastic coordinates.

3.3.2 Kinetic and potential energy of the flexible gear

The Lagrange's formulation needs the calculation of kinetic and potential energy of the gears.

Kinetic energy

The kinetic energy of the gear needs the calculation of the velocity for all the nodal point masses in the FE model. A general ij node presents the velocity:

$$\dot{\mathbf{r}}^{ij} = \dot{\theta}^i \mathbf{B}^i \mathbf{u}^{ij} + \mathbf{A}^i \mathbf{V}^{ij} \dot{\boldsymbol{\eta}}^i + \mathbf{A}^i \dot{\mathbf{V}}^{ij} \boldsymbol{\eta}^i \quad (3.21)$$

where $\dot{\mathbf{u}}_o^i = 0$ and $\dot{\mathbf{R}}^i = 0$, due to the fixed reference system of both gears and to the assumption that the centres of the gears are blocked in the space. The basis \mathbf{V}^i depends on the current interpolated global shape, therefore it can be made explicit w.r.t. θ^i and derive with respect to time as $\dot{\mathbf{V}}^i = \mathbf{V}_\theta^i \dot{\theta}^i$. Consequently:

$$\dot{\mathbf{r}}^{ij} = [\mathbf{B}^i \mathbf{u}^{ij} + \mathbf{A}^i \mathbf{V}_\theta^i \boldsymbol{\eta}^i \quad \mathbf{A}^i \mathbf{V}^i] \begin{bmatrix} \dot{\theta}^i \\ \dot{\boldsymbol{\eta}}^i \end{bmatrix} = \mathbf{L}_v^i \dot{\mathbf{q}}^i \quad (3.22)$$

where the vector of generalized coordinates of the i -th gear is defined as $\mathbf{q}^{iT} = \{\theta^i \boldsymbol{\eta}^{iT}\} \in R^{1 \times n_q}$. The kinetic energy T^i of the gear is obtained summing the kinetic energy of every node:

$$T^i = \sum_{j=1}^{n_n} T^{ij} = \sum_{j=1}^{n_n} \left[\frac{1}{2} \mathbf{r}^{ijT} m^{ij} \dot{\mathbf{r}}^{ij} \right] \quad (3.23)$$

n_n is the number of nodes in the FEM of the gear and T^{ij} and m^{ij} are the kinetic energy and lumped mass of ij -th node. Substituting $\dot{\mathbf{r}}^{ij}$:

$$T^i = \frac{1}{2} \sum_{j=1}^{n_n} [(\mathbf{L}_v^{ij} \dot{\mathbf{q}}^i)^T m^{ij} (\mathbf{L}_v^{ij} \dot{\mathbf{q}}^i)] = \frac{1}{2} \dot{\mathbf{q}}^{iT} \mathbf{M}^i \dot{\mathbf{q}}^i \quad (3.24)$$

Potential energy

The potential energy U^i has the form:

$$U^i = \frac{1}{2} \boldsymbol{\eta}^{iT} \mathbf{K}_{\eta\eta}^i \boldsymbol{\eta}^i \quad (3.25)$$

where $\mathbf{K}_{\eta\eta}^i$ is obtained through the reduction $\mathbf{K}_{\eta\eta}^i = \mathbf{V}^{iT} \mathbf{K}_{FE}^i \mathbf{V}^i$. The orthogonality between $\boldsymbol{\Phi}^i$ and $\boldsymbol{\Psi}^i$ allows to write the reduced stiffness matrix as:

$$\mathbf{K}_{\eta\eta}^i = \begin{bmatrix} \boldsymbol{\Phi}^{iT} \\ \boldsymbol{\Psi}^{iT} \end{bmatrix} \mathbf{K}_{FE}^i \begin{bmatrix} \boldsymbol{\Phi}^i & \boldsymbol{\Psi}^i \end{bmatrix} = \begin{bmatrix} \boldsymbol{\Phi}^{iT} \mathbf{K}_{FE}^i \boldsymbol{\Phi}^i & 0 \\ 0 & \boldsymbol{\Psi}^{iT} \mathbf{K}_{FE}^i \boldsymbol{\Psi}^i \end{bmatrix} \quad (3.26)$$

As seen in the computation of the global contact shapes, $\boldsymbol{\Phi}^i$ is composed of mass-orthonormalized eigenvectors, therefore the first sub-matrix in the above equation is a diagonal matrix whose diagonal entries are the squares

of the natural frequencies of the eigenvectors in Φ^i . The second sub-matrix can be expressed with respect to the parameter p :

$$\begin{aligned}\Psi^{iT} \mathbf{K}_{FE}^i \Psi^i &= [(1-p)\mathbf{S}_s^i + p\mathbf{S}_{s+1}^i]^T \mathbf{K}_{FE}^i [(1-p)\mathbf{S}_s^i + p\mathbf{S}_{s+1}^i] \\ &= (1-p)^2 \mathbf{S}_s^{iT} \mathbf{K}_{FE}^i \mathbf{S}_s^i + p(1-p) [\mathbf{S}_s^{iT} \mathbf{K}_{FE}^i \mathbf{S}_{s+1}^i + \mathbf{S}_{s+1}^{iT} \mathbf{K}_{FE}^i \mathbf{S}_s^i] \\ &\quad + p^2 \mathbf{S}_{s+1}^{iT} \mathbf{K}_{FE}^i \mathbf{S}_{s+1}^i\end{aligned}\tag{3.27}$$

The final obtained form of the potential energy is:

$$U^i = \frac{1}{2} \mathbf{q}^{iT} \mathbf{K}^i \mathbf{q}^i = \frac{1}{2} \mathbf{q}^{iT} \begin{bmatrix} 0 & \mathbf{0} \\ \mathbf{0} & \mathbf{K}_{\eta\eta}^i \end{bmatrix} \mathbf{q}^i = \frac{1}{2} \mathbf{q}^{iT} \begin{bmatrix} 0 & \mathbf{0} \\ \mathbf{0} & \mathbf{V}^{iT} \mathbf{K}_{FE}^i \mathbf{V}^i \end{bmatrix} \mathbf{q}^i\tag{3.28}$$

3.3.3 Equations of motion of the gear

Lagrange's equation for the construction of the equations of motion is:

$$\frac{d}{dt} \left(\frac{\delta T^i}{\delta \dot{\mathbf{q}}^i} \right)^T - \left(\frac{\delta T^i}{\delta \mathbf{q}^i} \right)^T + \left(\frac{\delta U^i}{\delta \mathbf{q}^i} \right)^T = \mathbf{Q}^i\tag{3.29}$$

T^i and U^i are defined in the last section, whereas \mathbf{Q}^i is the vector of generalized forces, collecting:

- External forces \mathbf{Q}_e^i
- Contact forces \mathbf{Q}_c^i

According to equation 3.24 the last equation can be written:

$$\frac{d}{dt} \left(\frac{\delta T^i}{\delta \dot{\mathbf{q}}^i} \right)^T - \left(\frac{\delta T^i}{\delta \mathbf{q}^i} \right)^T = \mathbf{M}^i \ddot{\mathbf{q}}^i - \mathbf{Q}_v^i\tag{3.30}$$

where the quadratic velocity vector containing the gyroscopic and Coriolis forces is defined as:

$$\mathbf{Q}_v^i = -\dot{\mathbf{M}}^i \dot{\mathbf{q}}^i + \frac{1}{2} \left[\frac{\delta}{\delta \mathbf{q}^i} (\dot{\mathbf{q}}^{iT} \mathbf{M}^i \dot{\mathbf{q}}^i) \right]^T\tag{3.31}$$

The derivation of potential energy substituting equation 3.28 leads to:

$$\left(\frac{\delta U^i}{\delta \mathbf{q}^i} \right)^T = \frac{1}{2} \left[\frac{\delta}{\delta \mathbf{q}^i} (\boldsymbol{\eta}^{iT} \Psi^{iT} \mathbf{K}_{FE}^i \Psi^i \boldsymbol{\eta}^i) \right]^T = \mathbf{K}^i \mathbf{q}^i + \left\{ \begin{array}{c} \boldsymbol{\eta}^{iT} \Psi^{iT} \mathbf{K}_{FE}^i \Psi_{\theta}^i \boldsymbol{\eta}^i \\ \mathbf{0} \end{array} \right\}\tag{3.32}$$

The quadratic elastic displacements vector $\boldsymbol{\eta}^{i2}$ obtained in the second part of the equation is negligible and the following expression is obtained:

$$\mathbf{M}^i \ddot{\mathbf{q}}^i + \mathbf{K}^i \mathbf{q}^i = \mathbf{Q}_e^i + \mathbf{Q}_c^i + \mathbf{Q}_v^i\tag{3.33}$$

The mass matrix M^i according to 3.24 varies w.r.t. the reduction space, and so does the quadratic velocity vector Q_v^i . Therefore these two terms can be separated in two components, one due to the standard multibody formulation, \bar{M}^i , and one to the dynamic variability of the gear's basis matrix, \tilde{M}^i . On the other side the stiffness matrix K^i according to 3.25 remains constant.

$$(\bar{M}^i + \tilde{M}^i)\ddot{q}^i + K^i q^i = Q_e^i + Q_c^i + (\bar{Q}_v^i + \tilde{Q}_v^i) \quad (3.34)$$

As stated in [5] and in [7] the terms \tilde{M}^i and \tilde{Q}_v^i become significant only when the gears rotate at high angular velocities and undergo significant elastic deformations. Such gears can be found in propulsion systems of rotorcrafts and aeroplane gearboxes which rotate at very high velocities. If relatively stiff gears rotating at moderate velocities are considered, the influence of these two parameters is negligible.

In this work static and quasi static analyses are performed with high stiffness gears, therefore these parameters are not taken in account in the equations of motion.

In flexible multibody dynamics the formulation of mass matrix and the quadratic velocity vector is made in terms of mass invariants, i.e. matrices that are computed prior to the simulation and that contain information regarding the mass distribution of the flexible bodies, enabling a more efficient computer calculation. Therefore the mass invariants are the actual matrices used in the solution of the equation of motion. This procedure is accurately presented in [6].

3.4 Computer implementation

The theoretical concepts previously summarized were implemented on a digital computer, leading to a novel code fully developed inside the PMA research group under the name of MUTANT. This research code is structured as a set of Matlab routines and is currently being extended for planetary stages, shaft bending influences, misaligned conditions, micro-geometry, etc.

In the pre-processing phase, the vectors of the gears basis matrices V^i with i indicating first and second gear, and the corresponding mass invariants are computed and stored. The equations of motion can now be constructed and in the processing phase are solved. For every time instant the parametric mass matrix is built and inverted and the vector of generalized coordinates of the gears is obtained. Finally, in the post-processing phase dynamic transmission error, stress distributions, contact forces and other relevant quantities are calculated for the simulated time.

Also static analyses can be computed in the processing phase considering a certain number of angles along one angular pitch.

3.4.1 The pre-processing phase: computing the basis vectors

A flow chart representing the different steps in the pre-processing phase is shown in figure 3.8. The inputs consist of the FE mass and stiffness matrices of the respective gears, M_{FE}^i and K_{FE}^i , and the corresponding vectors of not deformed nodal coordinates, u_0^i . The n_k lowest eigenfrequencies are

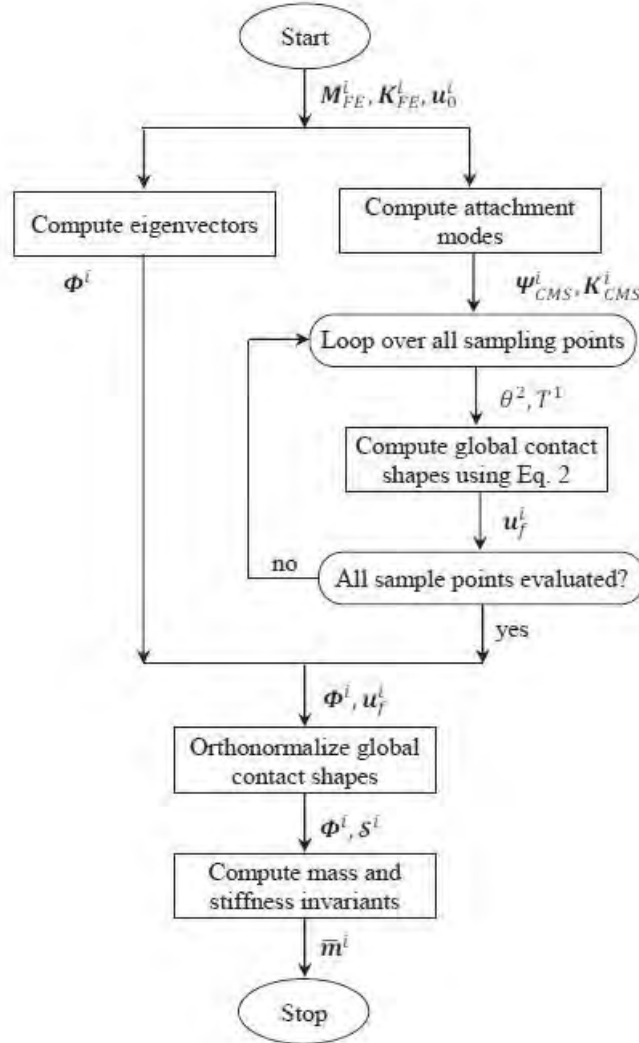


Figure 3.8: Flowchart of the preprocessing phase. Source: [7]

first obtained. These are the frequencies coming from a modal solution of the gears, and they vary depending on the boundary conditions. The gears are kept locked in their centres, allowed to only rotate around one axis. Consequently the calculated frequencies are the frequencies of fixed modes, resulting higher than frequencies values of free modes.

The global contact shapes are computed using a statically complete ROM that is based on a standard CMS approach, thereby limiting the overall cost of the pre-processing phase. The basis matrix of this ROM, denoted by Ψ_{CMS}^i , contains one static attachment mode for each nodal degree of freedom that can possibly be loaded during the computation of the shapes. This matrix is used to transform the contact problem system to an equivalent system of reduced dimension.

This system is then solved iteratively for a particular combination of T^1 and θ^2 to obtain the corresponding set of global contact shapes ($n_s = n_\theta \times n_t$). Once the global contact shapes have been computed, a mass orthonormalization procedure is performed to make these vectors residual with respect to the set of kept eigenvectors.

Finally in the pre-processing phase, the mass and stiffness invariants of the gears are computed and stored. These data, along with the eigenvectors and global contact shapes are sent to the preprocessing phase of the simulation.

3.4.2 The processing phase: solving the equations of motion

A flow chart representing the different steps in the processing phase is shown in figure 3.9. The inputs to this phase consist of the initial conditions $\mathbf{q}^i(0)$ and $\dot{\mathbf{q}}^i(0)$, the external loads $\mathbf{Q}_e^i(t)$ and the data computed during the pre-processing phase, i.e. the mass invariants and basis vectors.

The equations of motion have the form of a system of non-linear second-order ordinary differential equations. In the present work, these equations are solved using an explicit 2nd order Runge-Kutta solver, requiring the conversion of the equation of motion into a first-order form:

$$\dot{\mathbf{y}}^i = \begin{Bmatrix} \dot{\mathbf{q}}^i \\ \ddot{\mathbf{q}}^i \end{Bmatrix} = \begin{Bmatrix} \dot{\mathbf{q}}^i \\ M^{i-1} \mathbf{Q}_e^i + \mathbf{Q}_c^i + \mathbf{Q}_v^i - \mathbf{K}^i \mathbf{q}^i \end{Bmatrix} \in R^{2n_q \times 1} \quad (3.35)$$

where the state vector \mathbf{y}^i is twice the size of the vector of generalized coordinates \mathbf{q}^i .

Although the 2nd order Runge-Kutta solver is based on a two-stage integration scheme, only one stage is shown in the figure. At the beginning of each stage, three parameters τ , s and p are computed.

- τ : this parameter counts the number of angular pitches travelled by the driving gear and controls the rotation of the global contact shapes when $\tau > 1$.

$$\tau = \lceil \frac{|\theta^1 - \theta_1^1|}{\tau^1} \rceil \quad (3.36)$$

where θ_1^1 is the angle at which the first global contact shape S_1^1 was computed. $\tau^1 = 2\pi/z^1$ is the angular pitch of the driving gear, with z number of teeth.

- s : this parameter selects the global contact shapes S_s^i , S_{s+1}^i that will be interpolated to obtain the static shape matrix Ψ^i corresponding to the actual configuration of the gear.

$$s = \lceil \frac{n_\theta(|\theta^1 - \theta_1^1| \bmod \tau^1)}{\tau^1} \rceil \quad (3.37)$$

where n_θ is the number of angular sampling points within one angular pitch.

- p : this parameter is the actual interpolation parameter defined in the precedent section.

3.4.3 Contact forces computation

Contact forces Q_c^i are computed using a penalty based contact formulation.

A penalty based problem means that any violation of the contact condition will create a new force in the system.

A simple scheme of this condition is shown above, with the rising contact force directly dependent on the penetration between the two bodies. The contact spring will deflect an amount Δ , such that equilibrium is satisfied: $\epsilon\Delta = F$. Some finite amount of penetration, $\Delta > 0$ is mathematically required to maintain equilibrium. The value of stiffness must be chosen depending on the type of problem and this leads to some difficulties, but the algorithm was selected because of its computational efficiency and ease of implementation. The choice of

There are different types of contact detection between the surfaces (surface-to-surface, nodes only, etc.) and these are widely presented in [8]. First the followings are defined:

- *Master*: Master body nodes can't penetrate the slave body
- *Slave*: Slave body nodes can penetrate the elements of the master body

This formulation implements the node-to-surface contact, in which the slave node penetration is detected through the master elements. First one body is defined master and the other slave, a contact analysis is performed and then the two bodies switch their roles and the contact analysis is repeated. An average result is finally taken from the two solution. In order to improve the efficiency of this step, the computation of the actual contact forces is

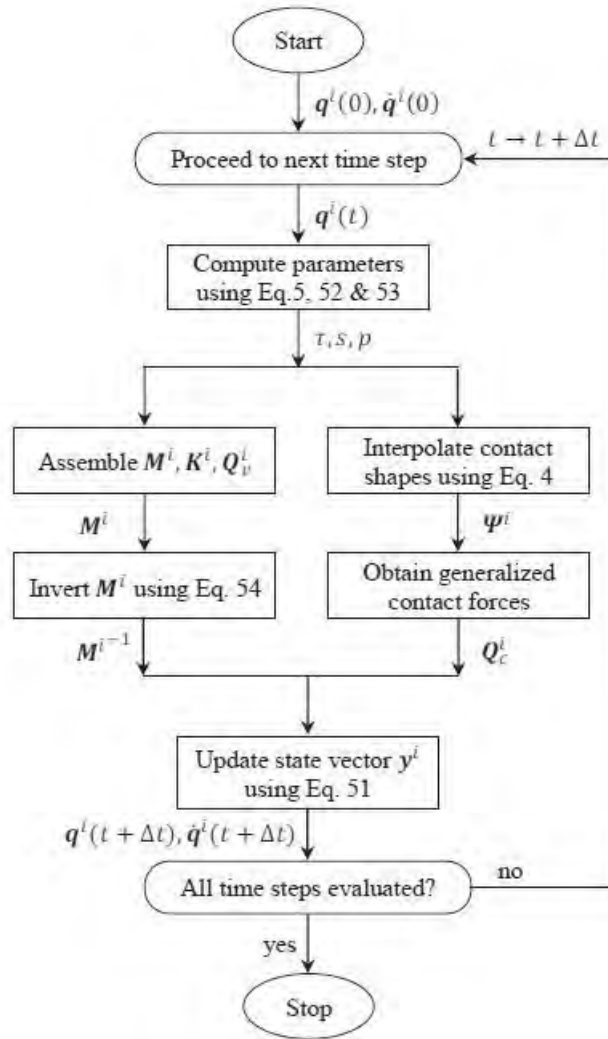


Figure 3.9: Flowchart of the processing phase. Source: [7]

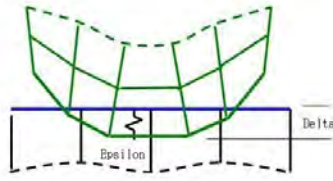


Figure 3.10: Illustration of penalty method for contact



Figure 3.11: Node-to-surface contact detection

preceded by a coarse contact detection phase during which a set of possible contact nodes is selected based on the not deformed geometry of the gear pair. These nodes are then evaluated for contact during the subsequent fine contact detection phase.

3.5 Chapter's remarks

In this chapter the implemented MOR method for dynamic flexible systems was discussed. First a brief introduction on main model order reduction techniques was presented, then the creation of the reduction basis matrix, which is the core of the discussion, was developed. The equations of motion were constructed and applied to the floating frame of reference approach. Along the chapter [7] was kept as the main reference, with focus on spur gears pair. After the theoretical bases, the method implementation is discussed in the last section, with focus on the main steps needed to build and reduce the model, to assemble the equations of motion and to solve the system in the processing phase.

Chapter 4

Correlation and model updating

The aim of the present work is the testing of the adopted spur gear pair on the test-rig and the simulation of the numerical model of the gear pair on the MUTANT code. In order to perform a comparison between numerical analysis and experimental tests, the parameters used to define the gears model must be updated.

The gear pair has two identical spur gears. In this chapter first a correlation between the numerical model and one tested gear is performed, then a quick model updating is made varying the most influencing parameters. Final parameters to be used in the numerical model are chosen.

4.1 Modal analysis

To obtain a reliable numerical model for following static analyses, only a correlation on the first normal modes of a single gear is necessary. As the higher normal modes are not excited with a quasi static test, the first three modes are taken into account to perform a model correlation. The assumed parameters introduced in the numerical model are the ones which should be updated to obtain good correlation of the model. Those are the Young's module and the Poisson's ratio.

A modal analysis of one gear was performed by Siemens Industry Software NV and the results are now courteously available for the present work.

Only one gear was tested as they were identical. The test modes are free-free modes, due to the fact that the modal analysis was performed with the gear hanged up with a soft elastic rope. The gear was tested with an impact hammer and a set of piezoelectric accelerometers placed on one of the gear's face. The correlation between the numerical model and the real gear is performed with focus on the first three normal modes coming out from the

experimental modal analysis. These modes were expected to be out-of-plane modes, as these types of modes, due to the geometry of the gear, are the most flexible ones. Results are shown in figure 4.1. The first two modes are

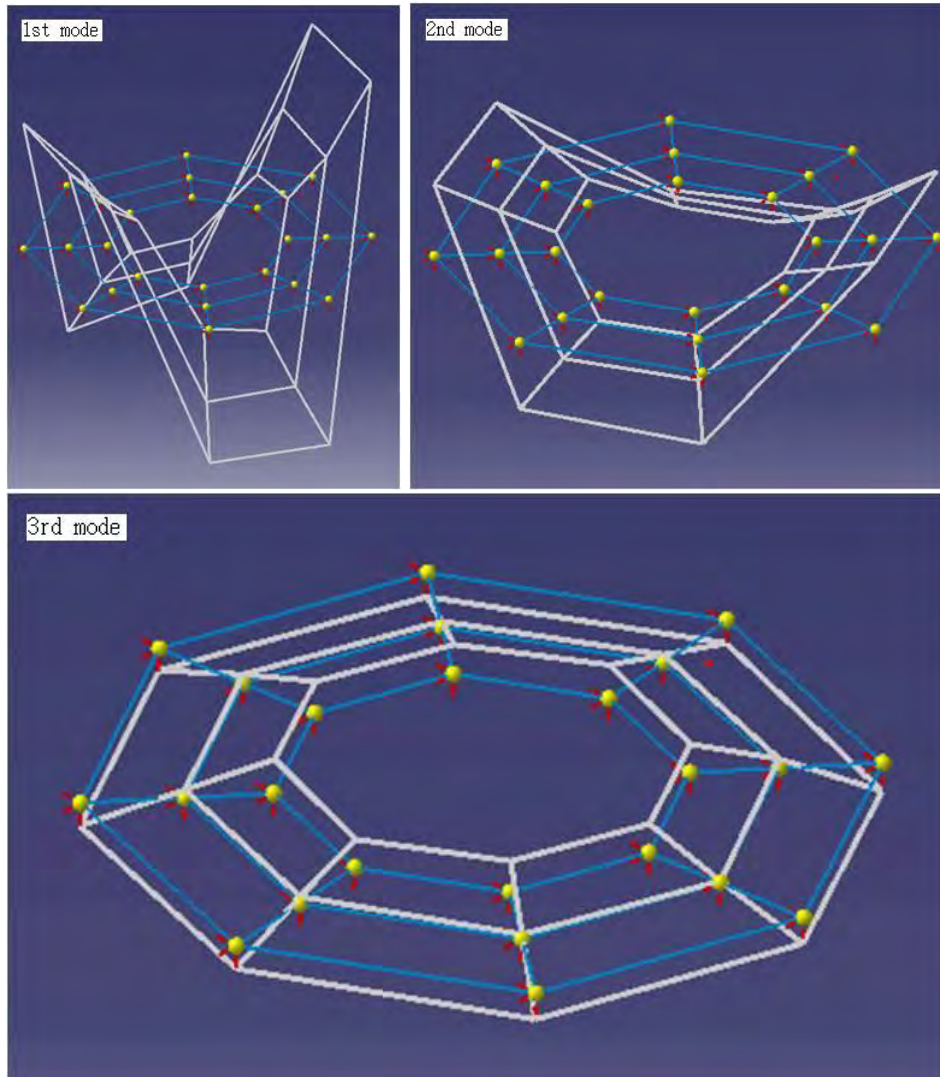


Figure 4.1: 1st mode: 4526 Hz; 2nd mode: 4554 Hz; 3rd mode: 8302 Hz.

very close in frequency, around 4500 Hz, as they are symmetric modes. The third one has a frequency of 8300 Hz.

4.2 Numerical model and design of experiments

The adopted numerical model has a relatively coarse mesh, because the first three normal modes are global modes, which only consider deformation of

the whole body of the gear and the local deformation of the teeth is not excited. The final mesh has around 110.000 degrees of freedom.

To obtain free-free modes the gear is not restrained. The modal analysis is performed through the software LMS Test.Lab [19], which easily allows to correlate experimental and numerical results through the Test.Lab Correlation environment [20].

Starting values for material coefficients were taken from the specification sheet of steel 16MnCr5: -

- Young's module 206 GPa
- Poisson's ratio 0.3

From those starting values a design of experiments (DOE) is performed, to better correlate the first three natural frequencies. In figures 4.2, 4.3, 4.4, 4.5 the DOE is shown, with various solutions of the same FE model with different material parameters. The experimental frequencies are represented by constant values all along the parameters ranges. The adopted borders of the DOE are: -

- $0.28 < p < 0.34$
 $E = 206000MPa$
step= 0.02
- $200000MPa < E < 213000MPa$
 $p = 0.3$
step= 1000Mpa

4.3 Model correlation

From the previous graphics the following values were taken to correlate the model: $E = 207000Mpa$, $p = 0.32$. The first three modes obtained from the numerical model are shown in Figure 4.6. It can be seen that the numeric modes found are very close in shape to the experimental ones. The first two have the same frequency, as expected for a structure with symmetry. Relative errors with respect to the experimental modes are:

1st frequency relative error = 0.53%

2nd frequency relative error = 0.09%

3rd frequency relative error = 0.28%

The Modal Assurance Criterion (MAC) is used to correlate the three modes. MAC matrix in figure 4.7 shows that the model is well correlated.

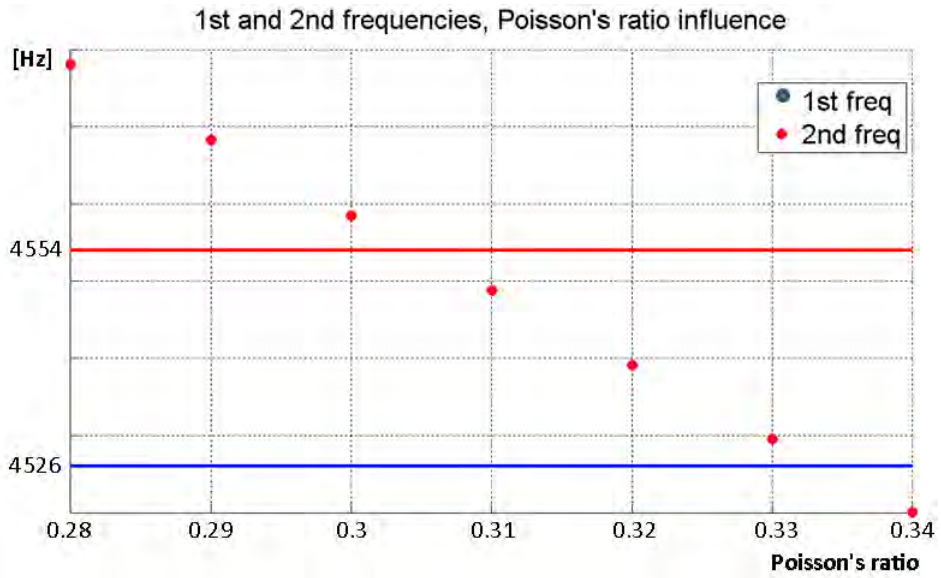


Figure 4.2: DOE varying Poisson's ratio of the numerical model

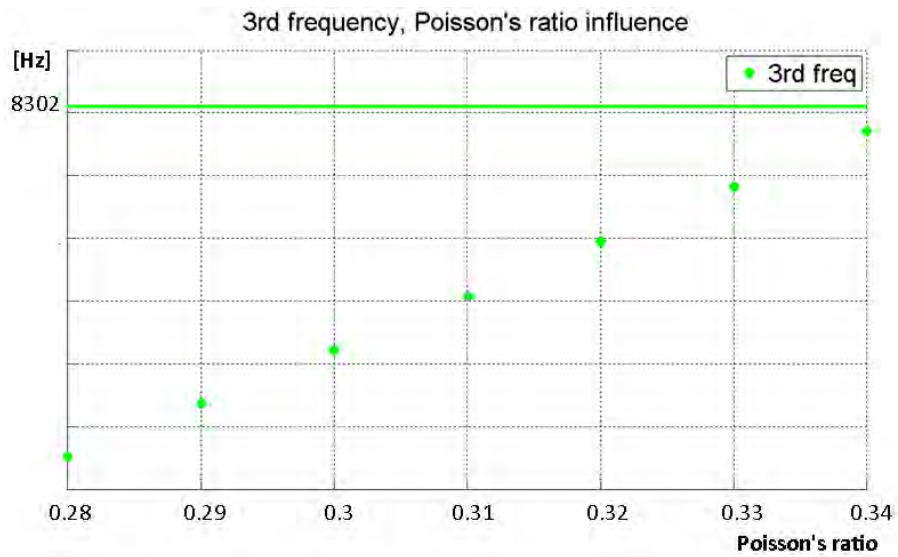


Figure 4.3: DOE varying Poisson's ratio of the numerical model

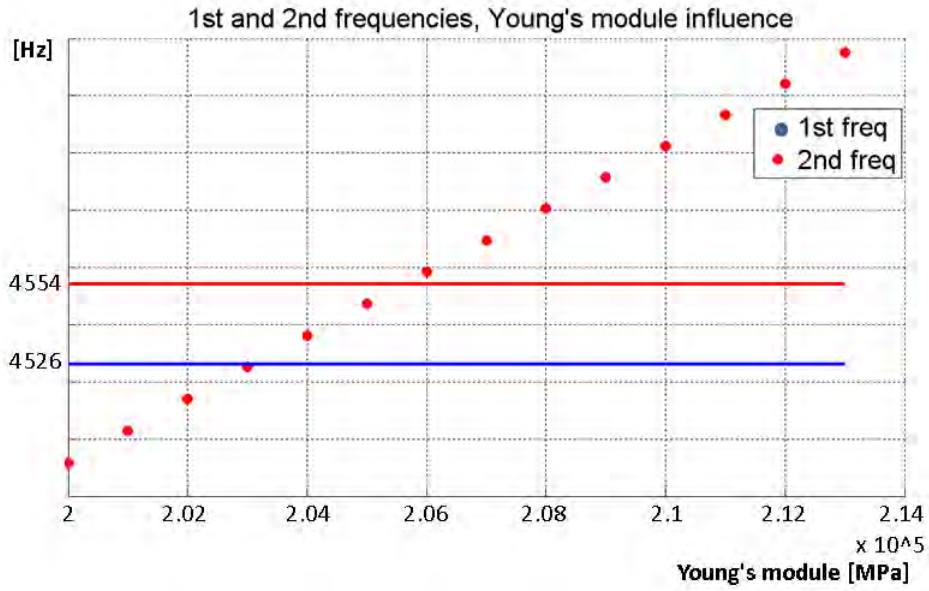


Figure 4.4: DOE varying Young's module of the numerical model

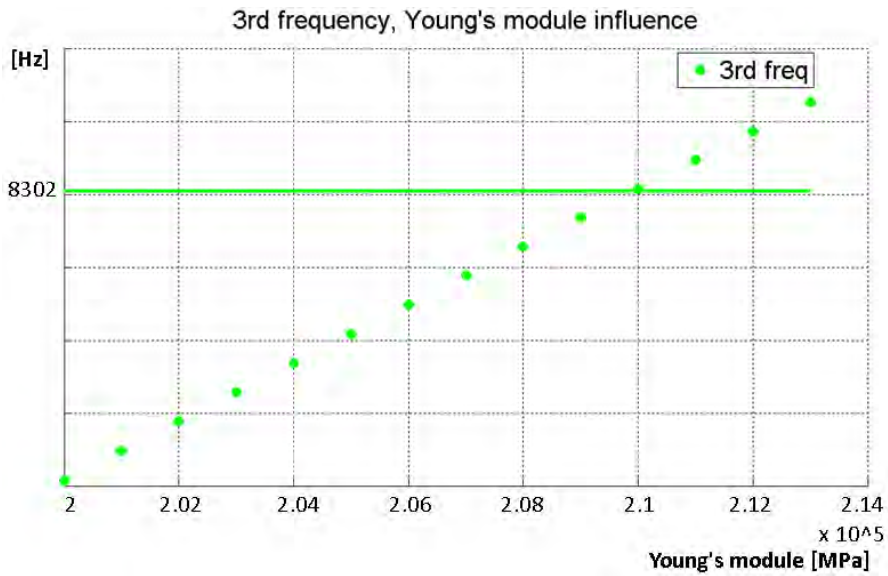


Figure 4.5: DOE varying Young's module of the numerical model

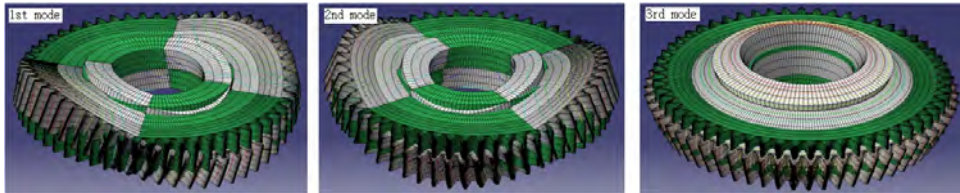


Figure 4.6: 1st mode: 4550 Hz; 2nd mode: 4550 Hz; 3rd mode: 8279 Hz

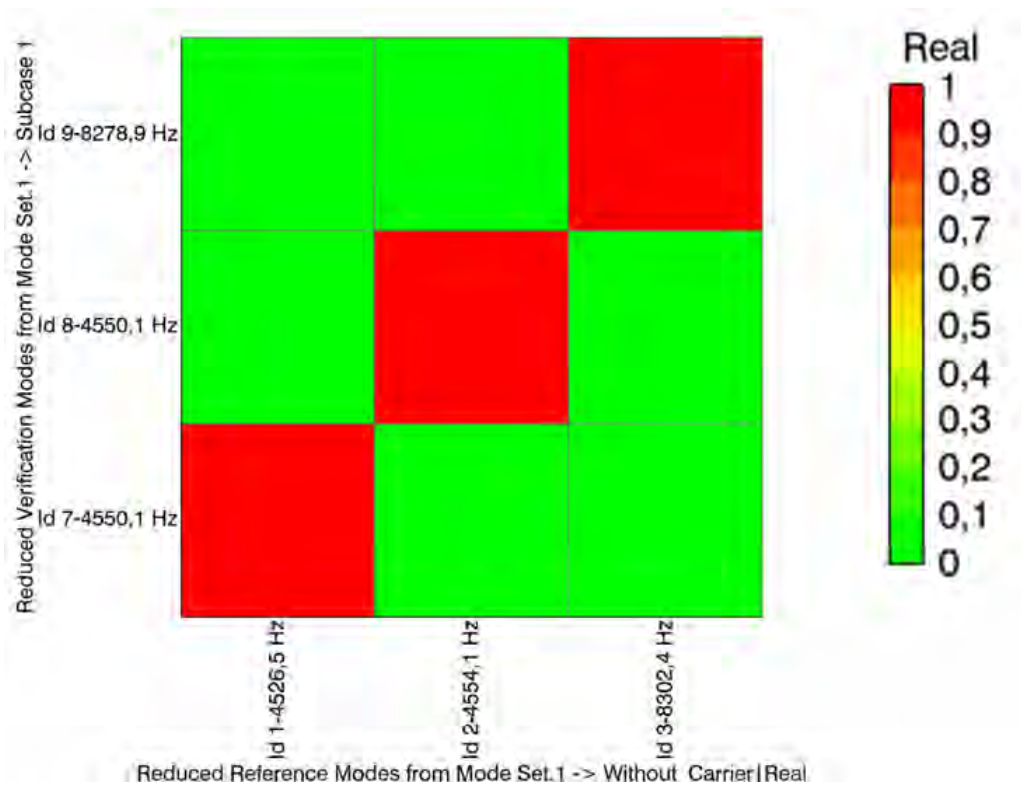


Figure 4.7: MAC matrix

4.4 Chapter's remarks

The modal analysis on the gear were provided by Siemens Industry Software NV, whereas in this work the numerical model has been built and updated. In this chapter experimental and numerical values of natural frequency are shown and it can be seen that they have reached very small relative differences after the model updating. The three natural modes taken in account are the first three modes observed with the modal analysis. The final MAC matrix shows a good correlation of the model.

Chapter 5

Simulation Parameters Analysis

5.1 System model and types of analysis

In the present work the novel code is tested with the gear pair shown in the previous chapter and here in this chapter, the various simulations performed are presented. The most influencing parameters are taken into account and the solution variability is analysed with respect to those parameters.

Working conditions of every parameter case are kept fixed referring to the model in figure 5.1.

If a dynamic simulation is performed, both gears are free to rotate, a torque is applied to the driving gear that acts on the driven gear which is submitted to a damping torque. After a transitory period a constant angular velocity of the gears pair is reached.

- Applied torque on driving gear $T = 100Nm$
- Damping torque on driven gear $D = 40Nm/rad$
- Angular velocity of the gear pair $\theta = 25rpm$

If the analysis is a static one, one gear is free to rotate and the other is locked at a certain configuration. The first one is brought in contact to the locked gear with a rotation angle increment, then a $100Nm$ torque is applied and the static solution for that particular configuration is calculated.

Static or dynamic solutions along one angular pitch are performed according to every parameter case. The analysis is divided in three parts. First a mesh analysis is performed, with focus on elements on teeth, then a penalty factor convergence analysis is presented for the contact force definition. Finally MOR parameters are varied to investigate their variability on the solution.

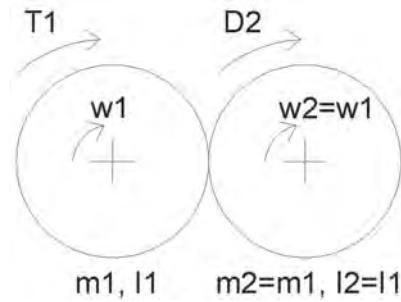


Figure 5.1: Gear pair simplified model

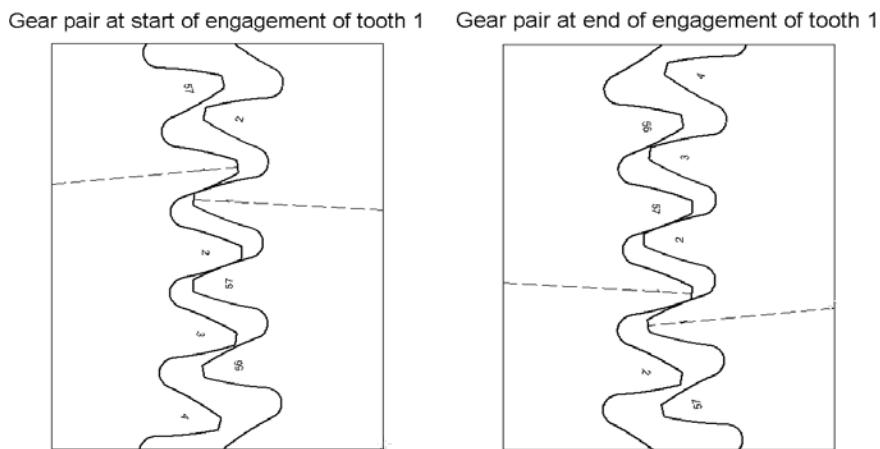


Figure 5.2: Angular pitch run during the simulation

Along the simulations different numerical effects are observed and they are also discussed in the final section.

Special focus is kept on the successive comparisons with test-rig results and TE is always observed because is the most suitable solution for successive comparisons with test-rig results.

5.2 Mesh analysis

In this section the convergence of the mesh is performed. The code presents a creation of the mass and stiffness matrices done through the FE software ABAQUS. Matlab creates the mesh, then the stiffness and mass matrix are assembled in ABAQUS, which sends back the stiffness and mass matrices for the created mesh [26].

The following simulations have the fixed parameters:

Applied torque [Nm]	100
Contact detection	Node-to-surface only on teeth flanks
Contact detection	Master-slave double pass
Penalty factor [N/mm]	500000
Normal modes	20
Global contact shapes	20

Table 5.1: Simulation parameters

5.2.1 Adopted model and meshing strategy

The model implemented is a 3D model, with bilinear 8-node hexahedral elements. Gears are fixed to the center allowing only one rigid degree of freedom, the rotation θ_z around the gear axis. Static and dynamic solution are obtained as shown before.

The 3D model is necessary for a correct representation of the system. Gears are spur type but the deformation along the width of the gears is not expected to be constant. There is a plane stress condition of the material on the sides of the gear width which leads to decreasing values of stress near the borders. The material in the central part presents a plane strain condition.

Evidently the crucial meshing is the one near the contact zone, hence all along the 57 teeth. The body of the gear doesn't sensibly affect the solution. As it can be seen from figure 5.4 the contact is supposed to be along the tooth flank. It has been verified with this pair of gears and the defined center distance, that the root fillet doesn't contact with the other gear. This leads to two convergence analyses:

1. Mesh refinement along the flank
2. Mesh refinement along the gear width

Must be taken in account that the root fillet should have elements size close to flank elements size, in order to correctly represent the deformation of the tooth. In fact the root is the mostly responsible part for the tooth bending because it has the highest values of stress after the contact zones.

5.2.2 Mesh refinement along tooth flank

Different meshes were implemented and static solutions were obtained, as a convergence analysis of the mesh doesn't need a dynamic solution. 20 static analyses were performed along one angular pitch.

The solution observed is the TE, which is given by the deformation of the

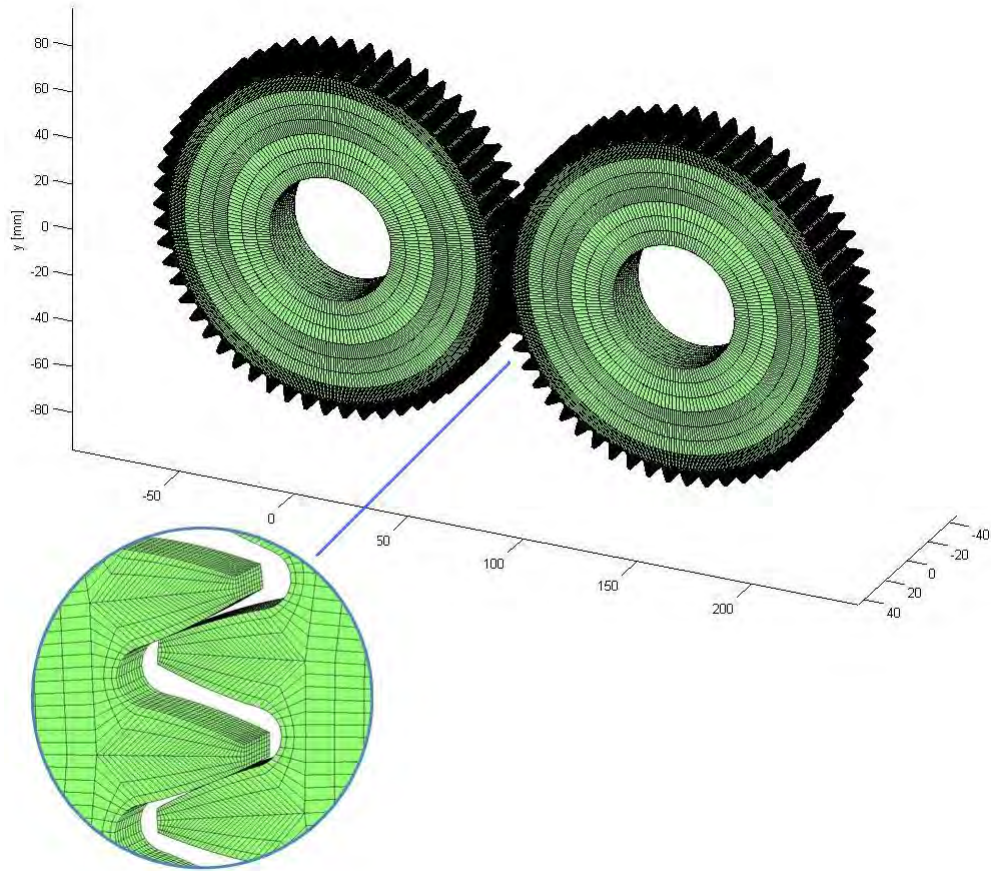


Figure 5.3: FE model of the gear pair

teeth and therefore is directly dependent on the mesh quality.

The number of elements along the flank goes from 10 to 35. Convergence is observed for 35 elements on the flank, which is evidently the case with the highest time needed. Referring to this solution two different errors are calculated.

- Relative peak to peak error:

$$err^i = \frac{|(TE_{top}^i - TE_{bottom}^i) - (TE_{top}^n - TE_{bottom}^n)|}{(TE_{top}^n - TE_{bottom}^n)} \times 100 \quad (5.1)$$

- Relative medium error:

$$err^i = \frac{|(TE^i - TE^n)|}{TE^n} \times 100 \quad (5.2)$$

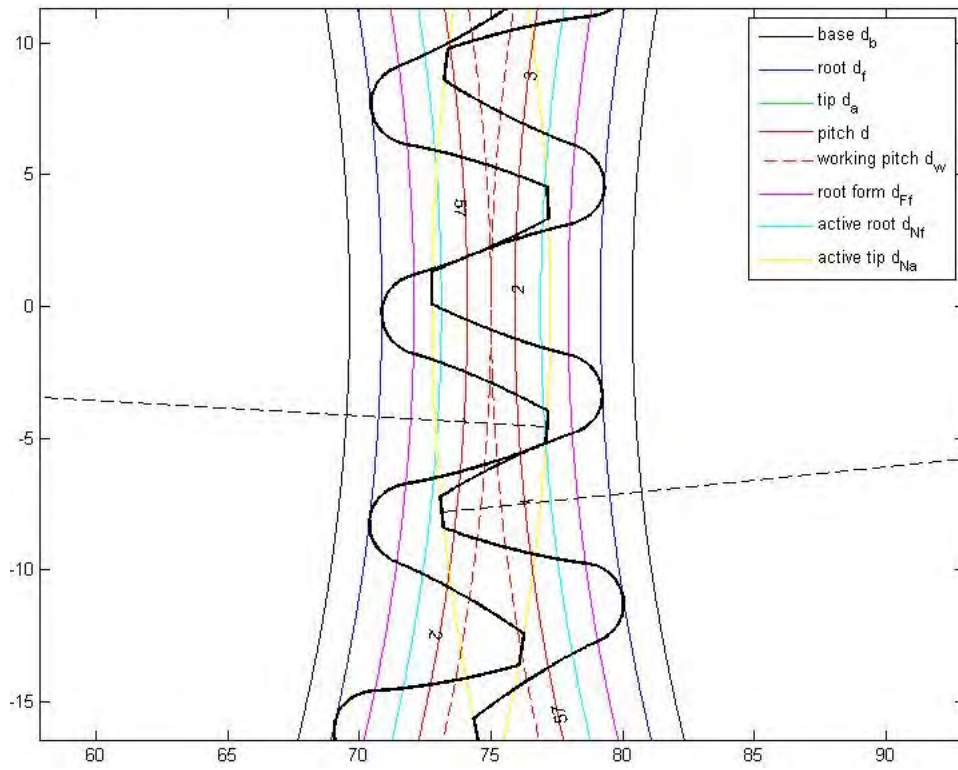


Figure 5.4: Teeth contact. The root fillet goes from d_f to d_{Ff}

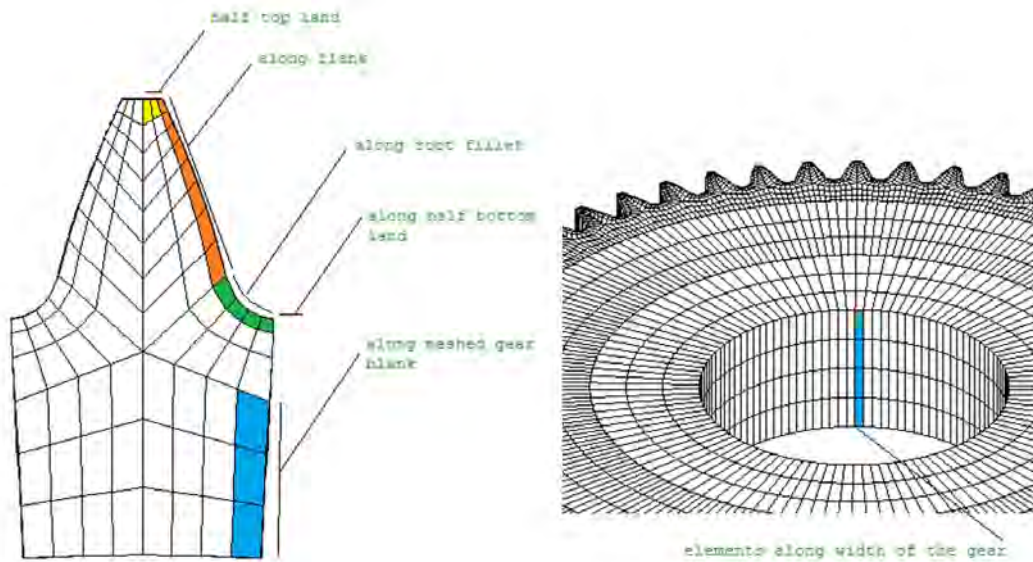


Figure 5.5: Mesh parameters

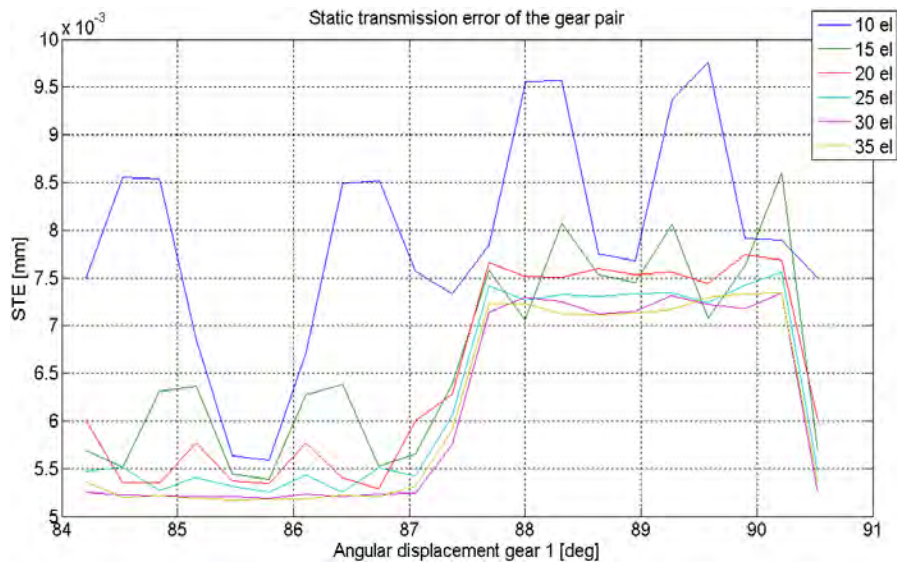


Figure 5.6: Mesh cases along tooth flank

where TE_{top}^i is the medium value of the points of the top part of the distribution of a single case i and TE_{bottom}^i of the bottom part. The case n is the converged case of 30 elements. TE^i and TE^n are the medium values given by all calculated TE points.

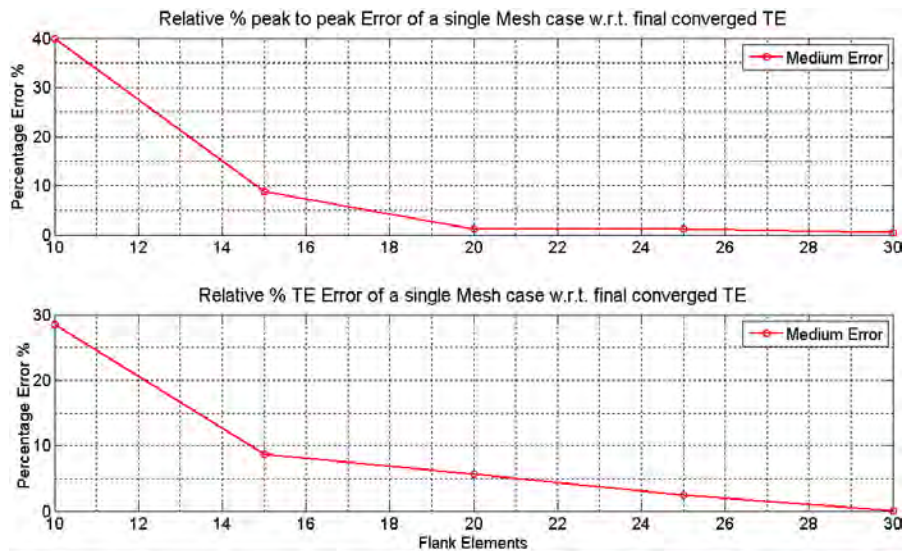


Figure 5.7: Relative errors of different mesh cases

Mesh refinement along width

The same conditions of the precedent refinement are kept for the refinement along tooth width. The number of elements goes from 8 to 14 elements (figure 5.8). Convergence is observed with 14 elements. A smaller deviation

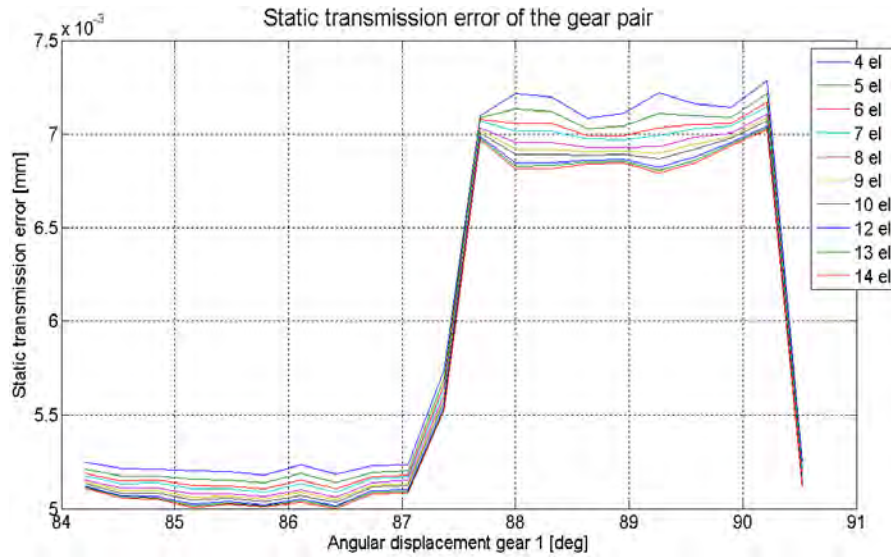


Figure 5.8: Mesh cases along tooth width

of the results is observed than the flank elements analysis. This is due to the convergence of the stress in the plane stress zones.

Relative errors are calculated as before in figure 5.9, based on the 14 width elements solution

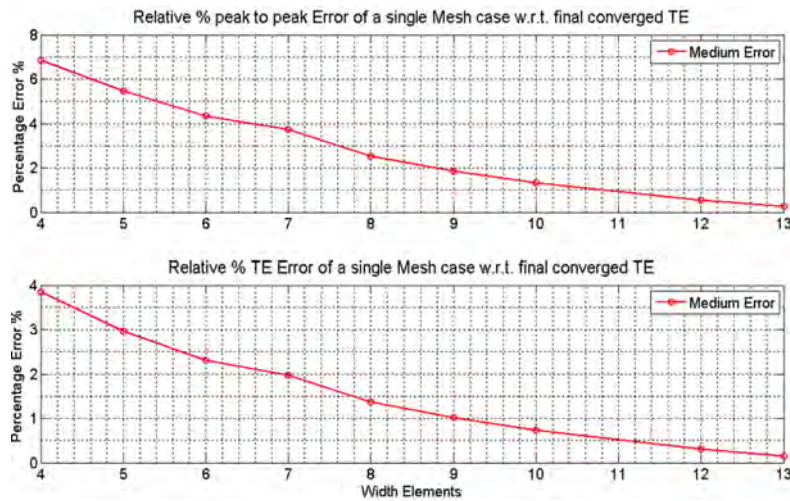


Figure 5.9: Relative errors of different mesh cases

5.3 Penalty factor analysis

Ideally the penalty factor should be set as high as possible, to correctly represent the physical phenomenon, where there is no penetration between the two bodies. On the other side the computational effort increases as the c_p value increases and for values of penalty factor too high the problem becomes ill-conditioned.

Keeping fixed all the simulations conditions and using the same mesh, the value of c_p is varied and the considered solution data is the STE. A convergence of the solution is expected.

As stated in [5] in the paper "On the applicability of static modes switching in gear contact applications" a check on the cinematic parameters should be done when varying the c_p factor, to observe the results are not cinematically different between each other.

Therefore to save time a convergence analysis of the c_p is performed on STE and then the final value obtained is checked with the cinematic parameters of a dynamic analysis. The c_p value is used for every contact problem that has to be solved, hence in the global shapes computation, in the static analysis and in the dynamic one. These three values are kept the same for every case studied. It has been chosen to increment the c_p factor from 50000 N/mm to 3000000 N/mm with variable steps, keeping the parameters of table 5.2 fixed:

Applied torque [Nm]	100
Contact detection	Node-to-surface only on teeth flanks
Contact detection	Master-slave double pass
Elements along tooth flank	25
Elements along tooth width	12
Normal modes	20
Global contact shapes	20

Table 5.2: Simulation parameters

Convergence of the solution to a unique value is observed. The shifting of each entire curve is seen, according to the increasing stiffness of the whole system.

Non convergence of one single shape is observed for the last cases, with high c_p values adopted. In every static simulation the rising contact forces depend on the spring stiffness and on the elongation of the spring. The last parameter is given by the penetration angle increment applied to start the solution of the contact problem. This angle increment must be accurately set

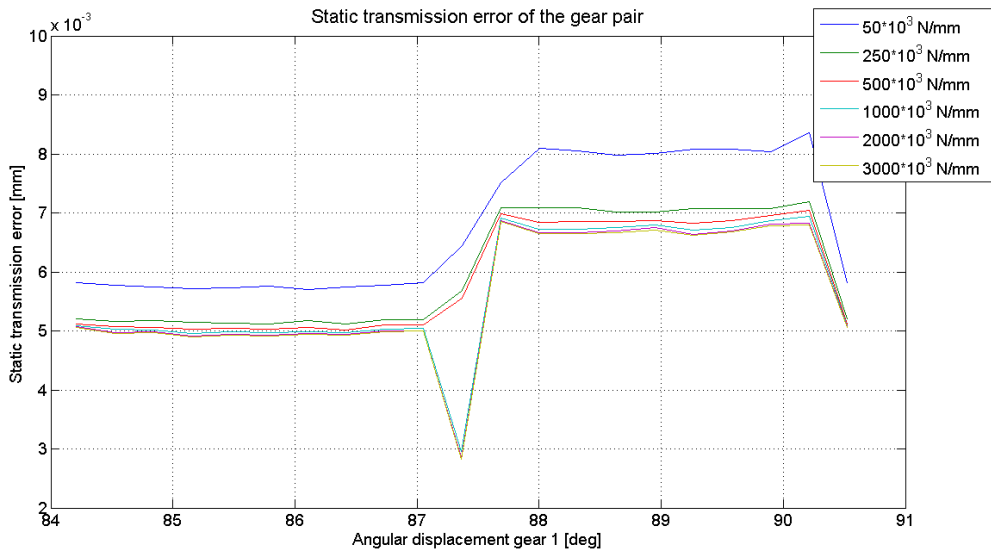


Figure 5.10: Cases with different penalty factors

for every penalty factor used, to obtain correct convergence of the solution.

Relative errors according to the precedent formulation are calculated. Single TE solutions calculated with non converged shapes are not taken into account.

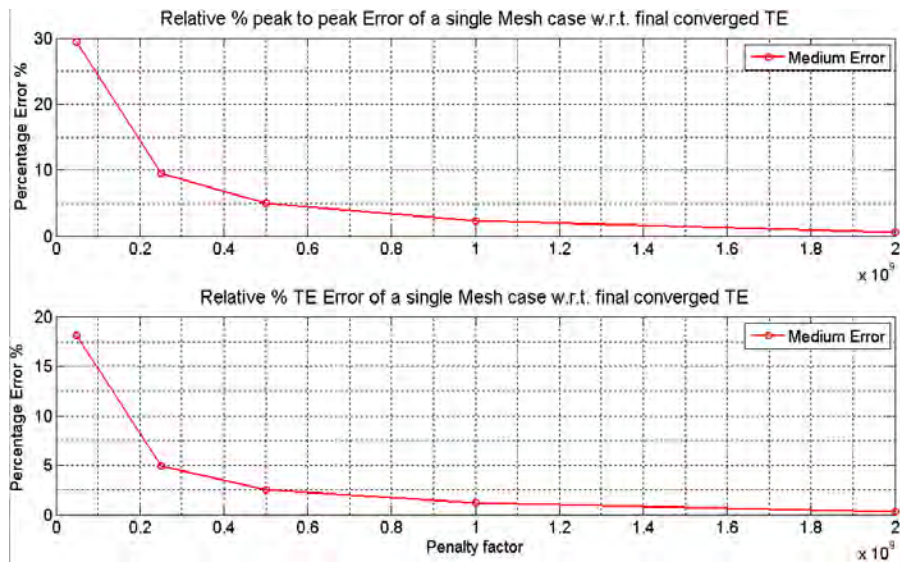


Figure 5.11: Relative errors of different penalty factor cases

Convergence of the analyses can be observed also through the errors rep-

resentation, with the relative peak to peak TE error around the double of the relative medium TE error for every c_p case calculated. This fact can also be noticed observing figure 5.10. It has been noticed an increasing numerical difficulty on the contact problem solution as the penalty factor value increased. Finally it can be stated that the optimal c_p value should be near $2 \cdot 10^9$ N/m, but assuming a lower c_p still low errors are reached. A final value of 500000 N/m is selected, giving a 2.5% relative peak to peak error. The analysis was more focused on the peak to peak error because this value is the most analysed in the followings chapters.

5.4 MOR analysis

The MOR elements which affect the solution are the vectors forming the reduction basis matrix, hence the number of kept normal modes and the number of global shapes.

- **Normal modes:** A quasi static analysis is the object of the present work; therefore high vibration modes of the system are not supposed to be excited. Normal modes are fixed-free, representing the real working conditions of the system. A relative small number of normal modes is expected to be sufficient to perform a good simulation.
- **Global contact shapes:** The number of global shapes depends on the number of divisions considered in an angular pitch. With more divisions a more accurate solution should be reached. On the other side, a too high value of divisions can bring to an ill-conditioned problem, due to the high similarity between two consecutive shapes.

These two different parameters vary, whereas the following remain fixed:

Applied static torque [Nm]	100
Applied dynamic torque [Nm]	100
Applied dynamic damping [Nm/rad]	40
Simulation time [ms]	55
Ramp-up time [ms]	5
Contact detection	Node-to-surface only on teeth flanks
Contact detection	Master-slave double pass
Elements along tooth flank	25
Elements along tooth width	12
Penalty factor [N/mm]	500000
Normal modes	20
Global contact shapes	20

Table 5.3: Simulation parameters

Normal modes analysis

A set of minimum 200 eigenmodes has been taken as a good value to obtain a reliable solution of a two spur gears system according to the simulations performed in [7] with similar rotational velocities. The DTE is the analysed

solution as it should be the result most affected by the normal modes number variation. Also the cinematic parameters are observed.

A 200 and 20 normal modes solutions are firstly compared: Observing these

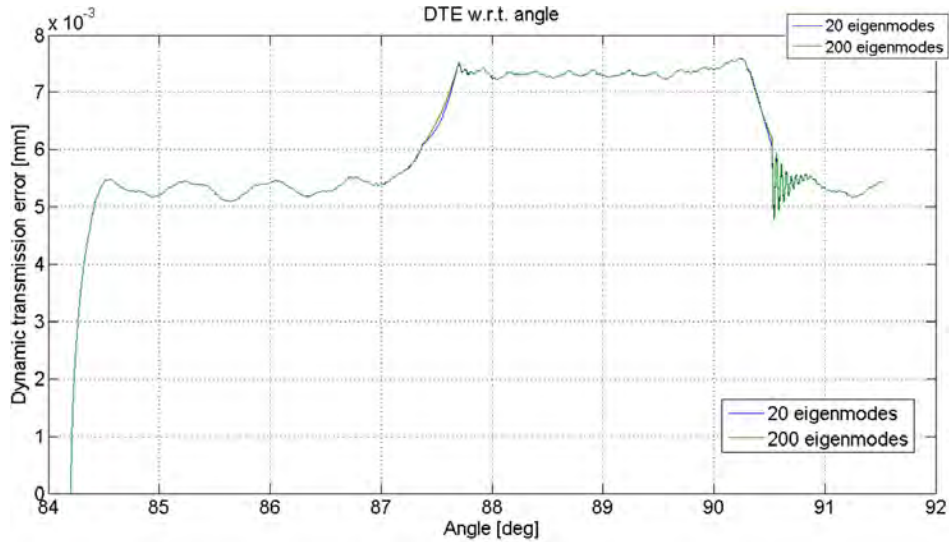


Figure 5.12: Cases with 200 and 20 normal modes adopted

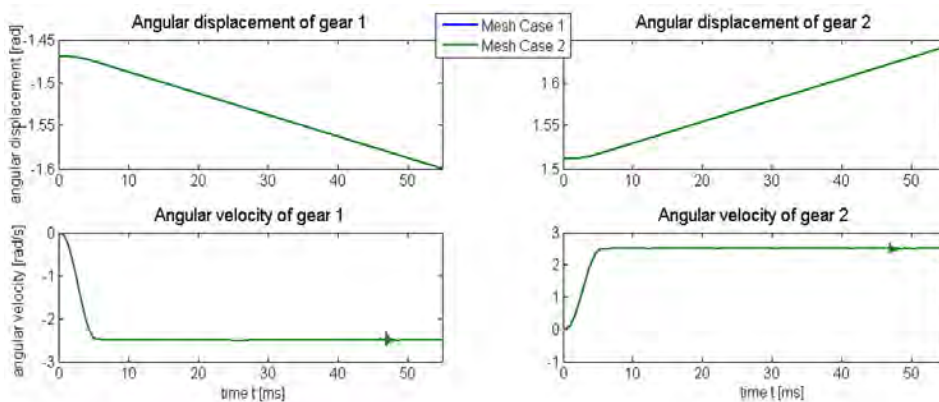


Figure 5.13: Cases with 200 and 20 normal modes adopted

two cases there are no evident differences in the shape of the transmission error. As expected the slow velocity of rotation cannot introduce high frequency dynamic effects in the solution, therefore using 20 normal modes is enough for taking into account all manifested dynamic effects.

Global contact shapes analysis

As seen in the theoretical chapter, global contact shapes are mainly responsible for the local and static solution definition, whereas normal modes are responsible for the global and dynamic solution definition. Therefore static analysis are implemented for the parameter n_θ , which represents the number of angular divisions taken along one angular pitch.

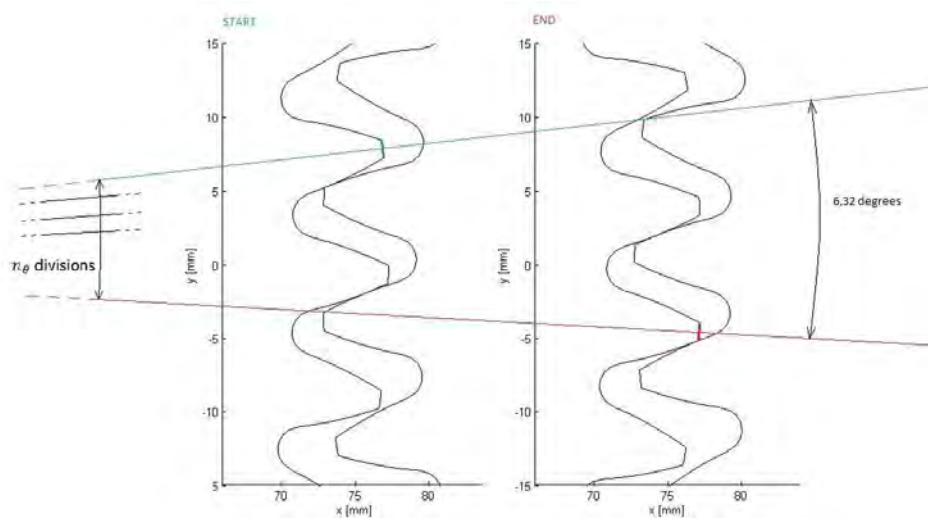


Figure 5.14: Angular divisions for shapes computation

To observe variations of TE shape, a higher number of static solution along one angular pitch was used (140). The number of normal modes is kept fixed to 20 and the divisions goes from 20 to 110.

Differences of TE shape are observed only in the right side of the central hill of the TE. This variation is calculated as area variation under every curve, with a spline of the data.

In this side of the curve an interpolation must be done between two consecutive shapes, one representing one tooth in contact and the other one two teeth in contact. This leads to an intermediate shape, which will make the system having an intermediate value of general stiffness between the two consecutive shapes. Therefore the TE will have a smoother distribution, given by a shape which is not physically correct, but comes from the interpolation of two consecutive states.

Peak to peak values are not affected by this parameter, and observing the calculated area, convergence of the side shape is nearly obtained with 80-110 shapes.

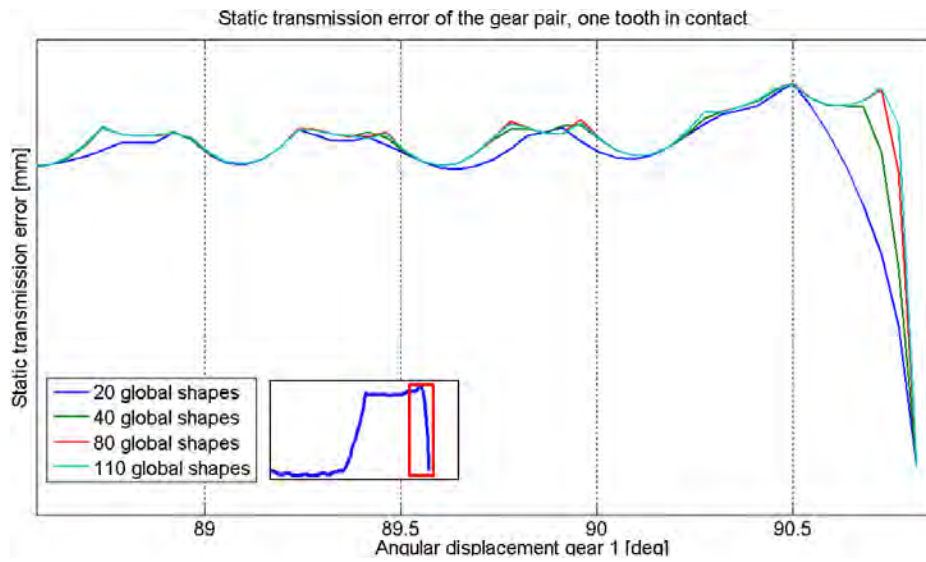


Figure 5.15: Cases varying the number of global shapes

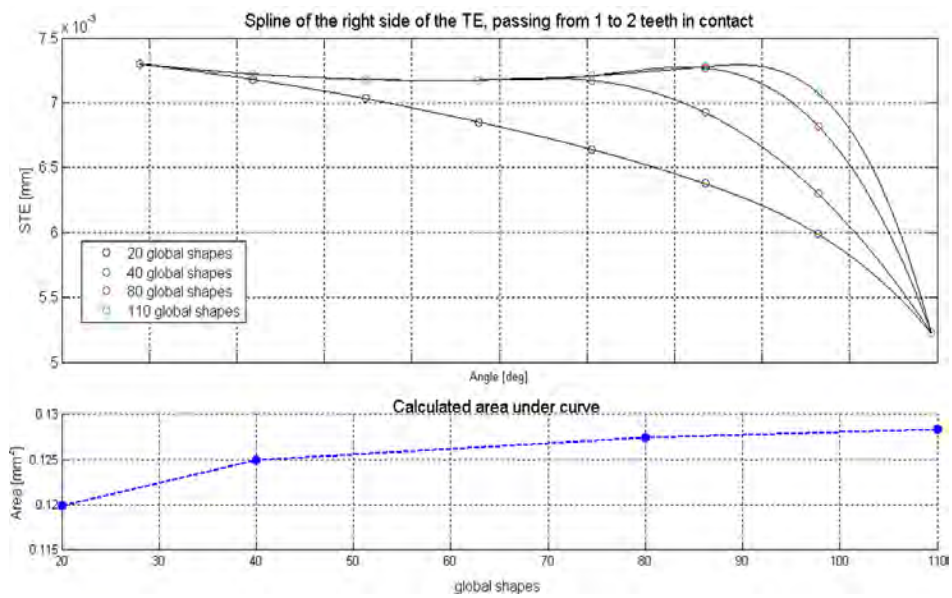


Figure 5.16: Global shapes influence

5.5 Numerical effects

Performing these analyses, different numerical effects have been encountered. In this section a briefly definition and explanation of them is gave. Most evident effects have been obtained in the DTE solution, which best collects all of them.

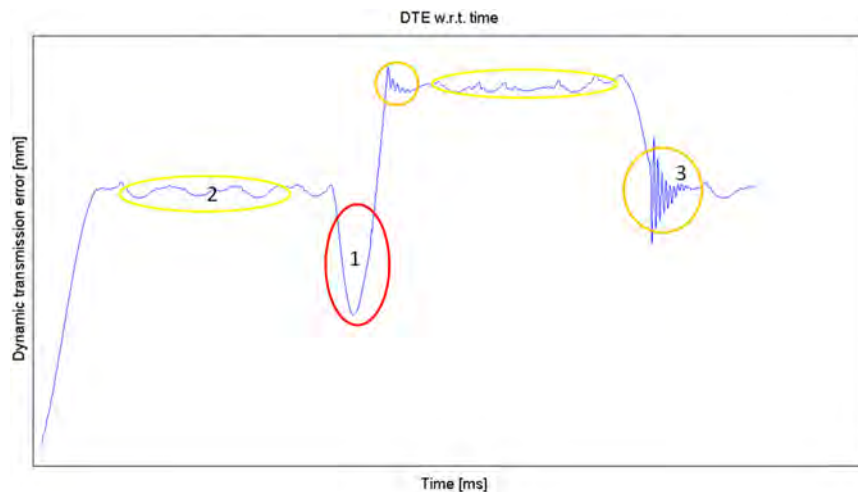


Figure 5.17: Main numerical effects: 1. No convergence of a single shape; 2. Oscillation on flat zones; 3. Oscillation on transitory zones.

5.5.1 No convergence of a single shape

This effect was previously observed. Changing the penetration angle, which brings the two gears in contact in the shape computation phase, convergence is obtained. In this example the same system was solved, varying only the penetration angle, from $8 \cdot 10^{-6} rad$ (red curve) to $5 \cdot 10^{-5} rad$ (blue curve).

5.5.2 Oscillation on flat zones

Both in static and dynamic TE solution, oscillation are observed along the flat zones, both with one tooth and two teeth in contact. The possible reason for this variation of the solution can be found in the number of elements in the FE model along the tooth flank. DTE has been calculated for different meshes in Figure 5.19. Contact forces are responsible for these oscillations as can be seen in Figure 5.21. Correlation between oscillation frequencies and number of flank elements is found, as shown in Figure 5.20. Therefore can be stated that TE oscillations are related to the switching of the elements rows in contact along the flank and increasing the refinement a more stable solution is observed. From this analysis further guidelines in choosing the mesh are found. Even though 25 elements have been found sufficient in the



Figure 5.18: 11th shape on 20 not converged

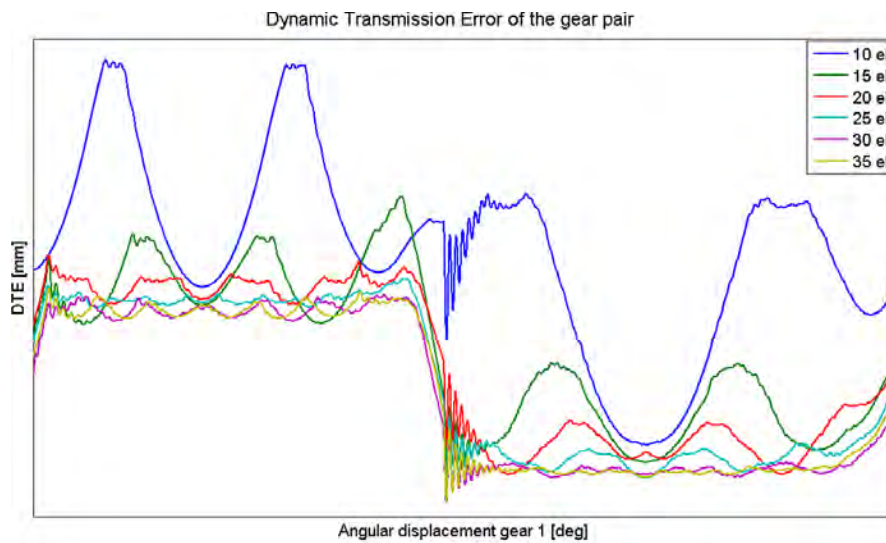


Figure 5.19: DTE oscillation with different tooth meshes

mesh analysis, to obtain a more stable solution in the flat zones at least 30 elements are required.

5.5.3 Oscillations on transitory zones

At the entrance and exit of a tooth, the contact zone changes, passing from only one tooth in contact to two and vice versa. Only in the dynamic simulation perturbation of the solution is observed mainly near those two transitory

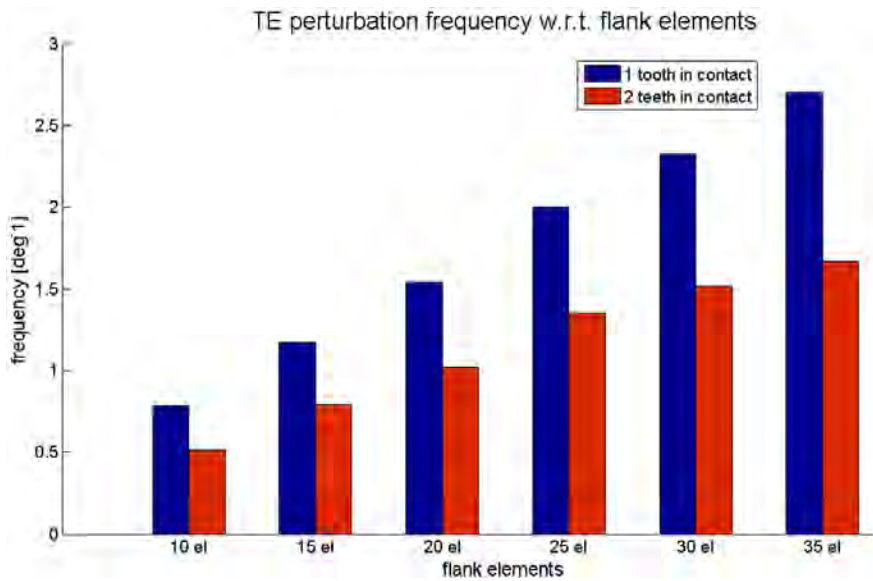


Figure 5.20: Oscillation frequency with different tooth meshes

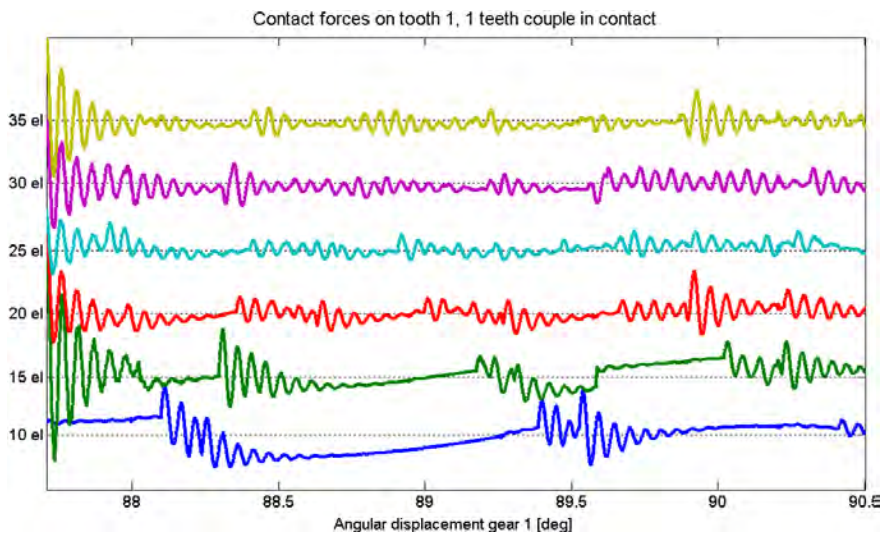


Figure 5.21: Contact forces with different tooth meshes

zones as shown in 3 in Figure 5.17. Forces rise at the contact detection and therefore their amplitude strictly depends on the time step (which defines the penetration at the following instant of time) and on the penalty factor. If the time step or the penalty factor are too high, too high contact forces rise and the applied torque is overtake by the contact forces, with following lose of contact between gears. The contact is after re-established with consequent oscillations.

The same system is solved for different values of time step, keeping constant all other parameters. Differences are observed mainly on the amplitude of the oscillation at the entrance of the second tooth (Figure 5.22) and also along the flat zones (Figure 5.23).

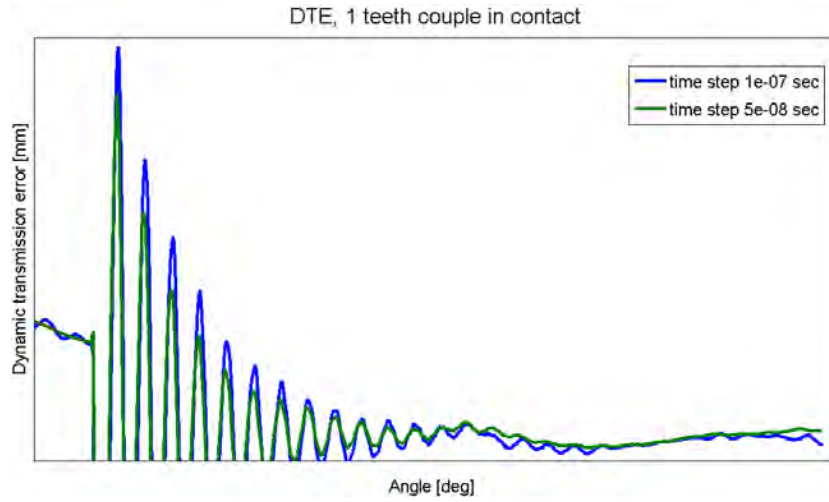


Figure 5.22: Different time step analysis

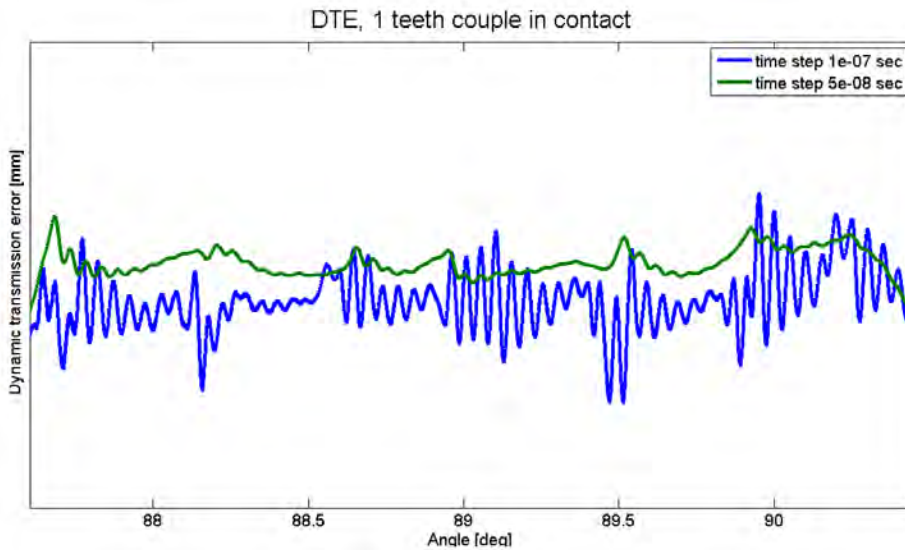


Figure 5.23: Different time step analysis

5.6 Chapter's remarks

In this chapter the updated gear pair has been simulated to investigate the main parameters of the code. The main solution taken into account in these analyses, is the static transmission error, as it will represent the main quantity measured on the test-rig.

First a mesh analysis was performed, defining a minimum number of elements on the tooth. Afterwards the penalty factor, responsible of the contact interaction between teeth, was discussed, together with related convergence problems.

The variation of the reduction basis was investigated varying normal modes and global shapes. Finally the principal numerical effects observed along the simulations were discussed.

Chapter 6

Experimental Measurements

6.1 Gear test-rig: basic concepts and instruments

The aim of the present work is the comparison of the novel code with experimental tests. Thanks to a collaboration between the University of Leuven and Siemens Industry Software NV, the gear test-rig at Testing and Simulation Division of Siemens in Leuven was available for this work. The test-rig was developed concurrently by KU Leuven, Siemens Industry Software NV and University of Calabria within the DEMETRA project [31].

DEMETRA project (DEsign of MEchanical TRANsmiissions) is an Industry-Academia Partnerships and Pathways (IAPP) project funded by the European Union under the FP7 Marie Curie Programme. It has the aim of developing technologies to enable green, silent and reliable mechanical power transmissions, by targeting the crucial subsystems (gears and bearing) for the efficiency noise, levels and durability of industrial machinery. New methods are currently studied for improved virtual prediction and optimization of the full system performance as a complete coupled dynamic system, as well as improved strategies to incorporate test data in the process.

The present gear test-rig was designed with the main objective of validation of computational gear methods. Focus is on gear pair belonging to families of spur or helical cylindrical gears. In order to have very well-known boundary conditions, all manufacturing tolerances were kept extremely tight. Further information on the present test-rig can be found in [13], [14], [15] and in the website [17]. In this thesis work, test results were measured working on the test-rig, checking all working conditions and input parameters used during the tests.

In this section main features of the test-rig are presented. A CAD model is shown in Figure 6.1 indicating all the main components.

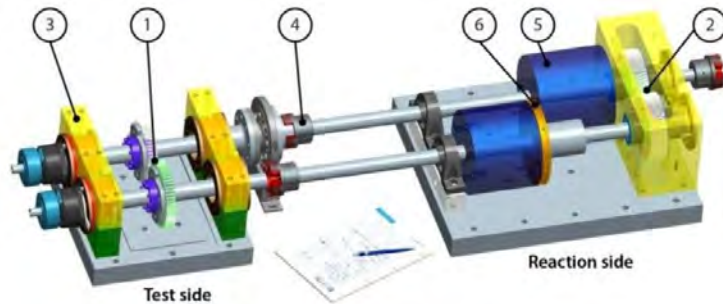


Figure 6.1: Test-rig representation: 1. Test gears; 2. Reaction gears; 3. Bearings support plates; 4. Flexible couplings; 5. Flywheels; 6. Clutch flange for preload. Source: [13]

Power circulation arrangement

Considering mechanical power, the present test-rig can be considered in the category of power circulation gear test-rigs, where the system is self-balanced and only one motor is required to overcome losses to spin the system. The discussed test-rig, through its power circulation arrangement, has two different sides, one dedicated to testing a cylindrical gear pair, and the other is needed for retaining a pre-load torque in the system by means of a second helical gear pair.

Imposing misalignments

Relative misalignments or center distance variations can be imposed on the test gears. Angular misalignments in an arbitrary plane and center distance variations can be set by a technique proposed by [16]. Bearings are mounted in eccentric caps and these caps can be turned to orient the eccentricity at a given angle. Same angles for the two caps on the same shaft result in imposing a center distance variation; opposite angles result in imposing an angular misalignment.

Adjusting shaft compliance

Shaft torsional and bending stiffness are placed in series with gear mesh stiffness and affect the total stiffness of the gearing. Expansion locking units are used to allow axial positioning of the gears and thus to adjust shaft stiffness. In particular, bending and torsional stiffness are maximum when the loaded shaft segment is the shortest. Two configurations are most relevant: gears at half shaft length and gears closest to the bearings.

Tested quantities and instruments

Static and dynamic testing is possible for the most important gear-related physical quantities: transmission error, relative displacements, tooth root strain, transmitted torque. Main devices to obtain TE measurements for the scope of this work are shown in figures 6.2, 6.3, 6.4. An LMS SCADAS Mobile 05 was used as sampling unit, receiving as inputs the signals coming from two Heidenhain ERN 120 encoders placed on both shafts, and from an HBM T40 torque meter placed on only one of the shafts.



Figure 6.2: Acquisition system: LMS SCADAS Mobile 05; 24 bit ADC sampling at 204.8 KHz; 820 MHz frequency clock, yielding 1.2 ns time resolution; 1 MHz maximum input pulse rate in digital mode. Source: [29]



Figure 6.3: Encoder: Heidenhain ERN 120 ; Digital output TTL ; 5000 divisions per rotation ; One rotation accuracy: ± 20 arcsec. Source: [29]



Figure 6.4: Torque meter: HBM T40 ; Analog voltage output ; Sensitivity: 10 mV/Nm ; Bandwidth: 6 KHz ; Accuracy: ± 1 Nm. Source: [29]

6.2 Experimental results

Experimental tests were conducted with the defined gear pair, effective applied torque and transmission error are measured, but only the TE is taken in account. In this section operating conditions are discussed, then the results components are identified and the final TE results are presented.

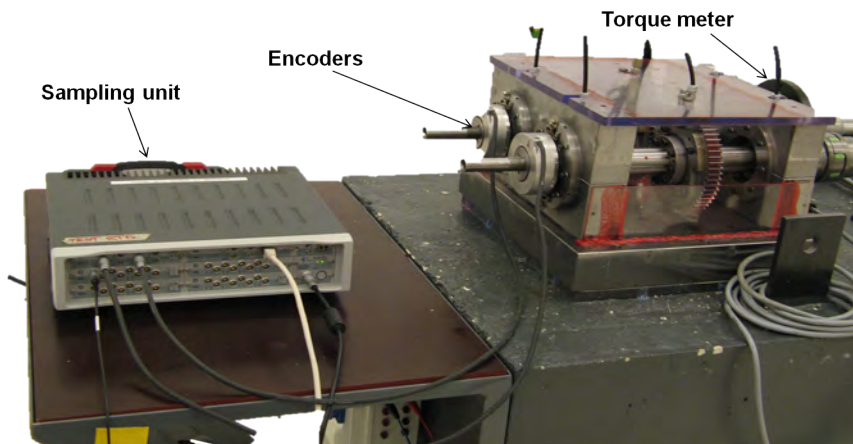


Figure 6.5: Measurement system

6.2.1 Test operating conditions

In order not to have initial misalignments between the two gears, those are placed at half of the shaft length, where the angular inclination, given by shaft deflection when torque is applied, is null. The present tests are

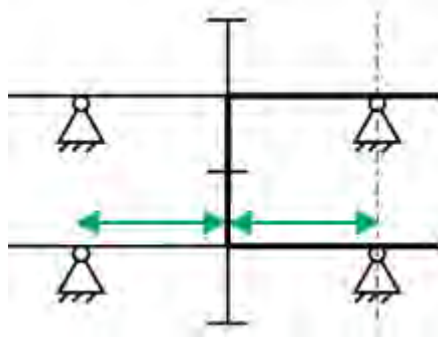


Figure 6.6: Axial position of the gear pair on the shafts

conducted with no misalignments condition. To achieve this the locking units of the gears are accurately fixed to the shafts with gradual tightening torque on the screws. If the locking conditions of the gears are not accurate, a 2nd order oscillation can be observed in the signal. The 2nd order oscillation (also called modulation of the signal [27]) comes from a rotation of the gears out of the plane leading to variation of the zone of contact on teeth along one round of the shaft. In figure 6.7 two maxima (90 and 270 degrees) and two minima (0 and 180 degrees) working distances appear in one round of the shaft, leading to a 2nd order oscillation. This effect implies a variation of TE amplitude along one round of the shaft, with consequent inaccuracy on measurement results.

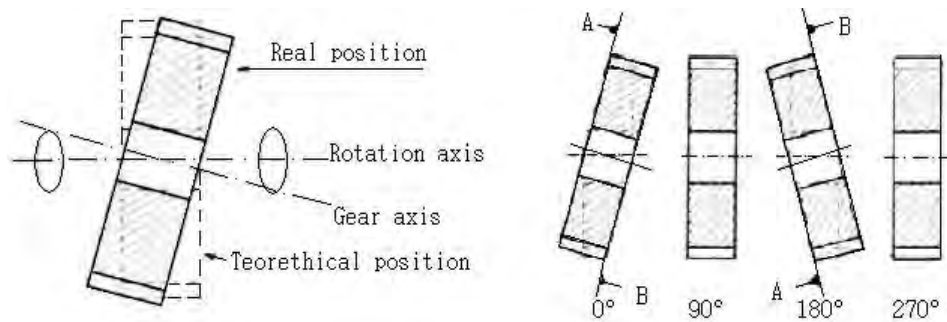


Figure 6.7: 2nd order oscillation: bad mounting conditions, the rotational axis is not parallel to the gear axis.

To approximately check the misalignment before acquiring data, the contact pattern between teeth is observed through a painting of the tooth surface using a permanent marker. Pictures of the painted tooth are taken every $2/3$ rounds of the shaft. In Figure 6.8 the pattern results to be correctly aligned, with constant development. The center distance was kept fixed at 150 mm, which is the nominal distance of the test rig with bearing

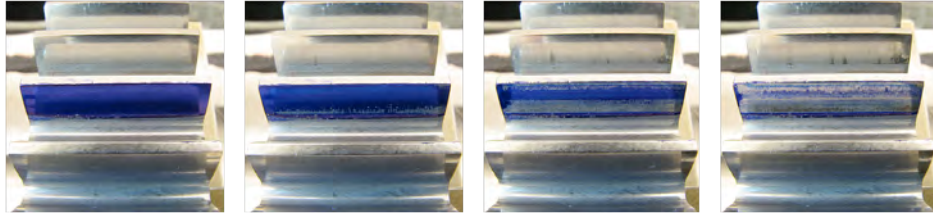


Figure 6.8: Contact pattern evolution

caps at their zero position and no torque applied. The measurements are conducted at different torque values, from 0 to 350 Nm with step of 50 Nm. Every applied torque gives a different shaft deflection which leads to a final different center distance. To control this parameter, the shaft deflection was measured for every torque value using a length gauge and a compensation of the center distance was made varying the bearing caps angular position. The defined center distance (150 mm) was re-established. To have a quasi static measurement, no dynamic effects have to be introduced in the system. Therefore the angular velocity of the gear pair is kept around 10-20 rpm.

6.2.2 Signal components

The measured TE contains different frequency components given by different causes. In Figure 6.9 a TE result is shown for 100 Nm applied torque. The lowest frequency component is the first order frequency, namely the frequency of rotation of the shafts. The cause of this order is given by the eccentricity of the whole rotating system which includes the eccentricity coming from the shafts, the gears and bearings. This component is called run out of the system.

The highest frequency components being observed are the 57th order frequency and its integer multiples, related to teeth passing. These components are given only by gears meshing, not including other parts of the system like shafts, bearings. It is impossible to obtain a system without eccentricity, therefore the total signal must be filtered to isolate these two components. In figure 6.10 the run out of the system can be observed and in figure 6.11 the meshing is shown. In figure 6.11 two facts can be noticed, which prove the good quality of the experimental data.

- The signal appears to be repeatable, observing low variations along the 57 teeth.
- The signal does not present modulation.

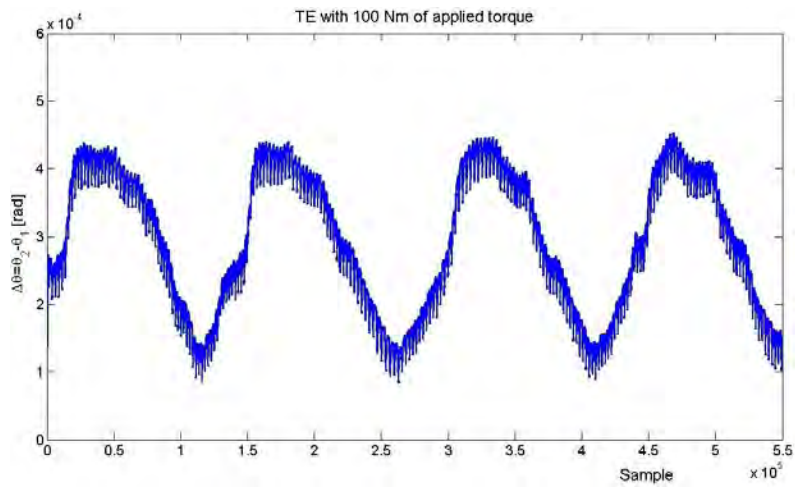


Figure 6.9: Total transmission error

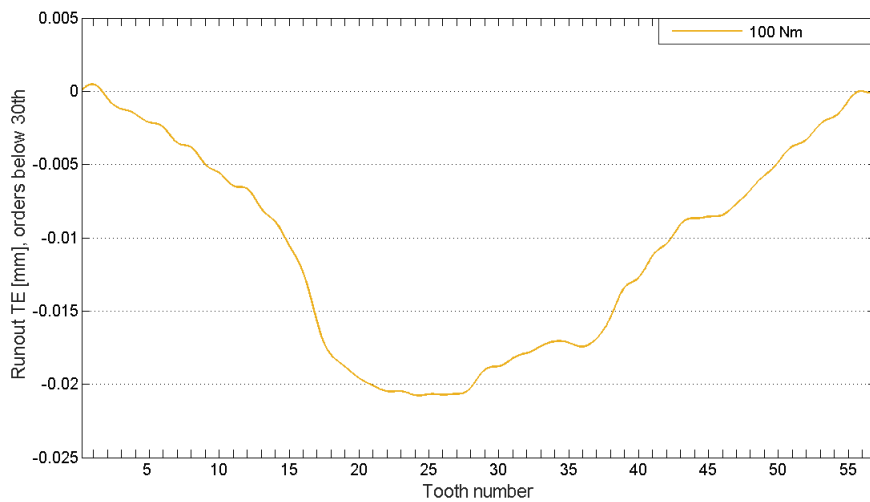


Figure 6.10: TE content below 30th order: run out

6.2.3 Experimental results

For the present work the operational conditions shown in figure 6.12, are used. Results for different torque values from 0 to 350 Nm are shown in figures 6.13 and 6.14. Low and high orders have been isolated through a spectral analysis, further discussions on this data elaboration are presented in next chapter. In figure 6.14, different torque curves are spaced along the y-axis to obtain a better visualization.

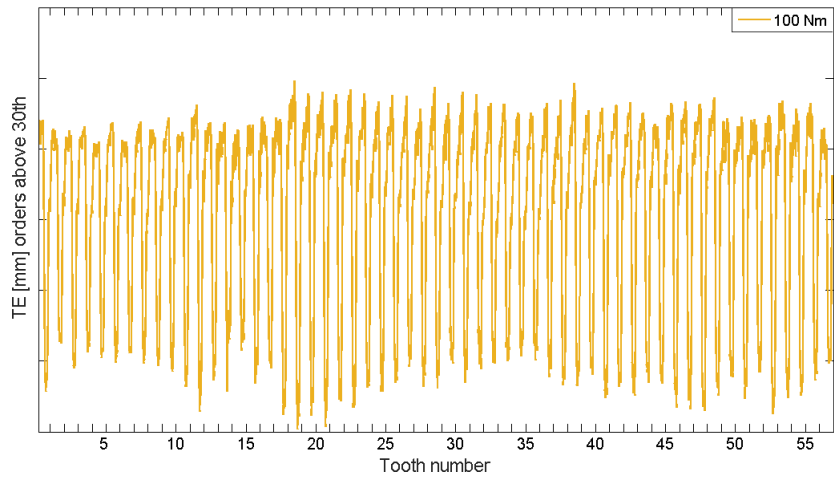


Figure 6.11: TE content above 30th order: teeth passing TE component

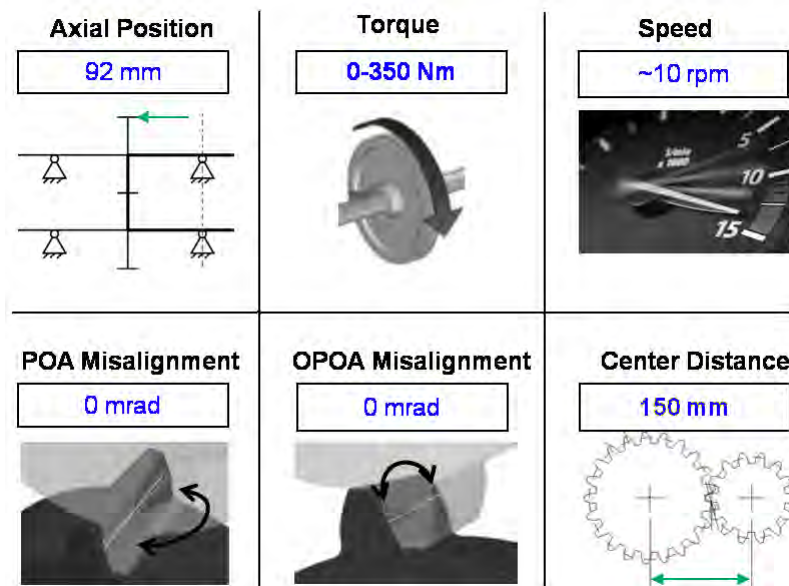


Figure 6.12: Testing conditions, torques from 0 to 350Nm. Source: [29]

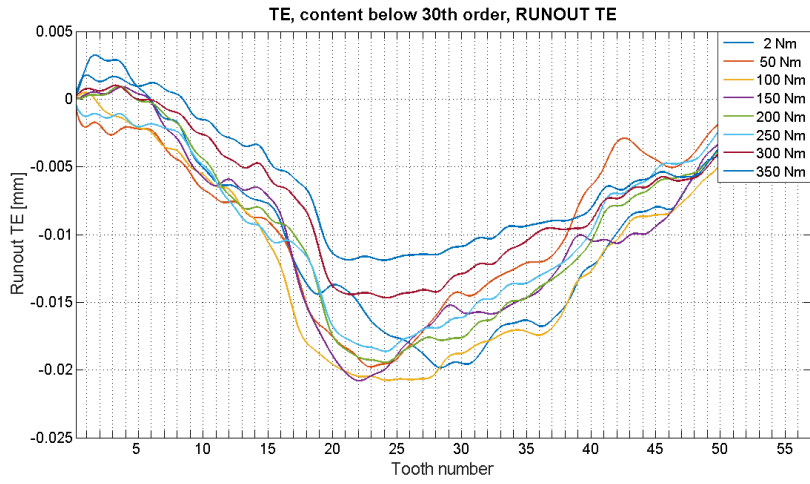


Figure 6.13: TE below 30th order, from 0 to 350Nm

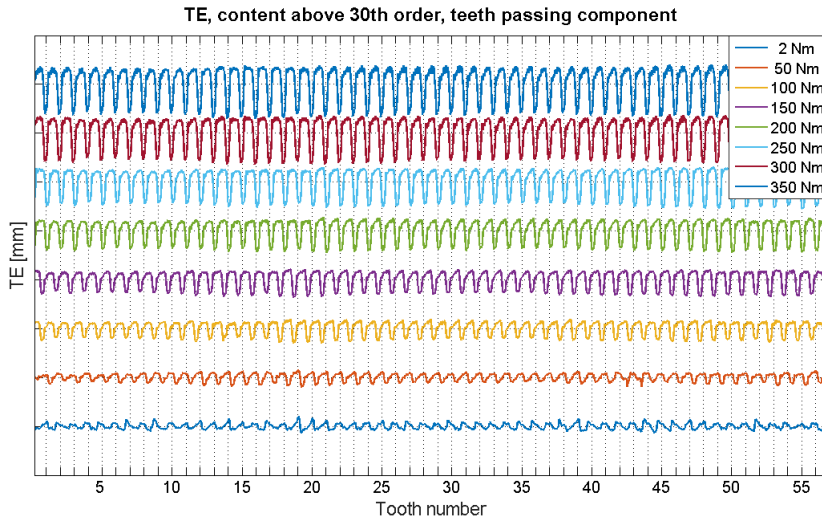


Figure 6.14: TE above 30th order, from 0 to 350Nm

6.3 Chapter's remarks

This chapter presented the high precision gear test-rig available at Siemens Industry Software NV. Its precision is given by various technical features, discussed in the first part together with different available set-up to impose different testing conditions. The main acquired data is the transmission error, needed to be compared with numerical simulations.

In the second part of the chapter test operating conditions are shown and the acquired signal components are discussed. Finally the measured TE for different torque values is split into the run out component and the 57th order component and the graphics are shown.

Chapter 7

Numerical results and comparison

7.1 Operating conditions

Along this chapter the numerical simulations performed on the adopted gear pair are discussed and results are compared with the experimental tests. The numerical model adopted and simulations strategy are presented in this section and the parameters used are chosen based on the performed analyses of the 4th chapter.

7.1.1 Numerical model

The mesh shown in figure 7.1 is the one chosen to perform the simulations. 10 elements on the width of the gear and 30 along the flank were chosen, according to the analysis made in the fourth chapter. In table 7.1 model and simulation parameters are shown.

Boundary conditions are defined with respect to the measurements performed. The gears are considered locked in their centres. This is done imposing zero displacements to all nodes along the inner diameter. Only the rotation along the perpendicular axis is allowed for the case of dynamic simulation. In the case of static solutions one gear is free to rotate and the other has all rigid displacements locked.

In the model updating phase a slightly different model was used, where the inner diameter presents a shoulder which there is not in the adopted FE model. This fact is assumed not to affect the quasi static analysis which is the aim of this work. For future developments dynamic simulations are foreseen, and the presence of this shoulder must be included in the numerical model.

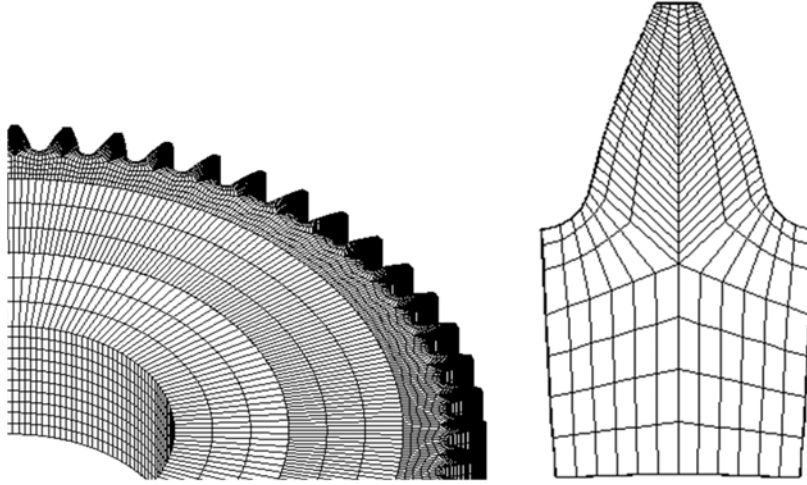


Figure 7.1: Implemented mesh

Elements along tooth flank	30
Elements along tooth width	10
Young's module [MPa]	207000
Poisson's ratio	0.32
Density [Kg/m ³]	7800
Penalty factor [N/mm]	500000
Center distance [mm]	150
Angular misalignments [rad]	0
Normal modes	20
Global contact shapes	40
Static solutions in one angular pitch	100
Simulation time [ms]	55
Ramp-up time [ms]	5
Contact detection	Node-to-surface only on teeth flanks
Contact detection	Master-slave double pass

Table 7.1: Model and simulation parameters

7.1.2 Pre-processing and applied torques

The discussed code needs the definition of two types of torques. A set of torques is used in the pre-processing phase to calculate the global contact

shapes that have to be inserted in the reduction matrix, and the applied torque is then used in the processing phase which is the real acting torque on the system. One of the advantages of this method is that with a set of 2 (or 3) pre-processing torques, a single pre-processing phase can be used to calculate various solutions with different applied torques, allowing to save time and maintain accuracy of the solution.

In this work seven different torques have to be calculated, from 50 to 350 Nm, therefore the scheme of table 7.2 of pre-processing and applied torques is used:

Pre-processing Torques: 50, 200 Nm	Torques: 250, 350 Nm
50, 100, 150, 200	250, 300, 350

Table 7.2: Torques in pre-processing and processing phases

7.2 Numerical results

In this section all static and dynamic results are collected. Special focus is kept on the amplitude of the TE results and on TE shapes. Differences between static and dynamic results are also investigated.

7.2.1 Static results

100 static solutions are calculated for every value of torque along one angular pitch. Two consecutive angular pitches are shown graphics 7.2.

To perform a comparison of the results, the first value to be analysed is the amplitude of the TE. In figure 7.2 static TE distributions for every torque value are shown and the difference of amplitude is evident when passing from two to one teeth pair in contact.

In figure 7.3 the amplitude of TE is represented. It was calculated as the medium of all results on the flat zone either for one and two teeth in contact. A quasi-linear distribution was expected, due to the fact that increasing the applied torque, the teeth deformation increases and the angular difference between the two gears increases. This fact is always present with unmodified spur gears, because the basic rack profiles allow a perfect meshing of the gear pair and the TE amplitude only depends on the applied torque. If one of the two gears has a modified profile, both the applied torque and the micro-geometry of the tooth affect the TE amplitude yielding to a non monotonic distribution as can be seen in [17].

Concerning the TE shape, it can be observed that there are oscillations

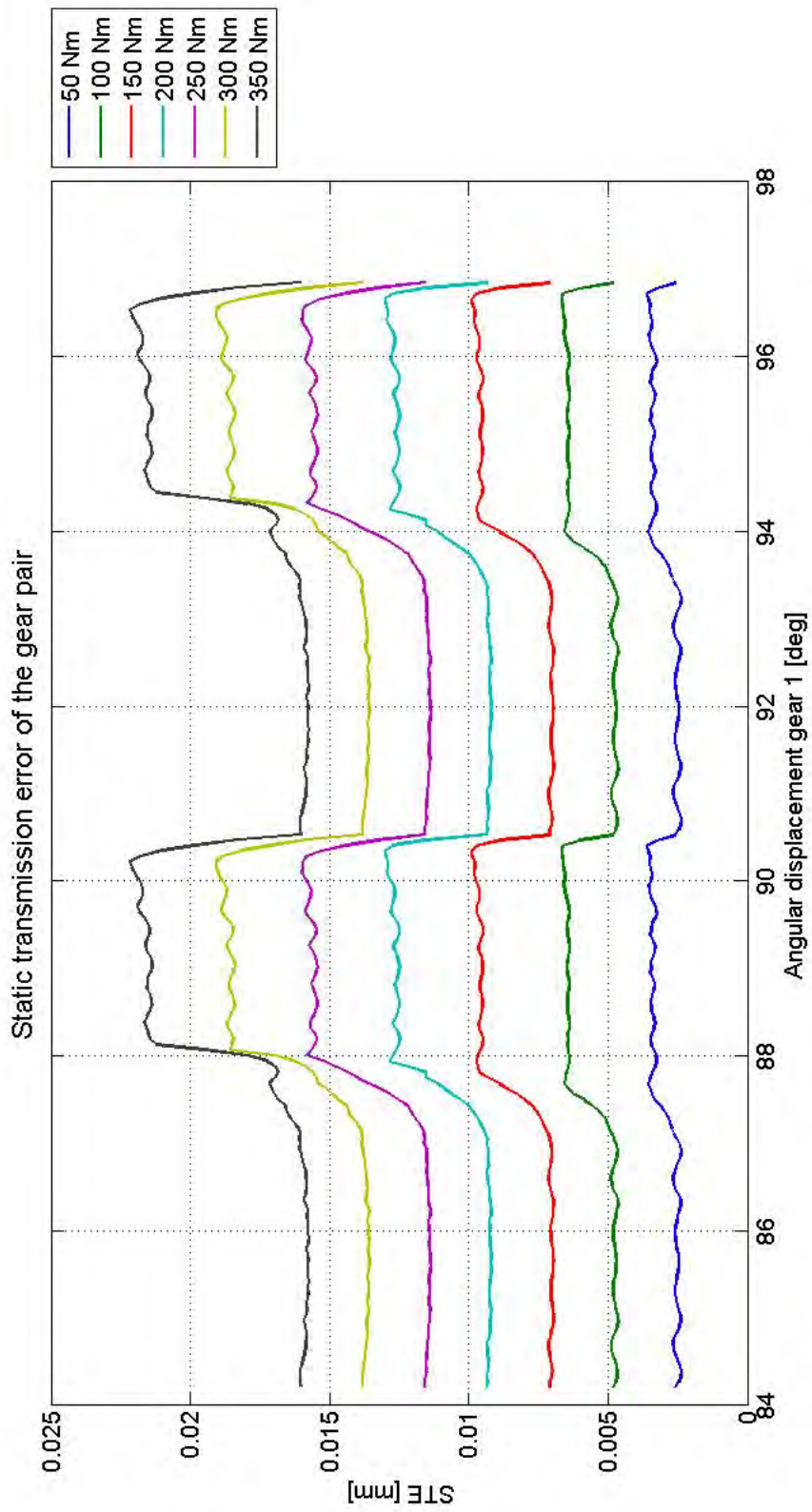


Figure 7.2: Static results of TE

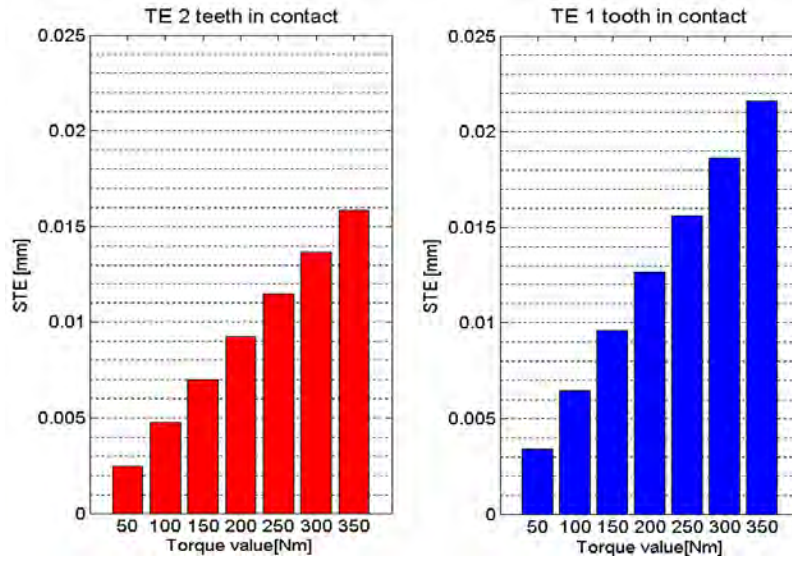


Figure 7.3: Average amplitude of static TE

along the one tooth contact part of the distribution. As seen in the 4th chapter this can be avoided increasing the number of elements along the flank, but this would sensibly increase the computing time. Decreasing the penalty factor is an other way to reduce this effect, without increasing the computing time but introducing a small error on the solution.

The penalty factor was set from 50000 N/mm to 10000 N/mm for 250, 300 and 350 Nm cases. Better distribution shape are obtained (Figure 7.4) whereas a small loss in amplitude accuracy is observed (Figure 7.5). In table 7.3 relative errors are calculated.

	250 Nm	300 Nm	350 Nm
Relative error: 2 teeth in contact	4.1%	2.8%	2.4%
Relative error: 1 tooth in contact	4.8%	3%	2.5%

Table 7.3: Relative errors between dynamic and static results

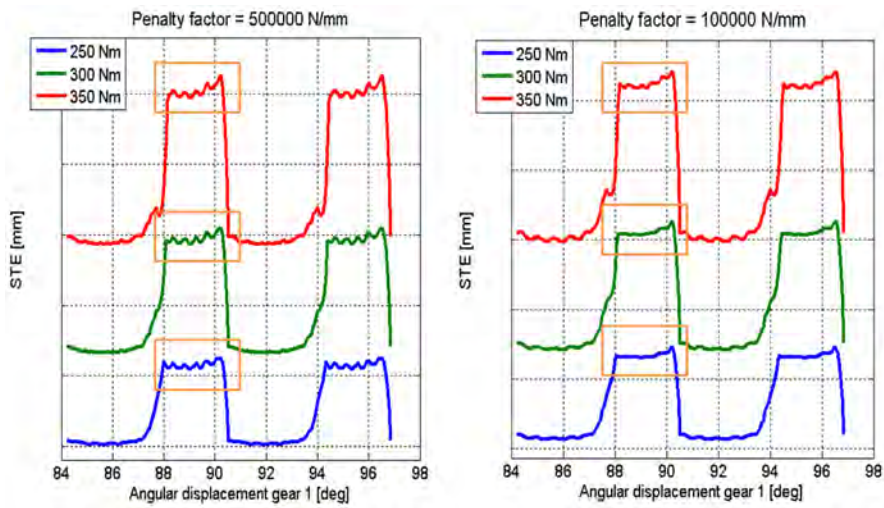


Figure 7.4: TE shape variation w.r.t. penalty factor

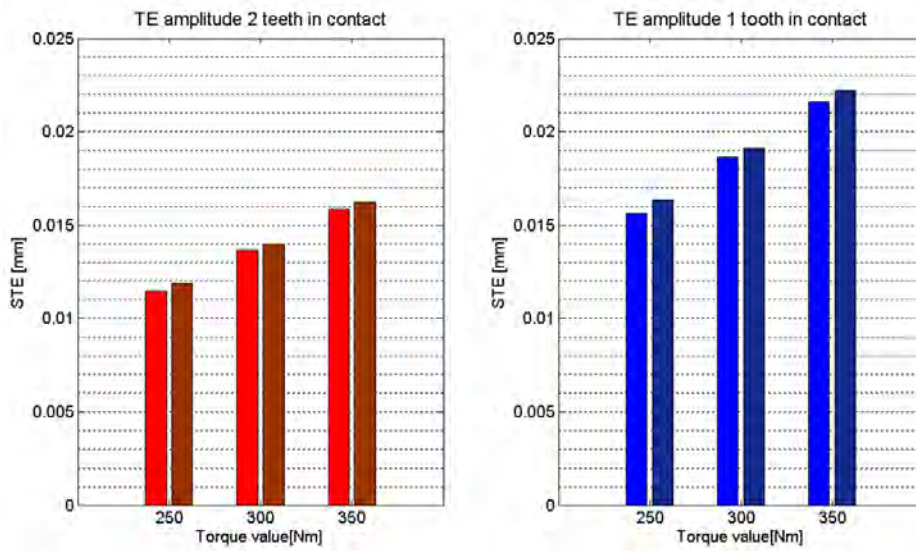


Figure 7.5: TE amplitude variation w.r.t. penalty factor

7.2.2 Dynamic results

Dynamic results are expected to be very close to the static results, because a quasi-static analysis is performed. According to this statement only three dynamic simulations are conducted (figure 7.7), with three values of torque: 100, 200, 300 Nm. Every dynamic simulation present different values of penalty factor and those values are the same used in the static solutions. TE amplitudes are compared showing in table 7.4 negligible variations of the results.

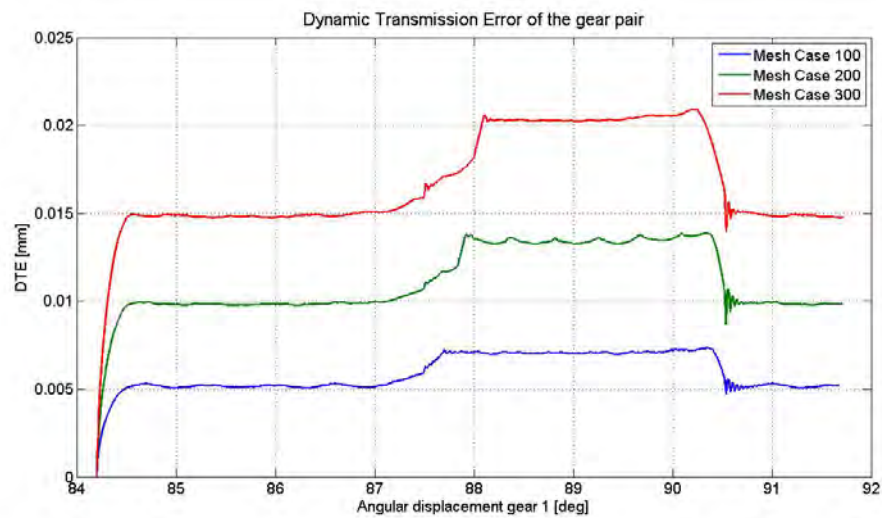


Figure 7.6: Dynamic results of TE

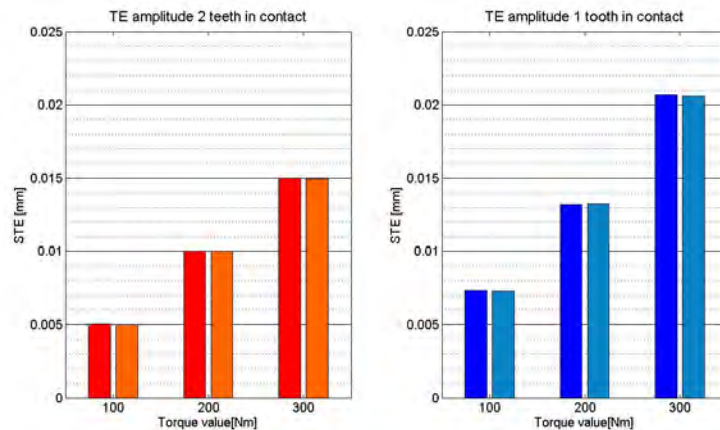


Figure 7.7: Comparison between static and dynamic solutions

The dynamic solutions result very close in amplitude values to the static

	100 Nm	200 Nm	300 Nm
Relative error: 2 teeth in contact	0.4%	0.3%	0.3%
Relative error: 1 tooth in contact	0.5%	0.4%	0.4%

Table 7.4: Relative errors between dynamic and static results

solutions. Therefore static values are acceptable to be compared with experimental results.

7.2.3 Contact evolution

As expected from the theoretical concepts on transmission error, a rectangular shape is obtained from the numerical simulations. This is due to the contact ratio that passes from 1 to 2 with a frequency directly related to the number of gear's teeth (57th order). The code also provides the calculation of displacements and stresses and their representation on the bodies, here in figure 7.8 the 100 Nm applied torque TE is shown. It can be observed the higher values of displacement and stress when only one tooth is in contact.

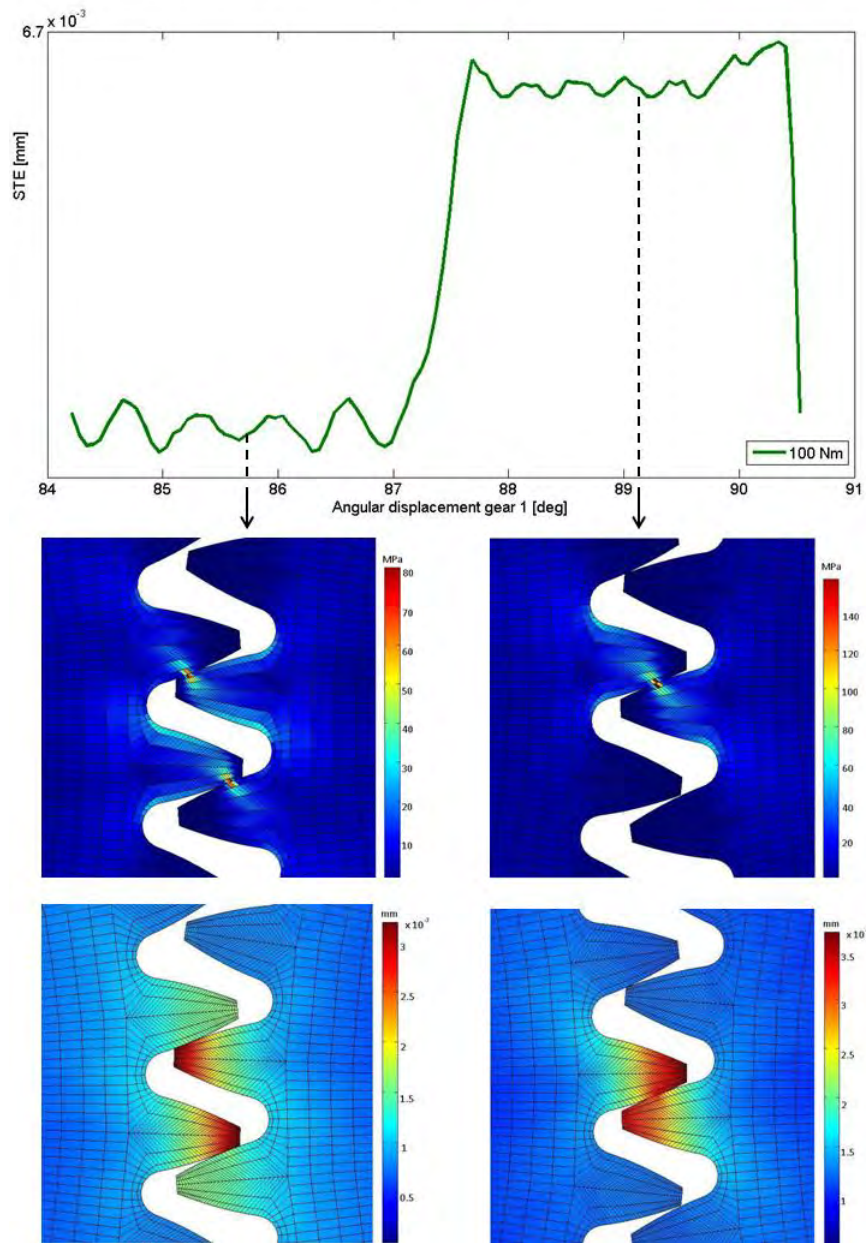


Figure 7.8: Von Mises stress [MPa] and displacements [mm] distribution for one tooth in contact configuration and two teeth in contact configuration.

Von Mises stresses are higher firstly on the contact path and then at the tooth's root. This stresses distribution mirrors the results shown by various literature sources, e.g. ([35]).

7.3 Comparison with experimental results

7.3.1 Signal decomposition

An analysis in frequency is performed for the measured TE. Different order components are obtained from order 1 to 500. The first order is the one related to the eccentricity of the system, taking into account shaft, bearings and gears eccentricity. Teeth passing effects should be observed near the 57th order and successive harmonics should be at orders 114th, 171st... In figure 7.9 the spectra of 100, 200 and 300 Nm are shown. In order to split the run

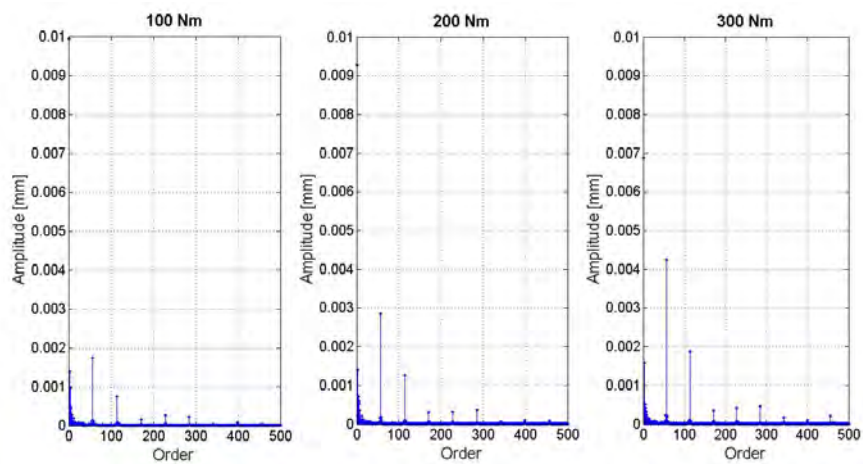


Figure 7.9: Spectra of measured TE

out component and the teeth passing component, a filter on every spectra is imposed, taking only the first 30 orders in the run out component and all the orders higher than 30 in the teeth passing component. Reconstructing the signal, two graphics can be obtained for every torque case, as can be seen in figure 7.10 and 7.11.

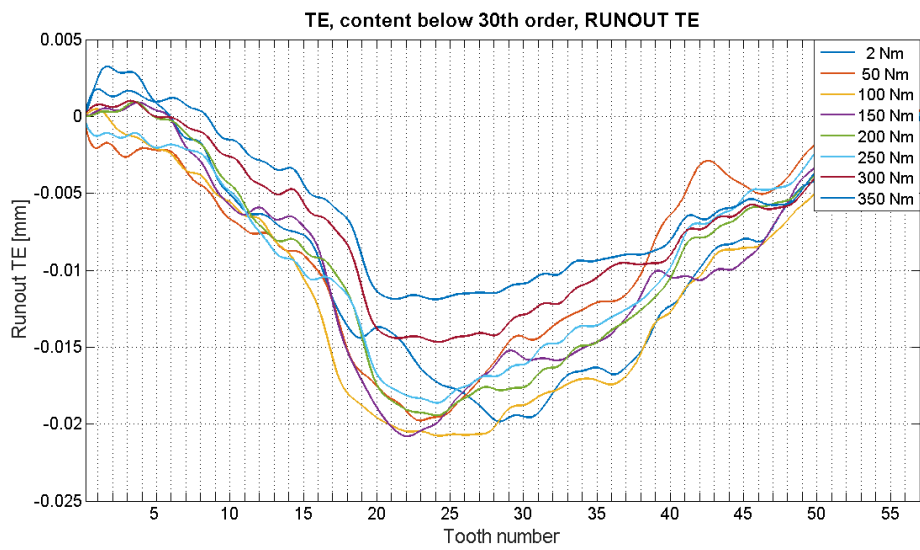


Figure 7.10: reconstructed TE, Run out

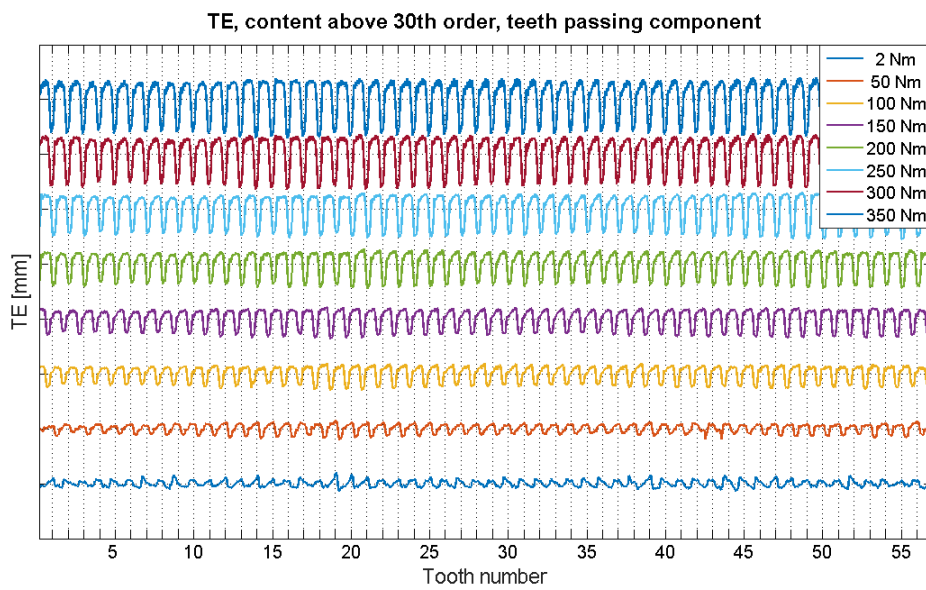


Figure 7.11: reconstructed TE, 57th order

Experimental amplitude is given by the 57th order amplitude. The higher meshing orders (114th, 171st...) have also been separated in the signal spectra, but they are not taken into account in this discussion. 57th, 114th and 171st orders are shown in figure 7.12.

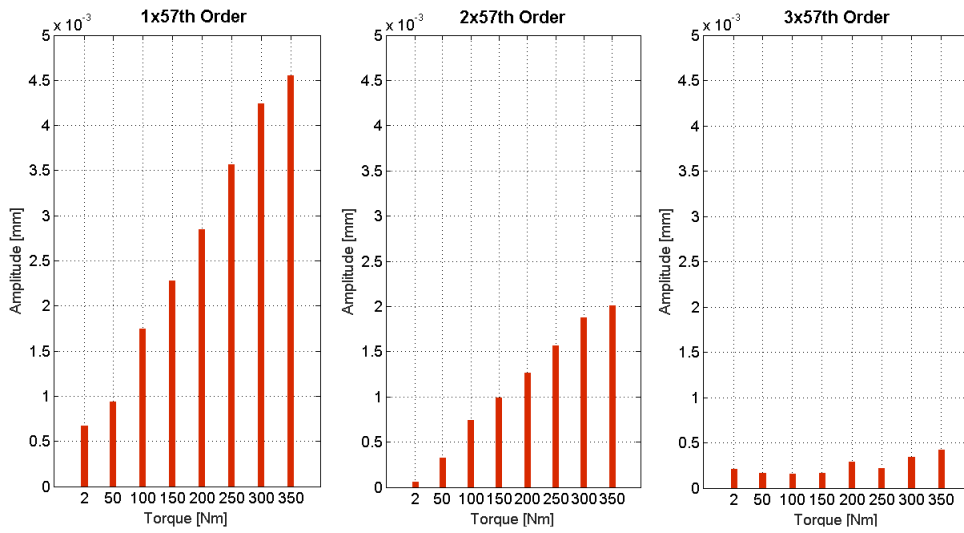


Figure 7.12: First three meshing orders

7.3.2 Amplitude

As the adopted gear pair presents a profile generated by a basic rack, the teeth in contact have to mesh perfectly in cinematic terms. Therefore with perfect meshing conditions and assuming no applied torque, the TE component given by teeth passing has to be zero. When the applied torque increases, teeth passing effects appear (e.g. 57th order effect). This brings to a defined linear distribution of the 57th order amplitude w.r.t. the applied torque as can be noticed in 7.3.

Experimental measurements give a TE of the gear pair for torque values in the range of 0 to 350 Nm. Observing the experimental curve at zero applied torque in 6.14, there is a TE component for teeth passing, probably given by manufacturing process or gears usage (figure 7.13). Therefore the TE for

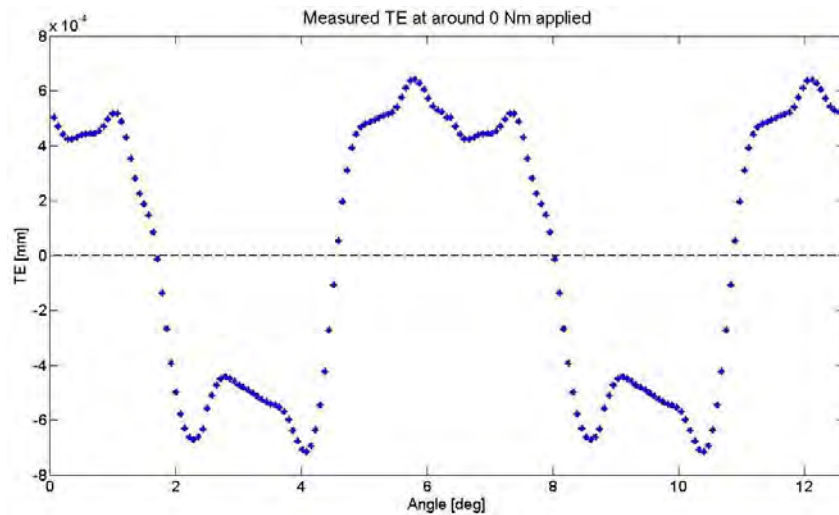


Figure 7.13: Averaged measured TE

the remaining torque values is adjusted taking off the TE with zero applied torque as can be seen in figure 7.14.

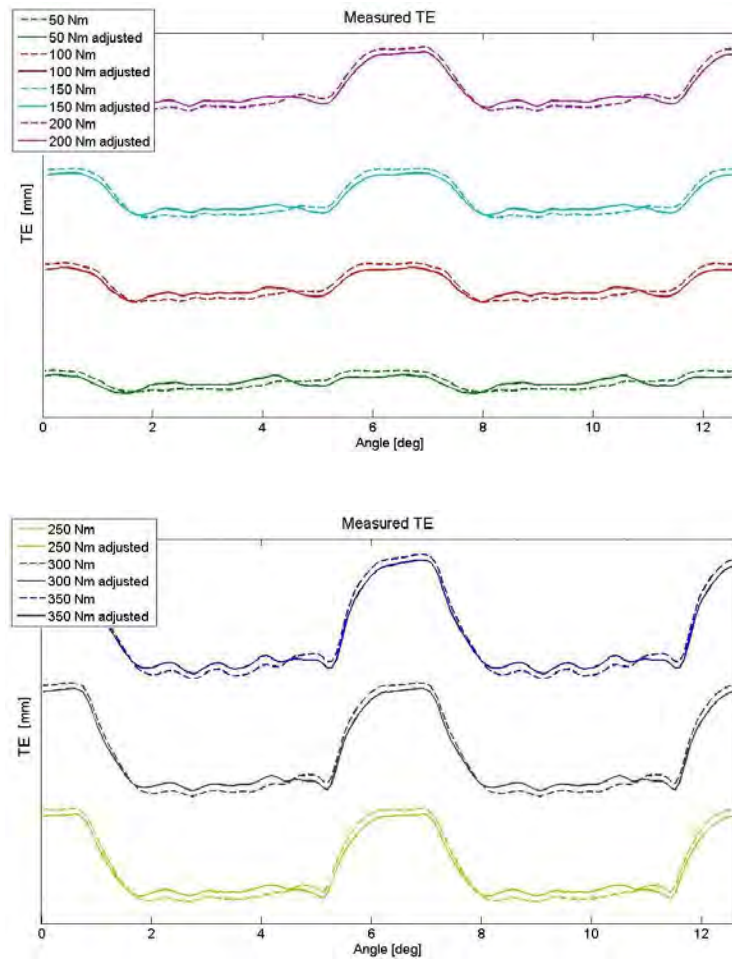


Figure 7.14: Adjusting of measured TE

Numerical results are given by perfect meshing conditions, where the geometry of the teeth pair is defined by geometrical functions. This fact leads to numerical solutions that are not affected by manufacturing or usage factors. Therefore the numerical TE results don't need the adjustment performed for the experimental ones.

The numerical amplitude is given by the difference between the 1-tooth-in-contact amplitude and the 2-teeth-in-contact amplitude divided by two (see Figure 7.3).

7.3.3 Shape

The experimental TE is given by a medium of 57 TE measurements along one entire rotation of the shafts. The different periods were phased and superposed leading to an averaged solution for every torque value. A Gauss

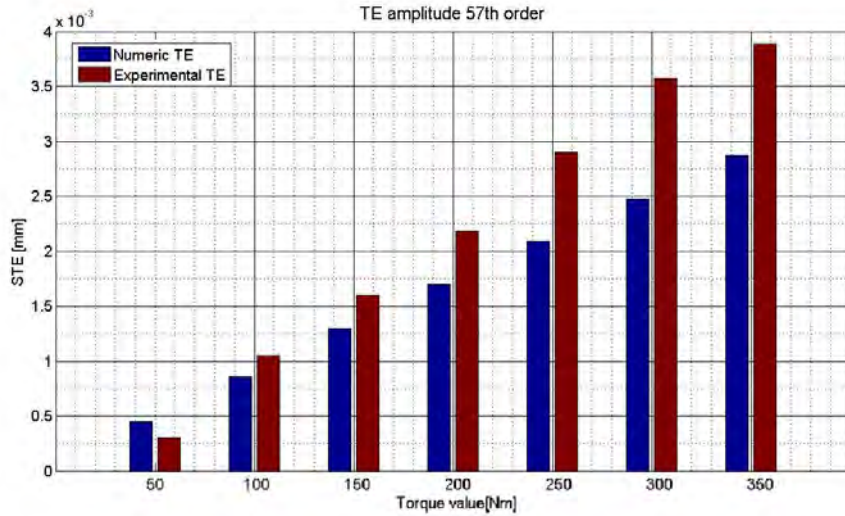


Figure 7.15: Amplitude comparison between numerical and experimental results

distribution is observed along every sample instant of the curve, then confidence bounds were calculated to observe the repeatability of the solution along one round of the shafts. 2σ bounds (95% confidence) are shown in 7.16. Some considerations on the processed experimental data can be made.

1. The variation of contact ratio is clearly evident. However the tooth handover is gradual, leading to shape results quite far from a square distribution. This can be due to:

Friction was not considered in the numerical model. It implies tangential forces in the contact path and sticking of the surfaces which both can increase the duration of contact between teeth leading to a gradual tooth handover. The gear pair has been tested several times and it has been used also for modal analysis with impact hammer, leading to high usage and oxidation of the surfaces, therefore friction between teeth can be a possible cause for the observed effect.

Edge contact appears with unmodified gears. At the start and at the end of the engagement of one tooth, the edge contact is the first and last contact interaction occurring. It can be responsible respectively for an anticipation and a delay of the teeth contact, increasing the average stiffness of the system.

2. The 2σ bounds are very close to the averaged value, but the variability increases when passing from one teeth pair in contact to two. This can be due to the edge contact phase, where the tooth's edge is the

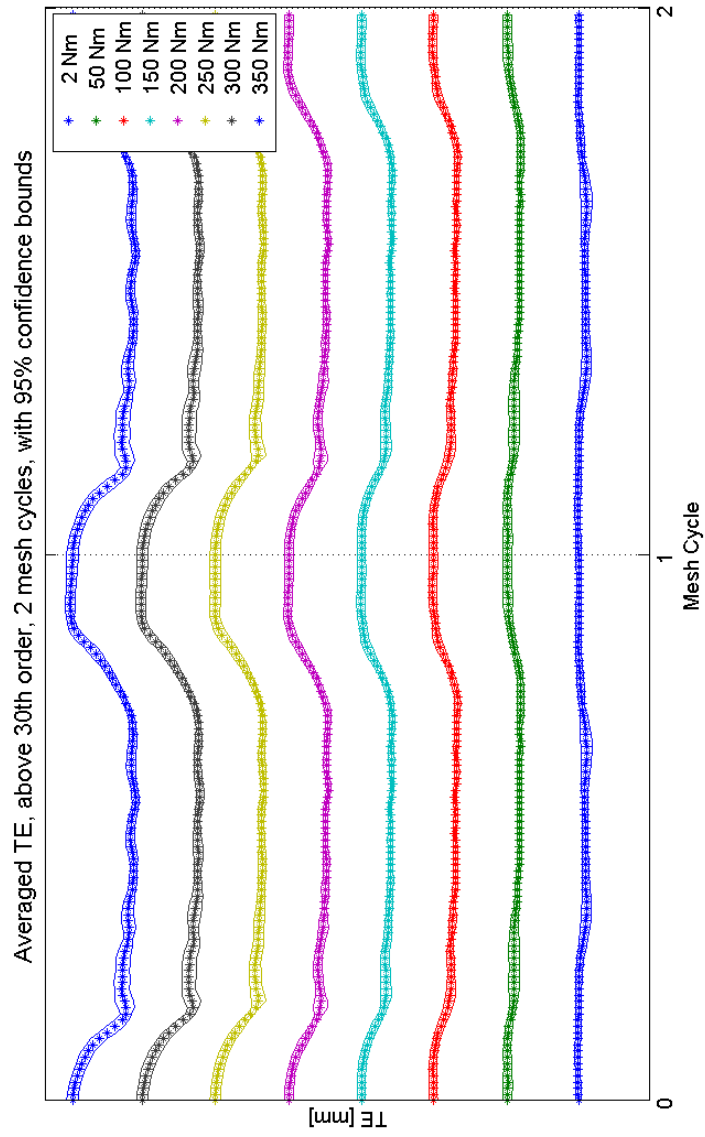


Figure 7.16: Averaged experimental TE

first part of entering in contact, making the contact interaction highly dependent on the tooth surface finishes.

- Oscillations are observed along the flat part where the contact ratio is higher. This fact can be due to the tooth's edge which impacts on the gear's flank and consequently excites the normal modes of the system. Considering figure 7.17, the frequency of those oscillations is around 170 Hz. In [13] the analytical equations of the rotational

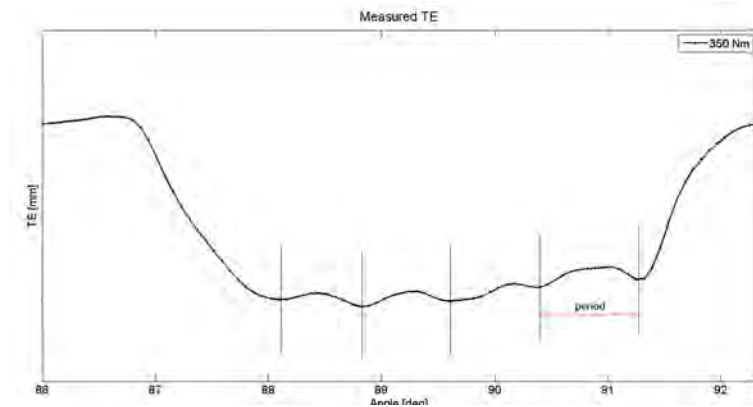


Figure 7.17: Measured TE at 350 Nm

model of the gear test-rig were solved to obtain the rotational natural frequencies. The first obtained natural frequency is around 280 Hz, which has the same order of magnitude of the experimental one, but they still present an high relative error. Further analyses should be conducted to investigate the origin of this measured frequency.

In figure 7.18 numerical and experimental data can be seen, underlining differences in the shapes, particularly in the transient zones.

7.3.4 Contact ratio

In this section the contact ratio of the gear pair is investigated on the TE graphics, both measured and numerical. In chapter 2nd the contact ratio definition was given, but it was also observed the more intuitive meaning of it. In TE graphics the contact ratio is calculated as described in chapter 2nd, comparing the percentage of two teeth in contact along one angular pitch. In table 2.2 the nominal contact ratio was calculated as $\epsilon = 1.45$.

It can be seen from figure 7.18, that the numeric TE presents a square shape more evident than the experimental TE, which has a gradual variation of stiffness in changing the number of teeth in contact. This implies more uncertainty in the measured contact ratio definition. Uncertainty boundaries

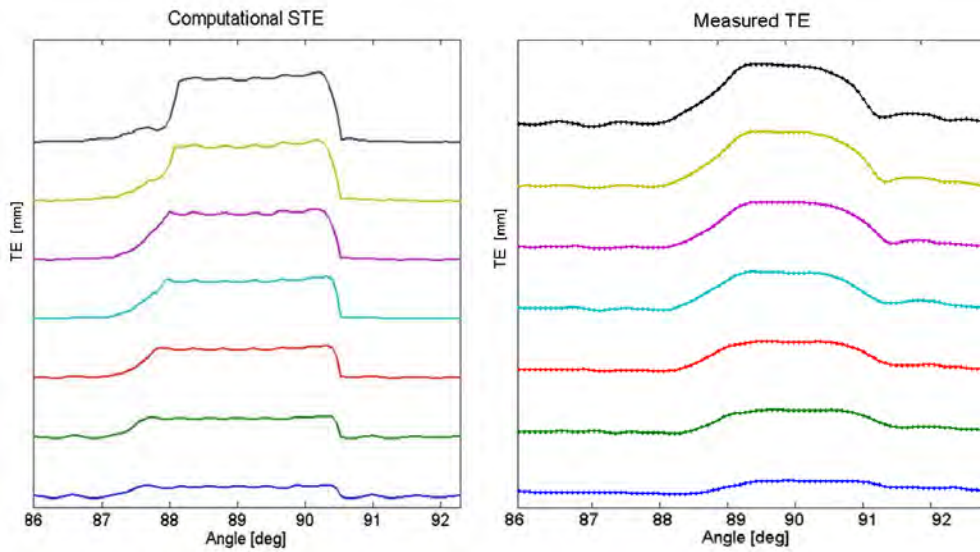


Figure 7.18: Shape comparison between numerical and experimental results

were taken into account in the contact ratio calculation. In figure 7.19 and in table 7.5, contact ratio values are shown. The numerical contact ratio is

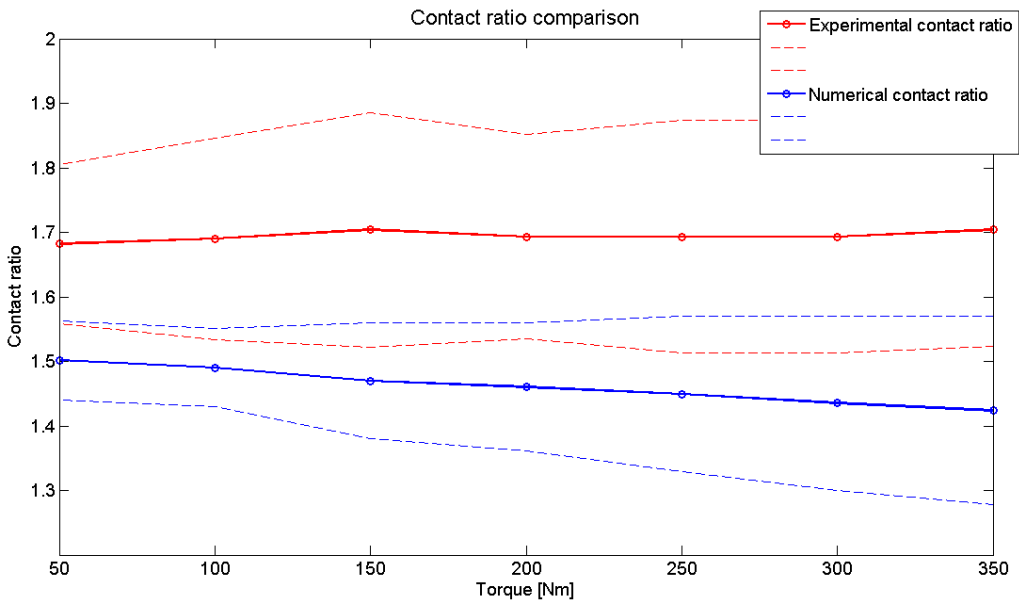


Figure 7.19: Contact ratio variation along torques

very close to the nominal value ϵ . There is a clear decreasing trend of the numerical contact ratio with respect to the applied torque. This is due to the fact that for higher values of torque, the tooth undergoes larger deflections,

50 Nm	100 Nm	150 Nm	200 Nm	250 Nm	300 Nm	350 Nm
1.6820	1.6899	1.7041	1.6930	1.6930	1.6930	1.7041
1.5016	1.4905	1.4699	1.4604	1.4494	1.4351	1.4241

Table 7.5: Measured and numerical contact ratio w.r.t the torque.

remaining more in contact in one angular pitch and leading to a lower contact ratio. The experimental contact ratios are far from the nominal value. Their calculation is affected by an high range of uncertainty.

7.4 Chapter's remarks

In this chapter the numerical model of the gear pair was defined, with focus on the results of chapter 5th. Numerical results were obtained for the seven values of torques, the static transmission error variation along torque was observed, with focus on amplitude and shape.

Experimental tests on the test-rig were discussed: first the decomposition of the signal was performed through a spectrum analysis, splitting the first 30 low orders (run out component) and the 30 high orders (TE component). Then comparison of numerical and measured results was conducted in terms of amplitude of the 57th order and observing the shape of both graphics. The amplitude of measured results does not match on every torque value accurately with the amplitude of the numerical TE. Observing the contact ratio calculation performed on numerical and measured TE, differences between the two solutions appear. However a high range of uncertainty is to be noticed in the experimental contact ratio definition, due to a different shape of TE distribution.

The experimental results in general do not match accurately with the numerical ones and looking at the contact ratio, ϵ , they are still distant from the analytical solution. On the other side the numerical results are very close to the analytical ones, with small errors between the numerical contact ratio and the analytical one.

Chapter 8

Conclusions

This thesis work analysed transmission error results of a gear pair, both with numerical simulation and experimental tests. A novel code by KU Leuven was tested, based on a new MOR approach. Theoretical aspects of the method and the code were presented in the firsts chapters, underlining the main advantages. The numerical model was correlated with an existing gear pair in order to perform numerical simulations on it (chapter 5th and 7th). The gear pair was tested at an available gear test-rig at Siemens Industry Software, obtaining measured transmission error for different torque values. These results were then compared in chapter 7th with numerical simulations performed with the same working conditions.

8.1 Simulation parameters analysis

In chapter 3rd, the main theoretical aspects of the method were discussed, underlining the most important parameters in the contact problem and in the model order strategy. In chapter 5th, these parameters were varied to investigate their influence on the solution, discussing some behaviours of the code.

Along these simulations various numerical effects were noticed particularly on the dynamic solution. Those effects were analysed and a explanation of their behaviour was given.

8.2 Correlation and transmission error results

Young's module and Poisson's ratio of the numerical model of the transmission were updated, showing good correlation with the test-rig gear pair. Quasi-static analyses of the gear pair were conducted on the test-rig, varying the applied torque on the system. Transmission error results were obtained. The gear pair was implemented in the novel code with the same working

conditions of the test-rig. Various transmission error results are shown, indicating some particular effects on the amplitude and contact ratio variation discussing possible explanations of them.

Finally a comparison between numerical and measured TE is presented. Experimental tests resulted to be not close to numerical ones and also to the theoretical value of contact ratio. A high range of uncertainty is noticed in the contact ratio calculation, whereas the amplitude of the 57th order of transmission error presents a match with the numerical amplitude for some values of torque.

The numerical results are close to the nominal contact ratio and a clear trend w.r.t. the applied torque is observed.

Future developments of this work can be conducted both on the test-rig and on the code, trying to obtain new measurements and simulations to investigate the variation of results for static and dynamic solutions. The numerical method proved to be stable and reliable, therefore efforts should be put on more developments of the code extending its range of application to different types of mechanical system.

Bibliography

- [1] Craig, Roy R Jr, *A Review of Time-domain and Frequency-domain Component-Mode Synthesis Methods*, NASA STI, 1985
- [2] Heirman G, Tamarozzi T, Desmet W, *Static modes switching for more efficient flexible multibody simulation*, International Journal for Numerical Methods in Engineering, 2011
- [3] Tamarozzi T, Ziegler P, Eberhard P, Desmet W. *Static modes switching in gear contact simulation*, Mechanism and Machine Theory, 2013
- [4] Rewienski M, White J. *Model order reduction for non-linear dynamical systems based on trajectory piecewise-linear approximations* Linear Algebra and its Applications, 2006
- [5] Tamarozzi T, *Efficient numerical simulation strategies for flexible multibody systems with variable topology*, PhD Thesis, University of Leuven (Belgium), 2014
- [6] Shabana A, *Dynamics of multibody systems*, John Wiley and Sons Inc., New York, 1989
- [7] Blockmans B, Tamarozzi T, Naets F, Desmet W, *A nonlinear parametric model reduction method for efficient gear contact simulations*, International journal for numerical methods in engineering, University of Leuven, 2014
- [8] Wang S, Nakamachi E, *The inside-outside contact search algorithm for finite element analysis*, International journal for numerical methods in engineering, 1997
- [9] *ISO 21771, Gears - Cylindrical involute gears and gear pairs - Concepts and geometry*, 2007
- [10] *KHK Gear technical reference*, Kohara Gear Industry Co. LTD
- [11] Henriksson M, *On noise generation and dynamic transmission error of gears*, PhD Thesis Royal Institute of Technology, Stockholm, 2009

- [12] *Transmission error: the metric for gearbox NVH quality*, Siemens PLM Software
- [13] Palermo A, Anthonis J, Mundo D, Desmet W, *A novel gear test rig with adjustable shaft compliance and misalignments. Part I: Design*, CMMNO Conference, University of Ferrara, 2013
- [14] Palermo A, Anthonis J, Mundo D, Desmet W, *A novel gear test rig with adjustable shaft compliance and misalignments. Part II: Instrumentations*, CMMNO Conference, University of Ferrara, 2013
- [15] Palermo A, Toso A, Heirman G H K, Cerd R, Gulinelli M, Mundo D, Desmet W, *Structural coupling and non-linear effects in the experimental modal analysis of a precision gear test rig*, International Gear Conference, Lyon, 2014
- [16] Hotait M, Kahraman A, *Experiments on root stresses of helical gears with lead crown and misalignments*, J Mech Des, 2008
- [17] <http://www.precisiongeartestrig.com/>
- [18] Tamarozzi T, Heirman G, Desmet W, *An on-line time dependent parametric model order reduction scheme with focus on dynamic stress recovery*, Computer Methods in applied Mechanics and Engineering, 2014
- [19] <http://www.plm.automation.siemens.com/it-it/products/lms/virtual-lab/>
- [20] Croes J, *Updating and correlation procedure*, Seminar structural dynamics, KU Leuven, March 2014
- [21] Van Langenhove T, Brughmans M, *Using MSC/NASTRAN and LMS/PRETEST to find an optimal sensor placement for modal identification and correlation of aerospace structures*, LMS International, Leuven, 2010
- [22] Irvine T, *An introduction to frequency response functions*, 2000
- [23] Pastor M, Binda M, Harcarik T, *Modal Assurance Criterion*, Technical University of Kosice, MMaMS, 2012
- [24] Langley R S, Bremner P, *A hybrid method for the vibration analysis of complex structural-acoustic systems*, Acoustical Society of America, 1999
- [25] MSC Nastran, *DMAP Programmer's guide*, MSC Software Corporation, 2012
- [26] <http://www.3ds.com/products-services/simulia/products/abaqus/>

- [27] *Controlli Ingranometrici*, Nuova PTM Meccanica, Info tecniche
- [28] Bianco G, *La rumorosit degli ingranaggi, 1, 2, 3 parte*
- [29] Palermo A, *Measurement Consolidation Procedure*, Siemens Industry Software, February 2015
- [30] Palermo A, Shweiki S, *STE measurement varying Torque, Unmodified spur gears*, Siemens Industry Software, February 2015
- [31] <http://www.fp7demetra.eu/>
- [32] Ricci A, *Model reduction techniques in flexible multibody dynamics with application to engine cranktrain simulation*, PhD Thesis, University of Bologna, 2013
- [33] Bruls O, Duysinx P, Golinval J C, *The global modal parametrization for non-linear model-order reduction in flexible multibody dynamics*, University of Liege, InterScience, 2006
- [34] Cantarini N, Chiarellotto B, Fiorot L, *Un corso di Matematica*, Libreria Progetto, 2006
- [35] Lewis W, *Investigation of the strength of gear teeth*, Gear Technology USA, 1992
- [36] Smith J D, *Gear noise and vibration*, Marcel Dekker Inc, 2003